THERMAL STUDY OF A TRIGLYCERIDE MIXTURE

by

Omar Abdel Muhsen Al-Qatami

Submitted in partial fulfilment of the requirements
for the degree of Master of Science

at

Dalhousie University
Halifax, Nova Scotia
June 2011

DALHOUSIE UNIVERSITY

DEPARTMENT OF PROCESS ENGINEERING AND APPLIED SCIENCE

The undersigned hereby certify that they have examined, and recommend to the Faculty of Graduate Studies for acceptance, the thesis entitled "**THERMAL STUDY OF A TRIGLYCERIDE MIXTURE**" by Omar Abdel Muhsen Al-Qatami in partial fulfilment of the requirements for Master of Science.

Dated: June 9th, 2011

Supervisor: _____

Readers: _____

_____

_____

DALHOUSIE UNIVERSITY

DATE: June 9th, 2011

AUTHOR: Omar Abdel Muhsen Al-Qatami

TITLE: THERMAL STUDY OF A TRIGLYCERIDE MIXTURE

DEPARTMENT OR SCHOOL: Process Engineering and Applied Science

DEGREE: M.Sc.   CONVOCATION: October   YEAR: 2011

Permission is herewith granted to Dalhousie University to circulate and to have copied for non-commercial purposes, at its discretion, the above title upon the request of individuals or institutions. I understand that my thesis will be electronically available to the public.

The author reserves other publication rights, and neither the thesis nor extensive extracts from it may be printed or otherwise reproduced without the author's written permission.

The author attests that permission has been obtained for the use of any copyrighted material appearing in the thesis (other than the brief excerpts requiring only proper acknowledgement in scholarly writing), and that all such use is clearly acknowledged.

_____
Signature of Author

TABLE OF CONTENTS

List of tables

List of figures

ABSTRACT

The heat capacity and the enthalpy of crystallization of the crystalline phases at the end of cooling must be known in order to determine the excess energy of mixing two pure triglycerides, trilaurin and trimyristin, cooled at different cooling rates. The present investigation was carried out using Differential Scanning Calorimetry, DSC, Modulated Differential Scanning Calorimetry, MDSC$^®$, and Thermal Relaxation (in a Physical Properties Measurement System, PPMS). It was found that enthalpy of crystallization values can be measured to within $\leq 2\%$ (SE) with DSC Q100 TA Instruments. To achieve this, an experimental procedure and a data analysis method are proposed.

It was not possible in this study to obtain accurate and reproducible heat capacity values using a DSC Q100 instrument. The values were shown to be significantly by the position of the sample pan in the measuring sensor. PPMS C_p values were within the literature values.

.

LIST OF ABBREVIATIONS AND SYMBOLS USED

DSC	Differential Scanning Calorimetry
MDSC	Modulated Differential Scanning Calorimetry
PPMS	Physical Properties Measurement System
LLL	trilaurin
MMM	trimyristin
OOO	triolein
SAXD	small angle X-ray diffraction
WAXD	wide angle X-ray diffraction
TAGs	triglycerides
3L7M	30% trilaurin: 70% trimyristin binary triglyceride mixture
5L5M	50% trilaurin: 50% trimyristin binary triglyceride mixture
7L3M	70% trilaurin: 30% trimyristin binary triglyceride mixture
T	temperature (°C)
ΔT	temperature difference between the sample and the reference sensors
C_p	specific heat capacity at a constant pressure (J/g°C)
ΔH_{crys}	the enthalpy of crystallization

ACKNOWLEDGMENTS

Chapter 1   INTRODUCTION

1.1   Lipids

The term "lipid" has evolved through "lipin", "lipine", "lipoid" and "lipide". In 1920, lipoids were classified into three major categories, simple lipoids (fats and waxes), compound lipoids (phospholipids and glycolipids) and derived lipoids (fatty acids, alcohol and sterols) (Bloor, 1920). This definition was accepted until 1940 when materials like caroteniods, terpenes and steroids were included in the term. Thus, it was necessary to have a more comprehensive definition based on the solubility. Christie (1987) proposed a definition consistent with modern views as "fatty acids and their derivatives, and substances related biosynthetically or functionally to these compounds." (Christie, 1987). It is a common mistake that the terms lipids and fats are used interchangeably; fats is a subgroup of lipids. The main sources of lipids are animals and vegetables. The main resources of fats and lipids are vegetable and animal fats and oils, which contain different molecular species having different chemical and physical properties (Sato, 2001a, 2001b).

Triacylglycerols (TAGs) are one of the main members of the lipid family. Almost all the commercially known fats and lipids, either from animal or plant origin, consist almost exclusively of TAGs. They are made of a glycerol moiety whose three hydroxyl groups are esterified to fatty acids. Based on the number of fatty acids esterified, lipids can be classified into three groups, monoacylglycerols, diacylglycerols and triacylglycerols which have one, two or three fatty acids esterified, respectively. An example of a TAG is shown in Figure 1-1.

$$CH_3(CH_2)_n-\overset{\overset{\displaystyle O}{\|}}{C}-O$$

$$O-\overset{\overset{\displaystyle O}{\|}}{C}-(CH_2)_nCH_3$$

$$CH_3(CH_2)_n-\underset{\underset{\displaystyle O}{\|}}{C}-O$$
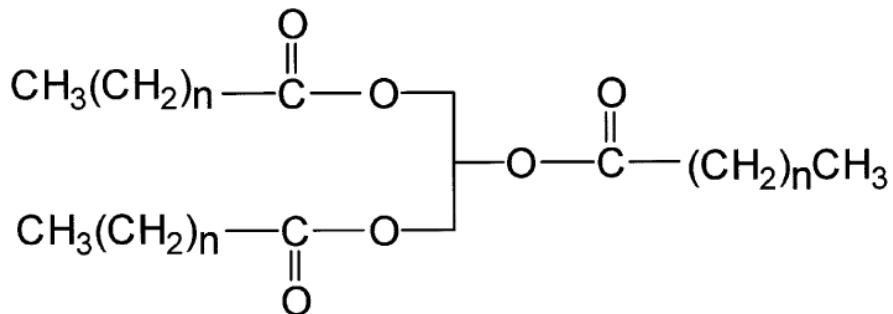
Figure 1-1: Schematic of TAG structure (Yeaman, 2004). (Permission has been obtained by PubMed).

Lipids can be classified based on their substituent fatty acids into two major categories, saturated and unsaturated. Saturated TAGs are mostly from animal origin and do not contain double bonds. Unsaturated TAGs, on the other hand, contain double bonds and are predominantly from plant origin. Cis-unsaturated TAGs have lower melting points due to the rigid kinks introduced in the aliphatic chain by the double bonds.

In the vast majority of the literature examined, TAGs are referred to according to the type of fatty acids esterified. For example, PPP represents Tripalmitin, which is a TAG with three molecules of palmitic acid. In cases where TAGs contain different fatty acids, the position of the fatty acid constituents should be indicated (Belitz *et al.*, 2009). For example, PSO is a TAG that contains palmitic acid, steric acid and oleic acid esterifies into the carbon one, two and three in the glycerol backbone respectively, and would be different from POS. In this thesis, the same way of naming was used.

Lipids have been studied for many years for their vital impact on human health and economy. Disturbances in lipids metabolism are involved in a variety of diseases, especially cardiovascular problems. Omega-three fatty acids are well recognized for their prevention of many chronic ailments such as coronary heart disorders and some types of

cancer (Nettleton, 1995). Lipids also play an important role in economy, as they are one of the main ingredients of all foods and contribute significantly in the food palatability, flavour and structure. In addition, lipids are of great importance in industrial applications as they are the starting materials for many other materials such as detergents and lubricants.

1.2   Lipids Crystallization

Crystallization of fats and lipids has been studied in detail due to its significance to consumers and the food industry. Most often, the study of lipid crystallization aims at obtaining crystals with well-defined physical structures that impart the desired physical qualities to the final fat-containing products. Crystallization can be defined as the process of formation of a solid lattice crystal from a supersaturated liquid or solution. In practice, in order for a crystal to form, it is necessary for the melt to go beyond the equilibrium state and become supersaturated. Supersaturation can be attained by either supercooling the melt, which is cooling beyond the melting temperature, or reaching a concentration level greater than the solubility concentration. The conditions in which supersaturation, or metastability are attained control the desired properties of the end products. A material is considered to be metastable when it exists in a state of apparent equilibrium but has the capacity to pass to a more stable state when the conditions change significantly or enough time is given.

Metastability is very important in lipids. Crystallization is a kinetic process that to start needs the melt undercooled below its melting point. The undercooling bears an

inverse proportion to the induction time of nucleation and the number density of nuclei. During nucleation, the molecules of the melt will arrange themselves to form stable clusters that eventually form a crystal lattice structures (Hartel, 2001). Figure 1-2 is a proposed schematic depiction of ordering liquid molecules to form a crystalline solid phase (Hartel & Kaylegian 2001). This hypothetical view is still being debated.
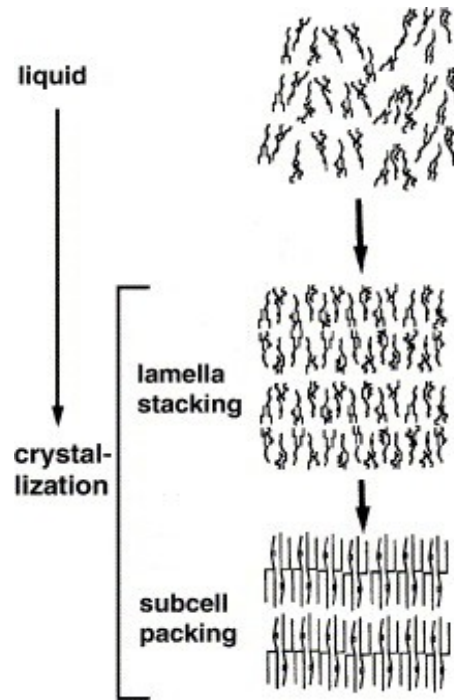
Figure 1-2: Schematic depiction of TAG liquid molecules rearranging themselves to form a solid crystalline phase (Hartel & Kaylegian 2001). (Permission has been obtained by Marcel Dekkar).

Subsequently, once a first crystal arrangement has reached a critical size to form a stable nucleus, it will start to grow in size to some extent depending on the degree of supersaturation in the solution (Coupland 2002; Lawler & Dimick, 2002; Sato *et al.*, 1989; Toro-Vazquez *et al.*, 2005). Thermodynamically, energy must be released, i.e., latent heat, from the aggregating molecules in order for a nucleus to reach a more stable state relative to the surroundings. However, surface tension at the solid-liquid introduces

a hindering force to the nucleation process. Nucleation is hence possible only when the total energy of crystallization of the nucleus exceeds the surface tension energy (Lawler & Dimick, 2002). In order for a nucleus to survive and consequently grow, its size must be above a critical radius where the activation free energy is lowered assuming that the substance is pure and the nucleation is homogenous (Marangoni & Narine, 2002). In addition, the interaction forces between TAG molecules in a nucleus must overcome the kinetic energy of the molecules in the melt generated by their Brownian movement; the latter effect is evident when shear flow is applied (Marangoni, 2005a).

In TAGs there are three types of nucleation that can take place. In the absence of impurities, fat molecules undergo homogeneous nucleation if they are substantially undercooled, since there are no foreign particles that would induce the aggregation of the molecules. On the other hand, heterogeneous nucleation takes place in systems that contain impurities (Phipps, 1964). TAGs almost always undergo heterogeneous nucleation since they contain preexisting foreign particle surfaces (Garti & Sato, 2001; Ghotra *et al.*, 2002). Even under homogeneous nucleation, the nuclei that have formed will act as impurities for further nucleation. There are types of impurities, such as diglycerides, that hinder the nucleation process if they are incorporated in the growing nuclei (McClements, 2005). Heterogeneous and homogeneous nucleation mechanisms are referred to as primary nucleation mechanisms. Crystals formed in primary nucleation may fracture, forming stable nuclei larger than the critical size. If the fragments are smaller they will re-dissolve in the liquid (Boistelle, 1988). Once the crystals have formed, they will start to grow by incorporating more molecules from the mother phase into the solid-liquid interface. During crystal growth, the incorporation of the growth

units onto the surface of the crystal depends greatly on the driving force or supercooling (Hartel, 2001). The growth rate increases with supercooling and is reduced by the viscosity of the melt as the diffusion of a molecule, i.e., mass transfer, is retarded (Timms, 1991). If the crystal grows slowly, the molecules will incorporate into the most energetically favourable sites, whereas if it grows rapidly, the incorporation will be favoured into less energetically favourable sites. Kinetically, under high supercooling, the least stable crystalline phase will form due to the lack of time for the growing units to optimally reorient themselves before incorporation takes place. Under low supercooling, however, more stable phases are more likely to form as that there will be more time for the molecules to rearrange themselves to the optimal configuration of the surface sites (Sato, 2001c). Further details about lipid nucleation and growth, including mechanism and theories, can be found in Garti and Sato (Garti & Sato, 1988, 2001), as well as in Widlak *et al.* (2000).

1.3   Polymorphism

More than a hundred and fifty years ago, the presence of different melting points in lipid materials was first explained by Duffy as polymorphism (Duffy, 1853). But it was not clearly understood until the 1930s, when Clarkson and co-worker (Clarkson & Malkin, 1934) clearly explained this phenomenon using X-ray diffraction experiments with pure TAGs. They proved that the presence of multiple melting points could be attributed to the fact that different crystalline nanostructures, having different diffraction patterns, were formed. Although the contribution of Clarkson was a pioneering step in

understanding fat polymorphism from the molecular basis, it created a lot of confusion in the literature. Ten years after Clarkson's demonstration, Edwin Lutton and others, whose work has been almost always referenced in the literature, came to clear up and correct some of the misunderstandings in Clarkson's work, such as the inconsistency in the nomenclature of different polymorphs (Lutton, 1945). Most of the literature now, however, uses the TAG nomenclature scheme adopted by Larsson (Larsson, 1966). Larsson in his studies saw that the nomenclature used by Lutton using short spacing lines in XRD patterns was convenient, yet incomplete, as some of the alternative chain packing had not been taken into account (Larsson, 1966). This step was important in uniting the variations in the nomenclature schemes used by different researchers and thus made it easy to characterize the crystalline properties of fats in different industrial applications.

Literally, the word "polymorphism" has a Greek origin composed of two parts; "poly" and "morphos" meaning "many" and "shapes", respectively. Chemically, polymorphism is a term usually referred to as the ability of a material to form different crystalline lattice structures of conformation and molecular packing under different conditions from the same chemical composition. TAGs can have different crystalline structures, or polymorphs, depending on the hydrocarbon chain packing and their angle of tilt. According to the studies conducted by Larsson, the polymorphic forms found in lipids can generally be classified into three main forms, α, β' and β based on the short spacing in the X-ray diffraction patterns. The α form is characterized by a single strong peak in the X-ray diffraction patterns near 0.42 nm. The β' form has usually four clear peaks (sometimes a few smaller ones), of which the stronger two peaks are near 0.38 and 0.42 nm. The β form exhibits many diffraction peaks, of which the three strongest peaks

appear around 0.46, 0.38 and 0.39 nm, respectively (Takeuchi *et al.*, 2003). As an example, Figure 1-3 shows a time resolved synchrotron wide angle X-ray diffraction pattern corresponding to different polymorphic modifications for a TAG binary mixture composed of 60% trilaurin and 40% tripalmitin by mass (Takeuchi *et al.*, 2003).
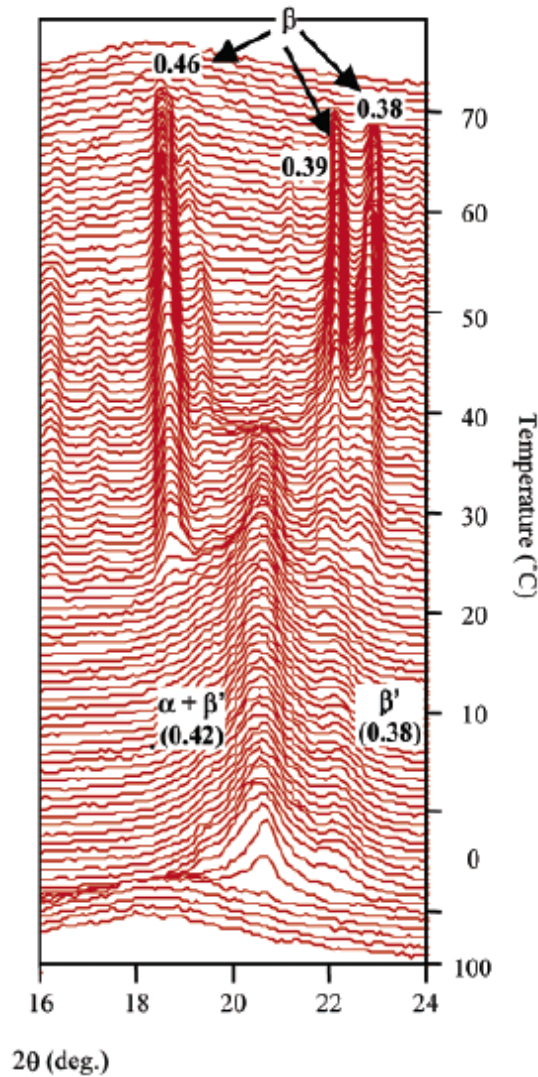
Figure 1-3: Time-resolved synchrotron X-ray diffraction pattern for 60% trilaurin and 40% tripalmitin by weight, where θ is the angle between the incident ray and the scattering planes according to Bragg's law, nλ=2dsin θ (where *n* is an integer, λ is the wavelength of X-rays, *d* is the spacing between the planes in the atomic lattice in nm) (Takeuchi *et al.*, 2003). (Permission has been obtained by ACS).

Lipid polymorphs can be classified using the concept of the chain packing sub-cell. A sub-cell unit is the smallest repetitive unit along the hydrocarbon chain axes within the unit cell. The arrangement of an ethylene group with another within the hydrocarbon chain, as a result of van der Waals interaction forces, in the crystal lattice of a polymorph gives rise to a 3D entity. Lipids usually show three main sub-cell structures, which are the hexagonal (α), triclinic (β or $T_{//}$) and orthorhombic perpendicular (β' or $O\perp$) (Chapman, 1962). A representation of the unit cell and the sub-cell structure of a TAG is shown in Figure 1-4.
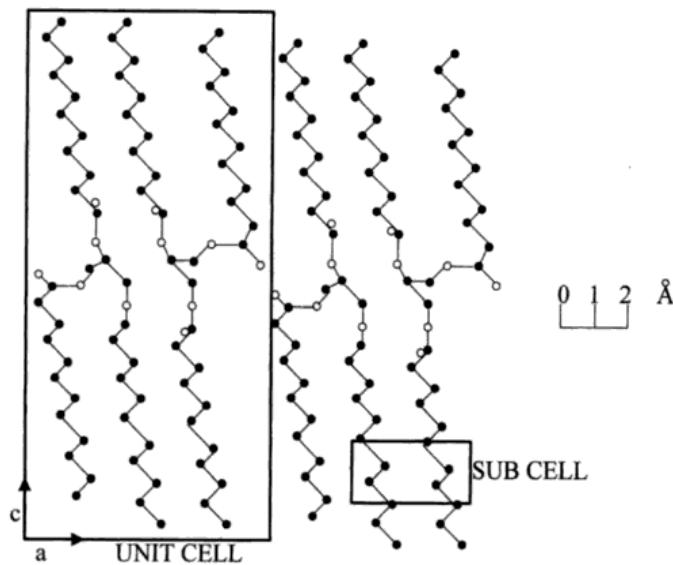
Figure 1-4: A depiction of the unit cell and the sub-cell of a TAG (Marangoni, 2005b). (Permission has been granted by Marcel Dekkar).

Moreover, the different geometrical arrangements of the different sub-cell structures directly affect the packing pattern each polymorph possesses in the unit cell. For instance, in the hexagonal sub-cell structure, the hydrocarbon chains are randomly oriented and have the ability to rotate about their long axis resulting in the formation of a loose packed unit cell. On the other hand, in the case of triclinic structures, there is only

one ethylene group per sub-cell and all zig-zag chains are parallel with respect to each other, giving rise to the most tightly packed structure. The possible geometric arrangements of the different sub-cell structures are depicted in Figure 1-5.
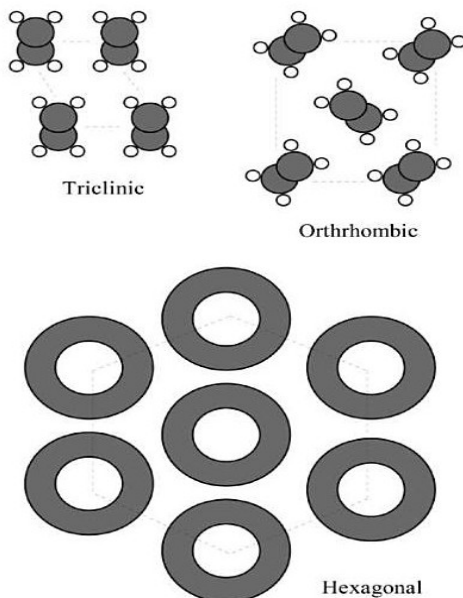
Figure 1-5: A TAG geometric packing arrangement for ethylene groups within the long hydrocarbon chain in a fatty acid (Marangoni, 2005b). (Permission has been granted by Marcel Dekkar).

TAG molecules tend to adopt the most suitable and stable sub-cell conformation and arrangement to accomplish the most efficient close-packing. This process is significantly influenced by the fatty acid make up: saturated or unsaturated, *cis-* or *trans* double bonds, odd or even number of ethyl chain carbons, stereochemistry and length of the hydrocarbon chain, as well as the purity of the lipid and the crystallization conditions (temperature, shear, rate of cooling, the presence of seeds, solvent) (Marangoni, 2005a). Other factors are the dipole-dipole interactions of the glycerol groups and the methyl end stacking (Sato, 2001b).

Usually, TAGs can be formed in either a double or triple chain structure and sometimes in quarto- and hexa- chain packing in asymmetric diacid TAGs as shown in Figure 1-6 (Sato, 2001a). TAGs tend to crystallize in a double chain length structure when the chemical properties of the fatty acids moieties are the same or very similar whereas a triple structure is formed when the fatty acid make up of a TAG is different. It was suggested by Lutton (1950) that a double chain packing structure is produced when the fatty acids of a TAG differ by two carbons in length.

hexa

double   triple   quatro
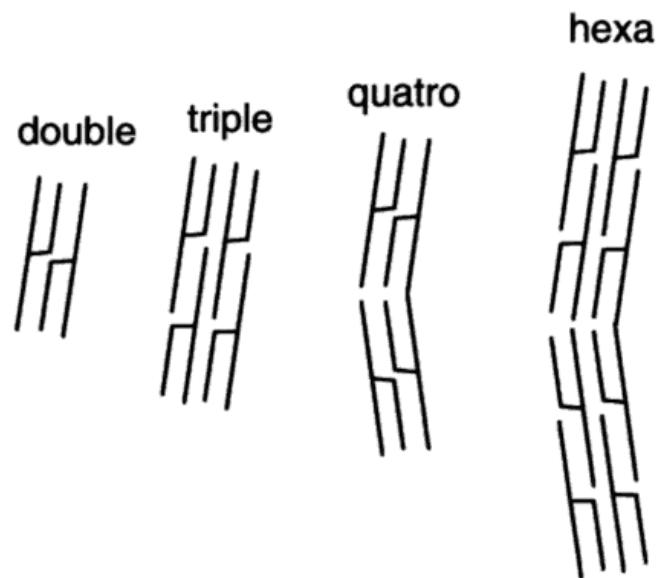
Figure 1-6: Typical chain length structures of TAGs. (Widlak *et al.*, 2001). (Permission has been granted by AOCS).

Two types of polymorphism occur generally in lipids: enantiotropic and monotropic. Crystalline forms are considered to be enantiotropic when they are thermodynamically stable in their respective ranges of temperature and pressure, so the transition from one form to another takes place at certain temperatures. Conversely, if the most thermodynamically stable form is produced when the surrounding parameters (temperature, pressure) change, this form is said to be monotropic (Hartel, 2001; Himawan *et al.*, 2006; Lavigne *et al.*, 1993). TAGs exhibit monotropic polymorphism

where the most stable crystalline modifications are sequentially and irreversibly formed from the unstable ones when given sufficient time. This transformation irreversibly takes place from α to β' to β in the order of increasing stability and reversibly from the melt as shown in Figure 1-7.
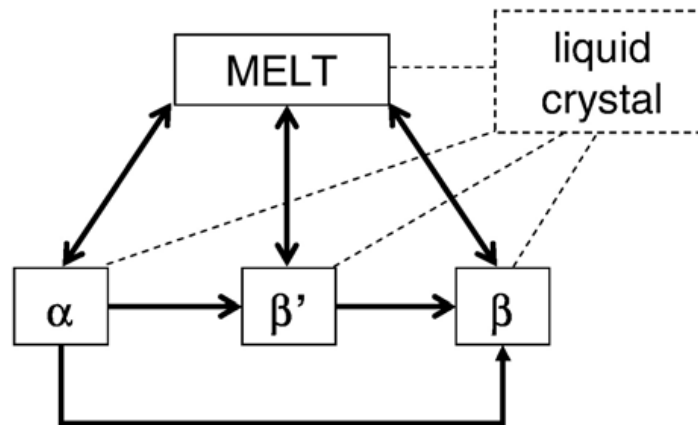
Figure 1-7: The monotropic transformation dynamics from the least to the most stable form in TAGs (Himawan *et al.*, 2006). (Permission has been granted by Elsevier).

The transformation process from the unstable to stable phases can be attained by a slight increase in temperature above the melting point of the less stable one in a process called melt-mediated crystallization, typically used in the tempering process of chocolate and other fat-based food products. In this process, less stable forms are melted leaving only more stable forms to solidify. In addition, transformation to a more stable phase can also sometimes be achieved without melting during solid-solid phase transition, which takes more time than the melt-mediated transformation and below the melting points of all the polymorphs involved (Sato & Ueno, 2005). Typically, the least stable forms crystallize first under strong supercooling or, in other words, when relatively faster cooling rates are applied, usually 10 °C/min or more (Himawan *et al.*, 2006; Metin &

Hartel, 2005). The duration of transformation from one form to another is dependent on the length of the fatty acid chain and is rapid with TAGs having shorter fatty acids (Metin & Hartel, 2005). As mentioned earlier, most of the lipid crystalline forms will eventually transform into the most stable modification, β. However, in some lipids as in some mixed acid TAGs, the β' polymorph is stable enough so that no β polymorph will form in any reasonable timescale.

At the melting point it takes a very long time for the hydrocarbon chains to align and form a stable nucleus and thus a crystal. However, when a fat melt is cooled well under its melting point, a stronger driving force for nucleation is created, which is proportional to some function of the undercooling. Subsequently, the system will try to relieve the imposed supersaturation by forming a crystal to achieve a state in which the Gibbs free energy is minimized. The α polymorph can therefore crystallize readily as its free energy of nucleation ΔG^* (energy barrier) is lower than the other polymorphs, even though its free energy of formation, ΔG_f, is smaller than that for the more stable polymorphs. Figure 1-8 is a schematic that shows the kinetic energy of nucleation, ΔG^*, and of formation, ΔG_f between the melt and the crystalline forms, for each polymorph from α to β' to β in the order of increasing stability (Larger. ΔG_f) (Himawan *et al.*, 2006; Marangoni, 2005b; Sato & Garti, 1988).
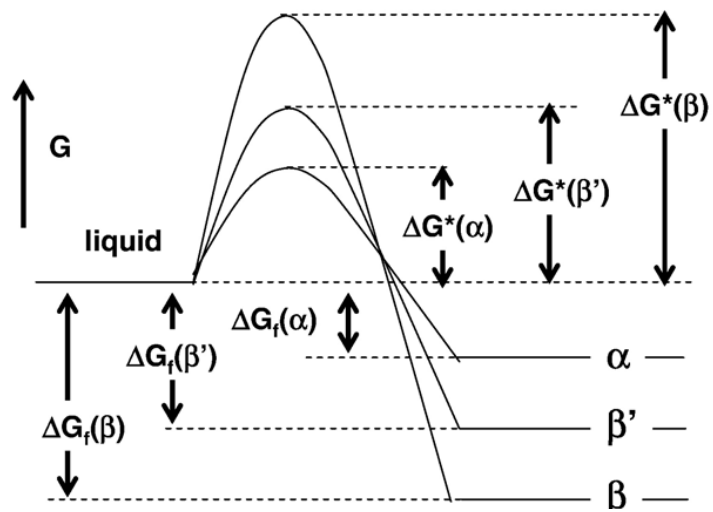
Figure 1-8: A depiction of the kinetic energy of formation for each polymorph (Himawan *et al.*, 2006). (Permission has been granted by Elsevier).

1.4 Thermal characterization and identification of lipid crystalline phases

Precise knowledge of the thermal behaviour of lipids is a prerequisite to understand the crystallization process in lipid-based foods. However thermal characterization of lipids is a complex and challenging task due to the great variety of TAGs, which may differ by the length of hydrocarbon chain, the degree of unsaturation and the position of the hydrocarbon chains on the glycerol backbone, not to mention their polymorphic state. For example, the presence of double bonds in unsaturated TAGs causes disrupted packing in the aliphatic chain which it turn lowers the melting point (Himawan *et al.*, 2006). For this reason, pure TAGs and their binary mixtures have intensively been studied as a first step to approach more complex systems in the future.

1.4.1 Heat of fusion (enthalpy) and melting points of pure TAGs and their mixtures

Melting temperatures T_m and enthalpy values ΔH_m of pure TAGs are essential for the thermodynamic description of solid-liquid equilibria in multi component fat systems, thus careful measurement is required. The different lipid polymorphic phases are characterised by their distinct enthalpy values and melting temperatures, which increase from the α form, through β' until β. This is directly attributed to the packing arrangement of TAG molecules. The least packed are in the α form and the tightest in β form. Precise measurements of the T_m of each specific crystalline phase is necessary to define the driving force required to induce the crystallization of that phase and ultimately define effectively its phase diagrams (MacNaughtan *et al.*, 2006; Metin & Hartel, 2005; Ueno *et al.*, 1997). When two TAGs are mixed, usually the T_m of the binary mixture is lower than

15

the T_m of the high melting point material and higher than the T_m of the low melting point material (Metin & Hartel, 2005; Takeuchi *et al.*, 2002). An example of this is shown in the study on the phase behaviour of three types of binary mixtures of saturated monoacid TAGs. Trilaurin/trimyristin (LLL/MMM), trilaurin/tripalmitin (LLL/PPP) and trilaurin/tristearin (LLL/SSS) were examined by Takeuchi *et al.* (2003) and the T_m of each binary mixture was determined by observing the phase melting in the SAXS (001) reflection spectra, when a sample rapidly cooled from the melt (100 °C/min) was subsequently heated (5 °C/min). Table 1-1 shows the T_m of each polymorphic phase for the pure TAGs used in this study. Generally, the melting points increase with increasing carbon number (Takeuchi *et al.*, 2003).

Table 1-1: Melting point and carbon number (C_n) of the fatty acid chain of the three polymorphic forms for trilaurin LLL, trimyristin MMM, tristearin SSS and tripalmitin PPP (Takeuchi *et al.*, 2003).

		melting point (°C)		
TAG	C_n	α	β'	β
LLL	12	15	35	46.5
MMM	14	33	46.5	57
PPP	16	44.7	56.6	66.4
SSS	18	54.9	64	73.1

Many of these TAGs, however, exhibit more than one β or β' polymorphic sub-forms. In some cases, the solid solution of two TAGs has a sub-form that is different from the one formed by the pure components alone. In the case of natural fats, there are no precise melting points, since they are multicompnent mixtures. Values are often given as the temperatures of the highest melting component, since natural fats are composed of a wide range of TAGs with different T_m (Timms, 1985). Different methods for the determination

16

of the melting points of natural fats have been summarized in the literature (deMan *et al.*, 1983; Wesdorp *et al.*, 2005). It seems that the first attempt to predict the melting points of different polymorphic forms of even and odd TAGs was carried out by Lutton and Fehl (1970). They found that odd TAGs resemble the even ones in showing three polymorphic modifications. They also found that the β form is the most stable form except for TAGs with n= 9 to 11 where β' is the most stable polymorph. Moreover, in the same work, the melting points of α and β' forms as a function of chain length showed smooth curves, which was ascribed to the similar packing of methyl group for odd and even TAGs. The β polymorphs of odd and even TAGs, on the other hand, show some alternations in the melting points which is attributed to differences in methyl group packing.

Thermal studies of monoacid TAGs have been extensively conducted using thermal techniques. Among these techniques, differential scanning calorimetry (DSC) has been the most used method in oil and fat characterization to determine melting and crystallization profiles, heats of transition, phase diagrams and even solid fat content. DSC is known for its sensitivity, and rapid and reproducible measurements are usually obtained, however careful interpretation is paramount. Several peaks, which reflect the presence of different thermal transitions, are observed upon heating or cooling of samples when calorimetry is used in the thermal investigation of fats (Keller *et al.*, 1996). When different cooling and heating rates are employed, different phase transition behaviours will readily be observed on DSC traces (Hagemann, 1988). The thermal behaviour of saturated mono acid triglycerides can typically be described by the heating and cooling curves of tristearin. In the work of Hagemann (1988), a single exotherm (crystallization) and an endotherm (melting) of the α form were observed when tristearin was cooled

very rapidly from the melt and reheated very rapidly. Soon after the melting of the α form upon heating, an exotherm appeared immediately as a consequence of the rearrangement of the α to β in a melt-mediated crystallization process. The β form was then melted when heating continued (Hagemann, 1988). A study was conducted to investigate the effect of using different cooling rates on the phase transition behaviour of a binary mixture of PPP and SSS using DSC, together with light microscopy and X-ray Diffraction (XRD) (Himawan *et al.*, 2007). The β and β' polymorphs were observed at cooling rates of 0.5 ºC/min and less, and α at higher cooling rates. Moreover, DSC cooling traces showed that two exothermic peaks appeared when mixtures containing more than 30% SSS were tested which correspond to the crystallization of α and β' forms when cooled at 0.5ºC/min. When cooling rates of 1 K/min or higher were employed, two exothermic peaks were observed corresponding to two α phases; likely one rich in PPP and the other rich with SSS. DSC has shown to be the most convenient method for determining the temperatures of the phase boundaries when two pure TAGs are mixed together. DSC has also been used to determine solid-liquid ratios in fats, although this application can be very limited by the uncertainty of the phases present (Biliaderis, 1983).

The enthalpy of fusion of the most stable polymorphic forms of different TAGs, saturated and unsaturated, was reviewed up to the year 1976 by Timms (1978). He indicated that the values obtained in his labs were in an excellent agreement with previously published data (Hagemann & Tallent, 1972; Hampson & Rothbart, 1969) when comparisons were possible. In addition, Timms rejected some values reported earlier as they were clearly high or low. Timms presented a method for the prediction of

heat of fusion of most of the glycerides that are of commercial and scientific interest, taking into account structural variations such as the presence of *cis* and *trans* double bonds, or mixed acid TAGs (Timms, 1978). Table 1-2 shows the heat of fusion of some mono acid saturated TAGs produced by Timms, where one can see that the molar heat of fusion of increases linearly with the carbon number.

Table 1-2: Heat of fusion of some mono acid saturated TAGs (Timms, 1978).

TAG	ΔHf (kJ/mol)
LLL	123.43
MMM	147.95
PPP	171.38
SSS	196.48

Most of the reported data are for the enthalpy of fusion of the most stable β form since Timms' work was concerned with mono acid TAGs (Hagemann & Rothfus, 1983; Ollivon & Perron, 1982). Many attempts have been carried out to find the best correlations for three polymorphic modifications of mono acid TAGs since Timms. Perron performed the most extensive work in predicting the enthalpy values using these correlations (Perron, 1984):

ΔH_f for α= 2.5*n-27.5 kJ/mol

ΔH_f for β'= 3.84*n-19.2 kJ/mol

ΔH_f for β= 4.20*n-29.92 kJ/mol

where n represents the carbon number. Different existing models for predicting the enthalpy of fusion and melting points of saturated TAGs have been reviewed in detail (Zéberg-Mikkelsen & Stenby, 1999). A more comprehensive and advanced model was

proposed by Wesdrorp *et al.* (2005) who developed a predictive method, the group contribution method, to find the enthalpy and melting points of saturated TAGs for different polymorphs as a function of carbon number and the position and chain length of the three acyl groups in TAG. Wesdorp compiled an excellent data collection from literature and the database of Unilever Research labs (Vlaardingen, Netherlands) resulted in 152 values of the enthalpy of fusion and 944 melting points for saturated and unsaturated TAGs for different polymorphic forms (Wesdorp *et al.*, 2005).

1.4.2 Heat capacity of pure TAGs and oils:

Heat capacity is one of the basic thermophysical and thermodynamic properties that characterizes the physical state of a material. It is an essential parameter for the calculation of thermodynamic functions. The knowledge of heat capacity is also needed in establishing energy balances, obtaining enthalpy and entropy values and evaluating the temperature effect on phase equilibria. It, therefore, serves as a sensitive indicator of any structural changes that happen to the material during phase transitions. Heat capacity is regarded as the most fundamental of all thermal properties since it is determined by the strength of intermolecular interactions, phase stability, thermal conductivity and energy storage capacity (White, 1999). Generally, the specific heat capacity of TAGs increases as a function of unsaturation, both in the solid and liquid states (Santos *et al.*, 2005). The numerical values for the heat capacities in the liquid state are often twice as large as those for the solid state (Morad *et al.*, 2000). The α form has larger values than the β form, due to higher freedom in mobility of the molecules. This freedom is highest in α and lowest in the β form (Santos *et al.*, 2005). Moreover, heat capacity values are important for the

fat industry to be used as a tool to distinguish between different polymorphic forms at low temperature ranges; and to be used for engineering and designing purposes for processes like deep-frying and hydrogenation at higher temperature ranges. DSC has been the most used instrument to measure the heat capacity values for TAGs and lipid materials.

1.4.3   The use of DSC to obtain heat capacity of TAGs and oils:

The heat capacity values of pure TAGs in their different crystalline phases and in the liquid state, vegetable oils, fish oils and innumerable food materials have been determined using, almost always, DSC (Hampson & Rothbart, 1983; Matovic *et al.*, 2005; Morad *et al.*, 1995a, 1995b; Morad *et al.*, 2000; Santos *et al.*, 2005; Simpson *et al.*, 1984; van Miltenburg *et al.*, 2003). Occasionally, other techniques such as adiabatic calorimetry and microwave oven have also been used (Matovic *et al.*, 2005; Santos *et al.*, 2005). Charbonnet and Sigleton (1947) measured the heat capacity values of the α and β forms of trimyristin, tripalmitin and tristearin and the β form of trilaurin as these phases are sufficiently stable at room temperature. They used a copper calorimeter enclosed in a semi-adiabatic calorimetric system and all temperatures were measured using a single-junction thermocouple. A plot of the heat capacity values vs. temperature from 200 to 300 K for SSS and MMM suggested the possibility of a polymorphic change, as the slope of the specific heat changed (Charbonnet & Singleton, 1947). In 1983, Hampson and Rothbart argued that the work of Charbonnet lacked accuracy in determining the purity of the materials used since gas liquid chromatography and thin layer chromatography were not available then and the specific heat values for intermediate polymorphs such as β' and α form for LLL were not shown. In the work of Hampson and Rothbart, a Perkin-

Elmer DSC was used to measure the heat capacity values. The α forms of LLL, MMM, PPP and SSS were obtained by quenching the melt to 180 K with addition of liquid nitrogen. It was possible to obtain the β' forms by quenching the melt to 2 to 5 K above the T_m of the α form and then maintaining the sample at that temperature until crystallization was achieved followed by quenching to 180 K, (Hampson & Rothbart, 1983). During any phase change, melting or recrystallization, a peak was produced and measuring the heat capacity values of the phases was not possible. At 190 K the specific heat values for tristearin were very close to each other for the three forms whereas the heat capacity for the α forms increased dramatically over that of the β forms at 210 K. Figure 1-9 shows the heat capacity values in the liquid and in different crystalline phases for LLL and MMM investigated.
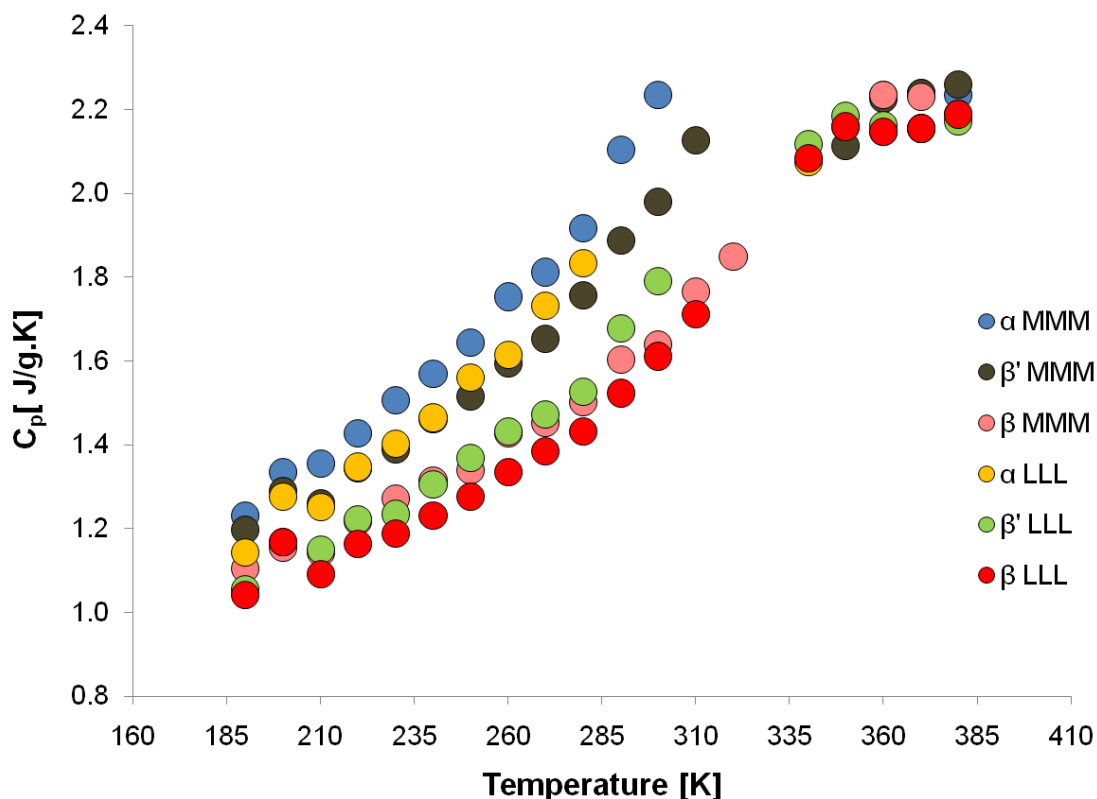
Figure 1-9: C_p values vs. temperature in the liquid state and in different crystalline polymorphs for trilaurin and trimyristin (Hampson & Rothbart, 1983).

All the heat capacity values were obtained according to the recommended procedure of Oneill (1966). This method, which is very frequently used to obtain heat capacity values from calorimetric techniques, is based on the idea that the heat flow rate measured from a sample is proportional to its instantaneous specific heat when the sample is subjected to a temperature ramp. The method essentially records three signals; the heat flow rate into an empty crucible, the heat flow signal into a standard material with known heat capacity values, and the heat flow rate into the sample. All these signals are obtained under identical experimental conditions (Oneill, 1966). This method is sometimes known in the literature as the classical three step method (Hohne *et al.*, 2003).

Simpson *et al.* (1984) obtained the specific heat values for the α, two β' and β phases of trimargarin, $C_n=17$, and SSS in the temperature range from 190-350 K using a Perkin-Elmer DSC and Oneill's method. This method, however, does not seem to be applied in the work of Eiteman and Goodrum (1994) in which another Perkin-Elmer DSC (Model DSC-2C) was used to obtain the heat capacity values of liquid tricaproin, tricaprylin and tricaprin with carbon numbers of 6, 8 and 10, respectively, and their binary mixtures. It was clearly shown that heat capacity values increased with increasing proportions of tricaprylin in the three binary mixtures made by combining tricaproin and trycaprlyin, C6:C8. Also for binary mixtures made by combining tricaprion with tricaprin, C6:C10, at different proportions, the heat capacity values followed the same behaviour as observed C6:C8 binary mixtures. However the absolute numbers were much larger in the case of C6:C10. This indicates that the heat capacity values in TAGs increase with increasing carbon number and with increasing proportions of the high carbon number TAG when they are mixed. The excess heat capacities for C6:C8 and C6:C10 binary mixtures were plotted as a function of varying mole fraction at 325 and 373 K. The excess heat capacity is a good measure of the non-ideality of the mixtures, if one assumes that they had formed only one phase of a homogeneus solid solution. It was observed that C6:C10 behaved as an ideal solution whereas C6:C8 exhibited significant departure from ideality by about 4% (Eiteman & Goodrum, 1994).

There has been no other work in the literature reporting the heat capacity values of TAG binary mixtures in their different crystalline modifications. This study will be the first work to find the heat capacity values of different crystalline phases made by varying proportions of LLL and MMM under non-isothermal conditions.

Morad *et al.* (1995b) measured the heat capacity values of four simple TAGs including LLL, MMM, PPP and SSS and four mixed TAGs including 1,2-dimyristoyl-3-oleoyl (MMO), 1,2-dimyristoyl-3-palmitoyl (MMP), 1,2-dipalmitoyl-3-oleoyl (PPO) and 1,2-dioleoyl- 3-palmitoyl (OOP) measured using a Seiko DSC 220 heat-flux instrument. They measured the C_p of the liquid state and then compared it with the literature values reported before their study and with optimal experimental methods reported earlier by the same authors (Morad *et al.*, 1995a). The heat capacity values were obtained between the melting point of each TAG and 523 K using the Round Robin Method (RRM). In this method the measurements are taken using different instruments from different operators and subsequently averaged. It was concluded in this study that the relationship between the heat capacity values of liquid TAGs and temperature can be described as a straight line from 50 to 150 °C. Also, the values reported by Charbonnet and Singleton (1947) from their experimental data, whose reliability was argued later on by Hampson and Rothbar (1983), agreed well with Morad's results for simple TAGs. Moreover, Morad *et al.* (1995b) found that the estimated heat capacity values by Phillips and Mattamal (1976) compared well to their experimental results. Furthermore, it was found that it was satisfactory to use DSC as a tool to measure heat capacity values, as long as the optimum experimental conditions, such a sample mass and heating rate, are determined in advance. In another work of Morad *et al.* (1995a), the optimum experimental conditions to obtain reproducible heat capacity values were determined using a heat-flux DSC instrument with liquid trilaurin as a sample in a temperature range from 50 to 150 °C. These parameters were found to be a heating rate of 17 °C/min, a sample mass of 21 mg and a nitrogen purge flow rate of 50 mL/min. Reproducible values of heat capacity of TAGs

were obtained within a precision of ±1%. However, the accuracy of the values was not discussed in this study.

1.4.4   The use of MDSC to obtain heat capacity of TAGs and oils:

Although DSC has been a successful technique in the calorimetric field for more than 40 years, it still has some limitations resulting in misinterpretation of the data. One of those intrinsic limitations is that DSC measures the sum heat flow rate from overlapping thermal events, which makes the quantitative analysis difficult, depending on the number of simultaneous events. Even in the simplest case of indium, melting of a pure metal element that does not exhibit polymorphism, there are three events happening during the melting.

These events are the heating of the solid remaining ($C_{p\,soild} \cdot \dfrac{dT}{dt} \cdot m_{solid}$), the heating of the liquid being formed ($C_{p\,liquid} \cdot \dfrac{dT}{dt} \cdot m_{liquid}$) and the delivery of heat of fusion ($\Delta H_f \cdot \dfrac{dm_{solid}}{dt}$), where $\dfrac{dT}{dt}$ and m represent the temperature ramp and the sample mass, respectively. Fortunately, the magnitude of the C_p terms is often small compared to ΔH_f. Thus, small errors in the estimate of the "baseline" under the melting peak are not too large with respect to the enthalpy measured, especially if a sigmoidal type of "baseline" is chosen. To further complicate matters, many materials exhibit a surface melting temperature that is lower than the bulk, and the DSC instruments are sensitive enough to pick up this signal.

More important for this work, the heat flux DSC used in this study lacks the ability to measure accurate C_p values at any given time or temperature throughout an experiment. However, the manufacturer contends that it can do it.

Even though it would seem logical to expect that $C_p = \dot{q}/(m_s \frac{dT}{dt})$ where $\dot{q}$ is the heat flow rate (per unit mass) at a given time or temperature, this is not the case. The value of $\dot{q}$ is altered by other thermal resistances and capacitances present in the instrument itself and between the instrument, the sample container and the sample. Even the sample positioning can change the ratio of these resistances. Thus it is not straightforward to estimate accurate C_p values directly from a single experimental measurement.

Modulated differential scanning calorimetry MDSC® has been claimed (the literature says "proven") to be an effective tool to overcome these drawbacks due to its high sensitivity and resolution and its ability to compute the specific heat capacity values at any given temperature or time throughout an experiment (Reading & Hourston, 2006). With the MDSC® technique, the temperature profile is produced when two simultaneous heating rates are applied to a sample: a linear heating rate as in DSC and a sinusoidal (modulated) heating rate (Reading & Hourston, 2006). Whether we have a single changing signal applied, or two is, however, a matter of interpretation. The strength of MDSC® is purportedly in it is ability to separate between temperature dependent and non-dependent thermal events that occur simultaneously. With the use of an oscillating temperature ramp, it is supposedly possible to produce two independent heat flow responses. The temperature-dependent heat flow response is used to obtain C_p values

(known as reversing C_p), whereas the other response C_p values associated with the change in the kinetics (known as non-reversing C_p), such as a first order phase transition.

In fact, the decomposition capability of MDSC$^®$ needs a closer look and requires more clarification. In the literature the conventional heating rate in the modulation signal is repeatedly described, or interchangeably defined, as the average heating rate from the sinusoidal profile (Hutchinson, 1998; Tomasi *et al.*, 1996; Van Durme *et al.*, 2004; Xie *et al.*, 2010; Zhao *et al.*, 2010). One may ask if there are actually two independent temperature ramps applied simultaneously or just one particular profile that is easier to describe mathematically as the sum of two functions. The importance of the distinctions lies on whether the information obtained represent two separate phenomena, or is an artefact of the mathematical decomposition.

Figure 1-10 shows, as an illustration, the modulated temperature signal and the corresponding reversing and non-reversing heat flow responses for a polyethylene terephthalate PET sample (Thomas, 2005).

The benefits of MDSC$^®$ over conventional DSC and its applicability and effectiveness to obtain absolute values has been argued and debated in the literature. The main dispute is on the use of modulation amplitude and the resultant heat flow. Verdonck *et al.* (1999) concluded that the MDSC$^®$ enables the separation of any overlapping phase transitions and computes the thermal conductivity of insulated materials; however MDSC$^®$ should not be used as a replacement for conventional DSC when investigating an unknown material (Verdonck *et al.*, 1999). Cao *et al.* (1997), however, indicated that MDSC$^®$ is incapable of determining C_p values, contradicting the work of Wunderlich *et al.* (1994) who concluded that the C_p of a material can be directly measured by MDSC$^®$.

In 2007, Cao came to the conclusion that the ability to separate the reversing and non-reversing heat flow signals is artificial. He also noted that terms like "reversing" and "non-reversing" are misleading; and the frequency used in modulation does not mean the frequency of crystal lattice vibration occurring in the sample (Cao, 2007), and therefore is not probing directly such lattices. The debate remains open, even if a large body of authors who use MDSC choose to ignore it in their publications.
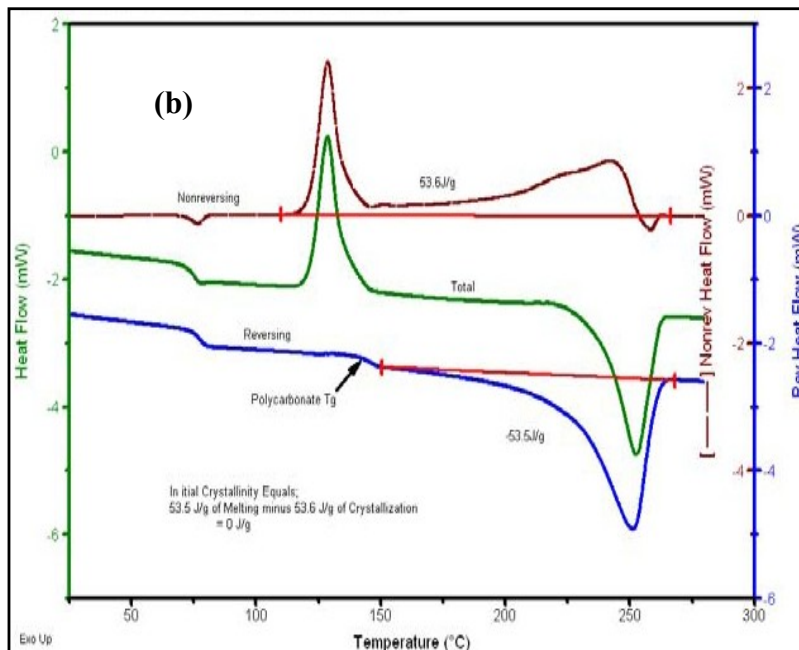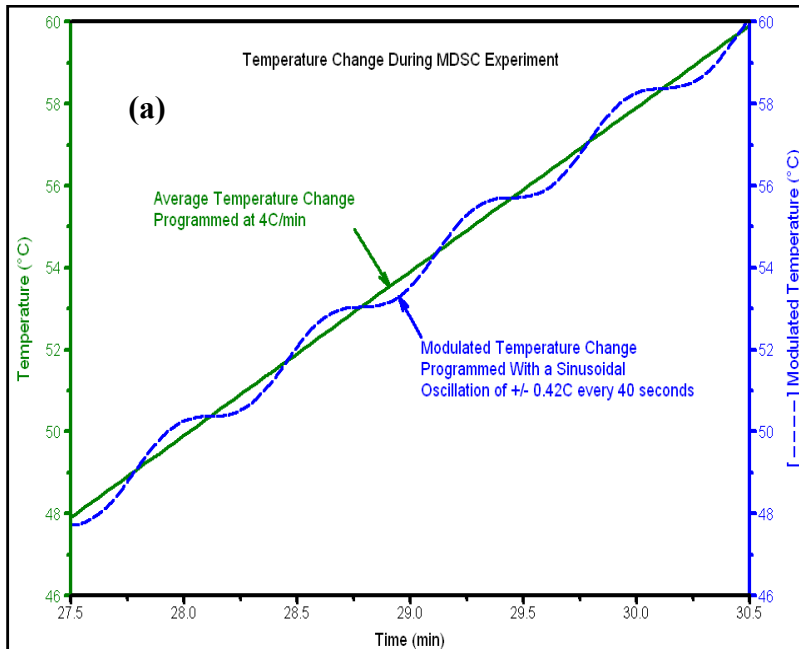
Figure 1-10: (a) temperature modulated signal and the average temperature ramp, and (b) the resultant heat flow signals (reversing, non-reversing and the total heat flow) from using the modulated temperature ramp (Thomas, 2005).

Under the benefit of the doubt, MDSC® was explored in this thesis. In order to get best quality data, optimum experimental conditions or parameters should be selected. MDSC® parameters include: modulation period, modulation amplitude and average heating rate. Modulation period is the time required for the modulated signal to complete one cycle represented as a sine wave superimposed onto the temperature ramp. Many circumstances should be considered in choosing the modulation period, such as the sample mass, thickness and thermal conductivity. The range of modulations periods provided by the typical DSC commercial instrument is from 10 to 200 s (Reading & Hourston, 2006). Modulation amplitude (±°C) is the sinusoidal change in temperature that is superimposed on the average temperature ramp. The typical commercial instrument allows a selection of modulation amplitudes from ±0.001 to ±10 °C; however not all of this range is practically possible. The reason is that when larger amplitude is applied (i.e. more than 3 °C) there will be a "smearing" of the transition signal and that, in turn, will decrease the resolution of the transition. Furthermore, if too large modulation amplitude is used, the linearity of the response will be significantly influenced leading to inaccurate data. On the other hand, using very low modulation amplitudes is not recommended because it gives poor sensitivity and decreased signal to noise. For that reason, the optimum modulation amplitude range has been suggested to be from ±0.1 °C to ±2 °C. For the average heating rate, it is important to be as fast as possible; however, slow enough to obtain the minimum number of modulation cycles over the desired transition, which is four cycles.

Most of the research published in the literature regarding the applications and uses of MDSC® is on polymers (Reading *et al.*, 1994; Wunderlich *et al.*, 1994), amorphous

lactose, polyethylene glycol glasses and glass–polymer composites but little work has been reported on lipid materials (Singh *et al.*, 1999). Singh *et al.* (1999a, 1999b) studied SSS as a model system to study the effectiveness of MDSC[®] and the impact of changing the operational parameters on the information obtained. They concluded that MDSC[®] techniques enabled the separation of the overlapping events in the melting of the α form and the crystallization of the β form during melting. It was also observed that cooling with modulation disturbed the crystallization process which in turn led to crystals with different nature. Accordingly, the option of turning off the modulation must be considered, thus defeating the purpose of using MDSC. It is worth noting that the usefulness of MDSC[®] to investigate lipid materials that exhibit polymorphism is then merely qualitative, since the "C_p values" obtained are influenced by different operational parameters used, i.e., are not the real C_p values of the material.

1.5 The use of the "Physical Properties Measurement System" PPMS[®]

A commercially available instrument from Quantum Design (CA, US), the physical property measuring system (PPMS), shown in Figure 1-11, is an important development in thermal instrumentations that allows for accurate determination of heat capacities of small samples (1-200 mg) in the temperature range of 0.4 – 400 K so long as the samples are stable enough to be prepared outside the instrument. The measurement principle is based on the determination of relaxation of the temperature following a heat pulse (Marriott *et al.*, 2006). Thus the instrument assumes that the thermal conductivity

of the sample is very high, and therefore the sample is isothermal. Other measurements that can be obtained with PPMS include thermal conductivity, electrical resistivity, DC magnetometry, AC susceptibitly, resistivity and magneto-resistance.

It was found that the accuracy of heat capacity determinations of sapphire and copper samples of ±1% or better was achieved in the temperature range from 100 to 300 K (Kennedy *et al.*, 2007). This was possible when solid samples were placed in intimate contact with the platform of the relaxation calorimeter Kennedy *et al.* (2007) and Lashley *et al.* (2003) showed that the accuracy of the heat capacity determination can be within 1% over the temperature range from 5 - 300 K and 5% over 0.7- 5 K. In the work of Kennedy *et al.*, it was mentioned that it is necessary to determine the heat capacity values for samples of different masses to obtain the highest degrees of certainties.

Kennedy *et al.* (2007) pointed out that sample size had a significant effect on the heat capacity values determined by PPMS for materials that are known to have low thermal conductivity. The results showed that poor thermal conductors can give precise but inaccurate results with PPMS since poor thermal conducting materials build up significant thermal relaxation within the sample.

Figure 1-11: Quantum Design, Inc. Physical Properties Measurements Systems, PPMS®
(http://www.qdusa.com/products/ppms.html)

It is necessary for the sample to have a good attachment to the sample platform in order to obtain accurate heat capacities. Usually a thin layer of thermal grease with good thermal conductivity between sample platform (puck) and sample is applied to enhance the thermal contact (Dachs & Bertoldi, 2005). It is crucial to apply the thermal grease (usually Apiezon N) as flat as possible to ensure optimal heat transfer since it was reported that having large amounts of Apiezon N grease produced heat capacity values several times lower than when lower amounts were used at low temperatures (Swenson, 1999). Figure 1-12 shows several pictures of the puck used in PPMS and a depiction of the chamber where the puck is installed.

(a)

PPMS Sample Chamber.
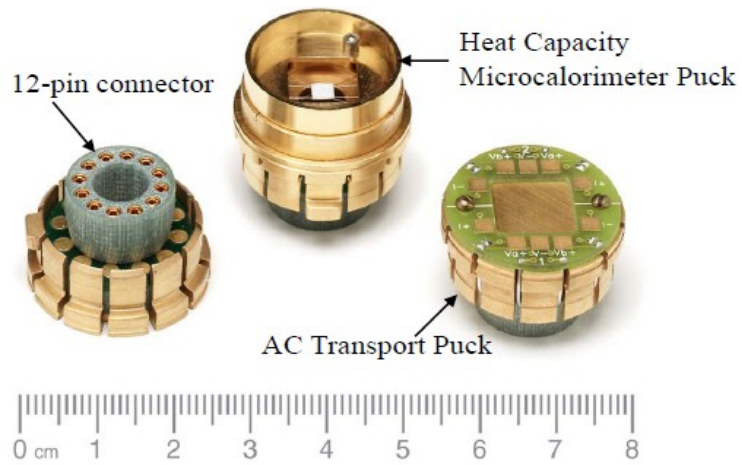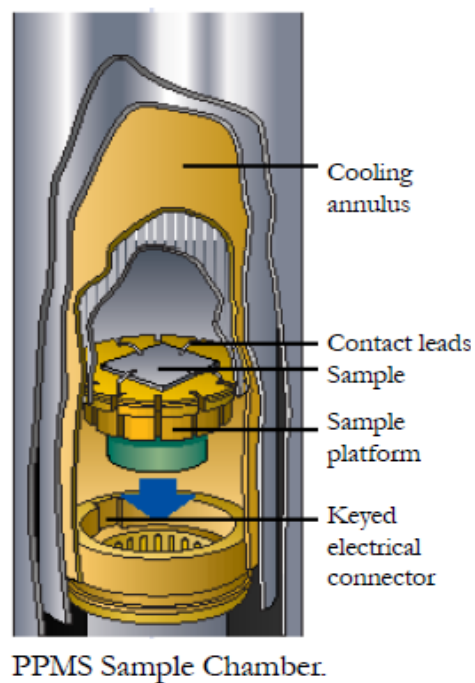
(b)

Figure 1-12: (a) PPMS puck, and (b) PPMS chamber with all its components (White & Johnson, 2009)

Measurements with PPMS calorimeters are done in three stages. In the first stage, the temperatures of the sample platform and puck are stabilized to a predefined temperature. The second stage is the application of a heat-pulse followed by the recording of the resulting temperature response of the platform (with and without the sample). The last stage is the analysis of the data to determine the heat capacity by applying a non-linear fitting technique (Dachs & Bertoldi, 2005). The heat capacity measurements obtained by PPMS are typically compared to those obtained by adiabatic calorimetry since the latter is an equilibrium technique and its results are most accurate, usually within 2% (Dachs & Bertoldi, 2005; Kennedy *et al.*, 2007; Van Oort & White, 1987).

Excellent heat capacity measurement agreement with adiabatic calorimetry results were obtained for a sample of corundum and fayalite in the form of single crystals, 10-50 mg, and powders, 48 mg, with reported relative uncertainty of 0.3 % for T>50 K and 0.5% T<50 K in the temperature range 5 to300 K. The relative uncertainties for sample powders contained in Al pans increased relatively, the precision was lower and the results were smaller than the adiabatic data by $1 - 2$ % (Dachs & Bertoldi, 2005).

There has been no work in the literature on the determination of heat capacity of TAG using PPMS. Therefore, the current work will be the first of its kind to obtain heat capacity values for LLL and MMM, and also to test the applicability of the instrument in measuring heat capacity for the samples under study.

1.6   The scope of the research

Studies of crystallization are usually limited to idealized conditions, in which external conditions are constant. In these conditions, the theoretical analysis is relatively simple and problems related to cooling rates and thermal gradients within the sample are avoided. In reality, though, external conditions change continuously. This makes the description of the crystallization process under non-isothermal conditions a big challenge. Nonetheless, the study of crystallization under these conditions is of great interest since crystallization in industrial processes takes place under such conditions.

TAGs represent an important class of materials for their wide application in food, cosmetic and lubrication industries. The crystallization of TAGs is heavily influenced by small differences in their composition, the processing conditions and subsequent storage environment. Industrial crystallization procedures to deliver adequate final properties are developed often in a semi empirical way. A better understanding of how the processing conditions affect the TAGs products can be obtained by mimicking these conditions in a smaller scale and in a controllable fashion in a laboratory setting. The investigation of these materials, however, is rather complicated due to their multi component nature and polymorphism. Therefore, investigating the crystallization behaviour, thermodynamics and kinetics of pure TAGs and their binary mixture is an inevitable necessary starting point.

This study seeks to investigate the thermal characteristics (heat capacity and enthalpy of crystallization) of two pure TAGs, trilaurin and trimyristin, and their binary mixtures when they are cooled statically (no shear) under different cooling rates by using differential scanning calorimetry (DSC), modulated DSC (MDSC), and thermal

relaxation (PPMS). The results of this study will be used to complement the findings of previous work done to identify the crystalline phases of the same materials under the same conditions using small-angle (SAXD) x- ray diffraction and wide-angle (WAXD) time resolved synchrotron radiation X-ray diffraction (SR-XRD).

In addition, an intensive and extensive amount of work has been put into understanding the DSC signal and how the measurements are produced. The heat capacity and enthalpy values obtained were critically investigated in relation to the experimental conditions in which they were obtained. This is important to differentiate between the values reflecting the actual sample behaviour and those caused by the instrument itself.

The long term purpose is to improve the prediction of the kinetic parameters under real processing conditions. This constitutes an important scientific and technological challenge in the field of crystallization of lipids.

1.6.1 Hypotheses and objectives

It is hypothesized that precise values of the enthalpy of crystallization of the pure TAGs and their binary mixtures can be measured using heat flux DSC, and with the use of these values the excess energy of mixing for mixed crystals can be estimated.

It is hypothesized that the heat capacity values of the crystalline phases formed by cooling two pure triglycerides (trilaurin and trimyristin) and their binary mixtures using seven cooling rates (20, 15, 10, 7.5, 5, 2.5, 2, 1 °C/min) can be determined using either heat flux DSC, MDSC$^{®}$ or PPMS. It is also hypothesized that the heat capacity values obtained can be correlated with the kinetic composition of the crystalline phases obtained at the end of cooling.

Chapter 2   EXPERIMENTAL METHODS

2.1   Materials

Samples of trilaurin (LLL) and trimyristin (MMM) were purchased from Fluka (Saint Louis, US) at purity levels ≥ 99%. The purity of these triglycerides was determined by gas chromatography (GC) and no further purification was performed. Three binary mixtures were prepared from LLL and MMM on a percentage weight by weight basis of LLL and MMM named 3L7M (30 % trilaurin, 70% trimyristin), 5L5M (50 % trilaurin, 50% trimyristin), and 7L3M (70 % trilaurin, 30% trimyristin).

2.2   Instruments and Methods

2.2.1   Differential Scanning Calorimetry (DSC)

2.2.1.1   The instrument

Differential Scanning Calorimetry, DSC, determines the heat flow associated with material transitions as a function of temperature or time, which are represented as either exothermic peaks (e.g., crystallization during heat evolution) or endothermic (e.g., melting or heat absorption) or as shifting in the baseline (change in the heat capacity). The versatility of the use of DSC makes it useful in investigations related to glass transition, melting and boiling points, crystallization time and temperature, heats of fusion and reactions, specific heat and heat capacity and purity.

All the experiments were performed using a TA Instrument differential scanning calorimeter (TA Instrument DSC Q100 V9.4 Build 287, Module DSC Standard Cell FC connected to a Windows-based computer system, New Castle, DE, US) equipped with a refrigerated cooling system, RCS, with an optional Modulated DSC MDSC®, touch screen and auto-lid connected to two gas cylinders, one for nitrogen and the other for air

as seen in Figure 2-1. The Q Series™ Explorer Window provided by TA instrument was used to setup, view and control the experiment after all the information about the sample have been input (e.g., sample name, sample weight, file directory, operator's notes etc).
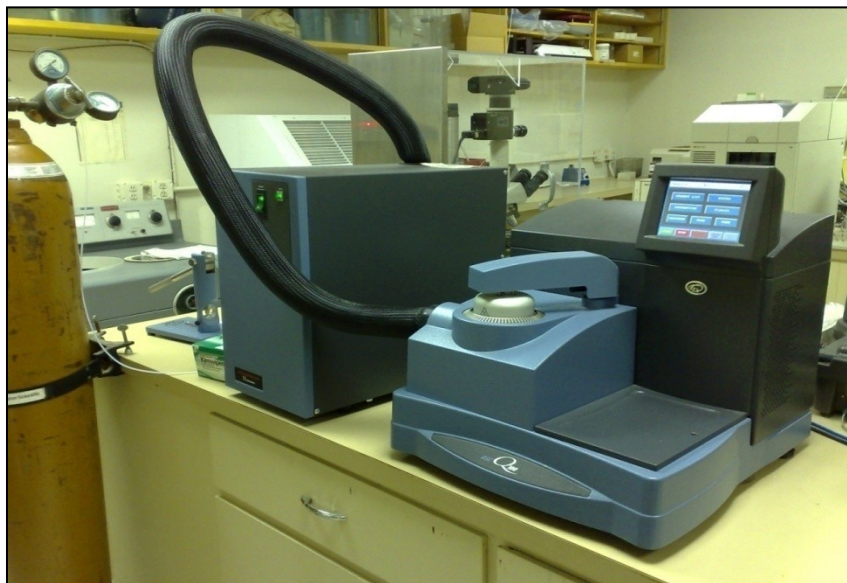
Figure 2-1: TA Instruments heat flux DSC Q100 equipped with modulated® DSC connected to a refrigerated cooling system, RCS.

2.2.1.2   Calibration

Prior to calibrating the DSC, it was ensured that the DSC cell, including the two sensors, was cleaned by brushing them using a fibreglass brush included in the accessory kit, and subsequently the residue was removed using clean compressed air. Figure 2-2 is a depiction of the DSC Q100 cell assembly with all its parts.
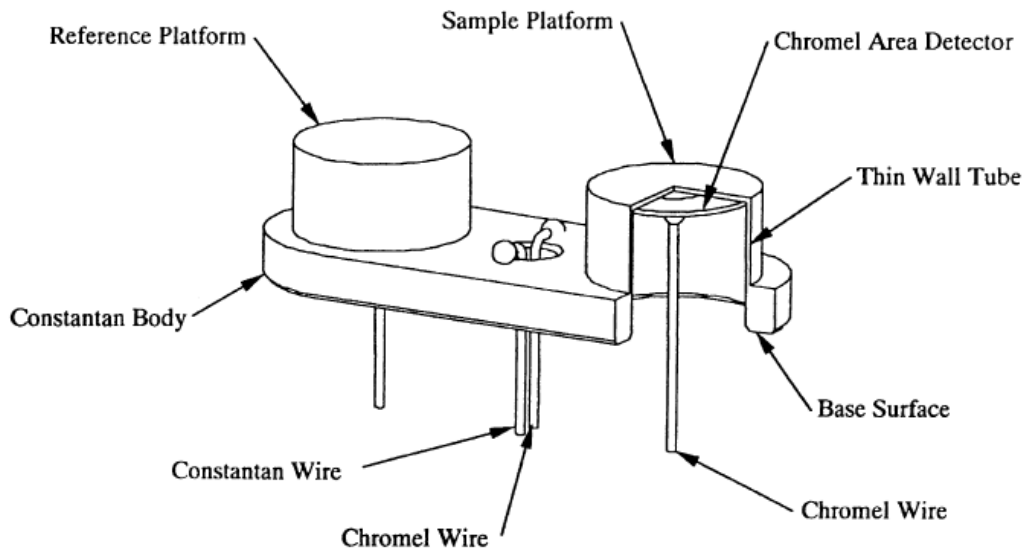
Figure 2-2: DSC Q100 sensor assembly with Tzero^{TM} technology (Danley, 2003)

To verify the efficiency of the cleaning process, an empty cell run (no sample or reference containers) over a temperature range from -60 to 200 °C using a heating and cooling rate of 20 °C/min was performed to remove any contaminants left from previous experiments. In instances where further cleaning was required, a cotton swab dampened with acetone was used to clean the cell. Subsequently, a dry cotton swab was used to dry off the cell followed by an empty cell run to verify that all contaminants were removed. If the cell was still contaminated, the cell was burned out as a last resort to remove all the contaminants from it. This process was done by heating up the DSC cell to 600 °C with the lid open under air flow at a rate of 50 mL/min. After ensuring that the cell was cooled to room temperature, an overnight cyclic test was performed on the empty cell. This was done to minimize the "first run effect" as suggested by TA Instruments over the temperature range aforementioned and to ensure that all contaminants have been eliminated. Calorimetric measurements usually drift from zero baseline during the first run compared with subsequent runs under the same conditions; this effect is called the

"first run effect". The calibration process was then repeated. This cyclic treatment to the DSC cell was strongly recommended by the TA Instruments support team that considered it to be a critical step to obtain a clean cell and thus a smooth baseline before the calibration process.

Subsequently, the instrument was calibrated using the calibration wizard option where the T4 heat flow option "cell resistance and capacitance, cell constant and temperature calibration" was selected. Another option available is the T1 heat flow but it does not make use of the Tzero^{TM} technology and produces measurements with poor quality. The T4 heat flow compensates for subtle differences in thermal resistance and capacitance between the reference and sample sensors in the DSC cell, i.e., corrects for the asymmetry between the reference and sample sensors.

DSC Q100 incorporates Tzero™ heat flow theory which is composed of four terms as follows: (Danley, 2003)

$$q = -\frac{\Delta T}{R_r} + \Delta T_0 \left(\frac{1}{R_s} - \frac{1}{R_r} \right) + (C_r - C_s)\frac{dT_s}{dt} - C_r \frac{d\Delta T}{dt}$$
[2-1]

where q is the heat flow rate, ΔT is the measured temperature difference between the sample and reference calorimeters, ΔT_0 is the measured temperature difference between the control sensor and the sample calorimeter, T_0 is the control temperature, R is the sensor thermal resistance, C is the sensor heat capacity and subscripts r and s represent the reference and sample, respectively (Danley, 2003). This calibration method includes three separate calibration runs. The first is performed with an empty cell, and the second with two sapphire discs with similar masses, to determine R and C values for the reference sample sensors in the equation [2-1]. The first two runs are heated through the

same heating range using the same heating rate, usually 15 or 20 °C/min. The third calibration run involves running indium as a standard with known enthalpy to determine the cell constant. The cell constant is a correction factor calculated by dividing the theoretical enthalpy value of indium by the one measured during the calibration process. Appendix A has a more detailed discussion about the calibration process.

2.2.1.3 Sample preparation

The samples were melted using an oven (Precision Scientific Co. Thelco 18, US) set at 80 °C for at least 10 min to insure that the sample is melted, and the sample containers were occasionally gently agitated to allow for uniform mixing of the binary triglyceride mixtures. Hermetic aluminum pans and lids purchased from TA Instruments were cleaned by immersing into mildly heated acetone, about 40 ºC, and left to dry in the oven. All the tools were handled using cleaned tweezers to avoid any contamination. Five to ten mg of molten samples were then transferred to cleaned pans using disposable capillary tubes with a wire plunger (Drummond Scientific Company, Wiretrol® II, US, 5 µL and 10 µL). All the weighing measurements were carried out using a microbalance (Cahn Instruments, C-33 Microbalance Model Number 13633-013, US) with a precision ≤ 0.001 mg. The pans and lids were encapsulated using a TA Instruments blue encapsulating press.

2.2.1.4 Procedure

Each sample pan containing binary mixtures of trilaurin and trimyristin at a given ratio was put into the DSC cell with a hermetically sealed Al empty pan as a reference after making sure that the RCS and nitrogen gas were turned on for at least 1 hour to

attain a steady flange temperature of about -85 °C. The flange temperature is the lowest temperature obtainable using RCS. It is important to make sure that the flange temperature is steady at about -85 °C before starting the experiment for a better cooling performance. All the samples were initially heated to 80 °C at a heating rate of 20 °C/min, held at this temperature for 15 min and then cooled using 7 cooling rates: 20, 15, 10, 7.5, 5, 2.5 and 1 °C/min in a successive fashion without taking the sample out. All the samples were cooled to an end point where the sample was completely solid (-10, -15 or -20 °C) , held for 10 min and then reheated to 80 °C at a rate of 5 °C/min and kept there for 15 min to melt the sample for the subsequent cooling rate. The whole process using all the cooling rates explored was regarded as one run; each run was repeated two times to test the repeatability of the experiment.

Two or three pans were prepared for each sample. All the thermograms obtained from the DSC experiments were initially analyzed using the TA Instruments Analysis program.

2.2.1.5 Calculating the enthalpy of crystallization

The crystallization traces of the samples were first plotted as heat flow vs. temperature using the Universal Analysis software (TA Instruments) followed by performing a zero baseline (absolute integral) integration. The integration process was carried out over the whole temperature range starting from the temperature at which the samples were totally melted, i.e., 80 °C all through to a point where the samples were entirely crystalline, i.e. -10 °C. An example of this process is shown in Figure 2-3.
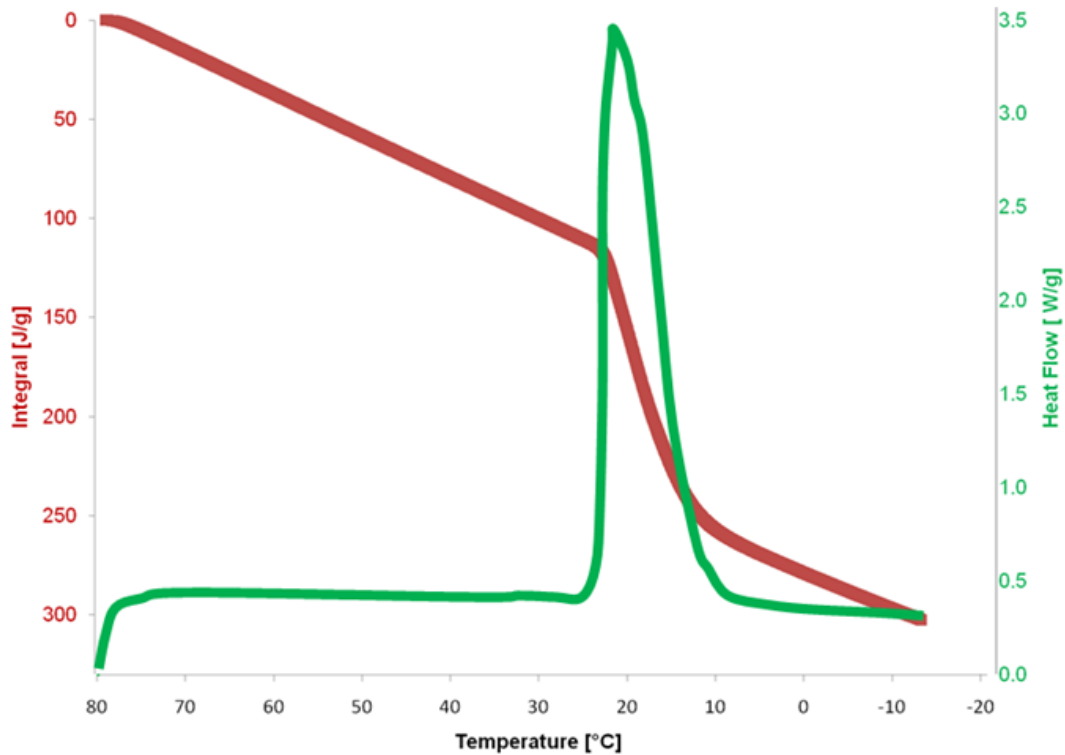
Figure 2-3: DSC cooling trace of 3L7M cooled from the melt at 80 °C to -15 °C using 10 °C /min (green line). The absolute integration of the peak from 80 °C over the whole range is shown (red line).

Afterwards, the values of the temperature, heat flow and integrated heat flow signal for all samples were extracted to an Excel spreadsheet for analysis. Performing the integration process using this automated fashion is important so that the variability of the data (due to pan position and other artefacts) is reduced to a minimum. Foubert *et al.* (2003) indicated that when integration limits, i.e., temperatures or time, are determined visually during the integration process of the DSC peak signal, the result will be dependent on the operator and will differ even when the same operator performs the integration several times. This was not an issue in the current work as the whole trace was integrated by selecting the start and end temperature well above and below the transition interval respectively as shown in Figure 2-3. An advantage of this procedure is

that one could avoid discrepancies, which depend on how the interpolated baseline underneath the peak is constructed (Matovic *et al.*, 2005).

When different cooling rates are applied to a sample, the resultant heat flow signals exhibit variation and shifts and so do the integrated signals. Therefore, it was necessary to normalize the crystallization traces for a sample at different cooling rates to make the integrated lines comparable. The normalization process was done for each sample using its liquid state signal as a reference.

The enthalpy of crystallization at -10 °C was determined by calculating the difference between the enthalpy values of the solid and the liquid state (ΔH_{crys}). This was carried out by subtracting the total integrated heat flow up to -10 °C (in the solid state) from an extrapolated line fitted to the liquid integrated heat flow using a quadratic function, as shown in Figure 2-4. The quadratic function was chosen because, as indicated in the introduction, it has been found that the specific heat capacity for liquid TAGs follows a linear relationship with temperature (Morad *et al.*, 1995b),. Therefore its integral, the enthalpy, will follow a quadratic function.
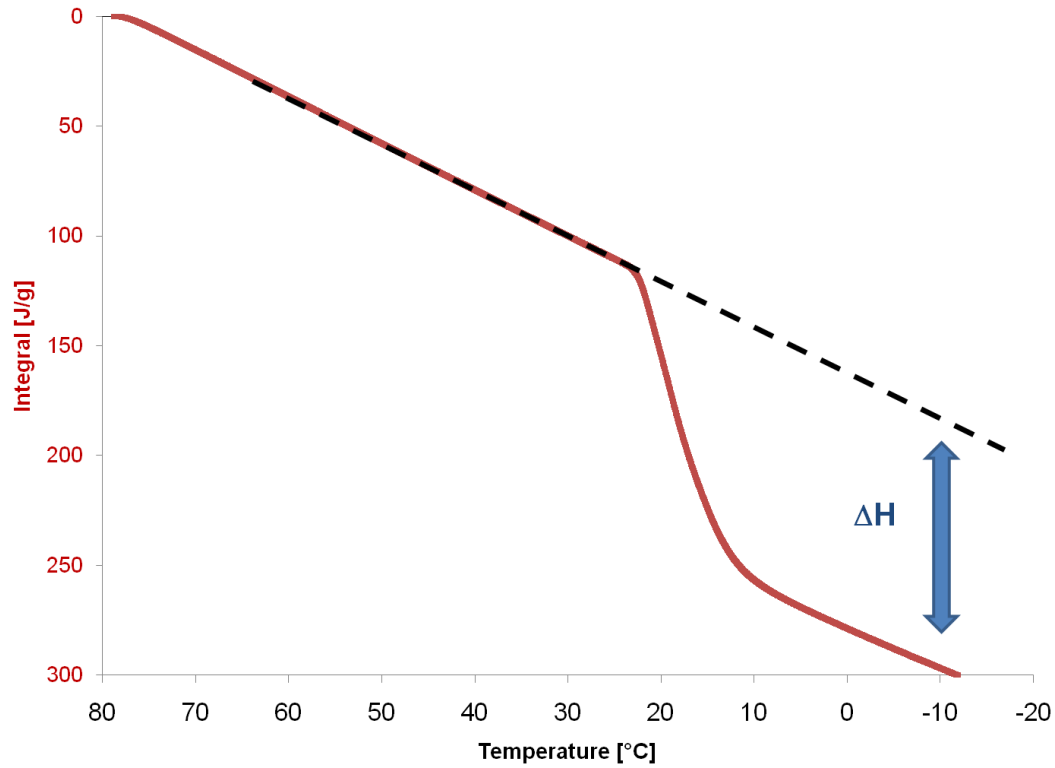
Figure 2-4: Determining the enthalpy of crystallization at a given temperature by calculating the difference between integrated heat flow values of the solid and an extrapolated line that was fitted linearly through integrated heat flow values for the liquid.

The liquid state was used as a reference to normalize the integrated heat flow traces obtained at different cooling rates, sample sizes and pan position. The mathematical integration used to obtain enthalpy of crystallization can be described as follows:

$$\Delta H_{-10} = \left(\Delta H_{80} + \int_{80}^{-10} C_{p(solid)} dT \right)_{R.I.} - \left(\int_{80}^{-10} C_{p(liquid)} dT \right)_{Extr.Liq.} \qquad [2\text{-}2]$$

The running integral (integrated heat flow) and the extrapolated line fitted to the liquid integrated heat flow are represented with the subscripts "*R.I*" and "*Extr. Liq*", respectively. The enthalpy of crystallization here represents the enthalpy difference at a

given temperature between the integrated heat flow in the solid and liquid values as a function of temperature.

2.2.2   Modulated Differential Scanning Calorimetry (MDSC®)

2.2.2.1   The instrument

All the experiments were performed using the same Q100 DSC. The main operating difference between MDSC and conventional DSC is that MDSC operates under two concurrent temperature ramps. One is the linear heating rate that produces the same information obtained by DSC, and the other is a sinusoidal or modulated heating rate that is supposed to allow direct calculation of the sample heat capacity. This modulation signal is created by the operator's selection of the modulation period and amplitude. The equation that describes the heat flow signal from MDSC experiment is as follows (Reading & Hourston, 2006) :

$$\frac{dH}{dt} = C_p \frac{dT}{dt} + f(T,t) \qquad\qquad [2\text{-}3]$$

where $\dfrac{dH}{dt}$ is the total heat flow rate in mW resulting from the underlying heating rate. This is also obtained by standard DSC, C_p (J/°C), and is regarded as the reversing component. It is the sample's heat capacity which is equal to the specific heat of the sample multiplied by the sample mass (mg) and is calculated from heat flow produced from the underlying modulated temperature ramp $\dfrac{dT}{dt}$ (°C/min). $f(T,t)$, regarded as the non-reversing component, is the heat flow that is a function of the temperature, time and history of the sample. It is the kinetic heat component of the total heat flow. It is

computed by subtracting the in-phase heat capacity component from the total heat flow. The specific heat of the sample is found by dividing the reversing heat flow amplitude by the temperature ramp amplitude and then multiplying by the calibration constant KC_p predetermined in the calibration process. The calibration constant KC_p is obtained by dividing the theoretical value of a standard (sapphire) by the experimental value obtained for the same material (sapphire) at a given temperature under the same conditions of the runs that will be done with the TAGs mixtures. This is similar to the three-step method mentioned above, but without subtraction of the empty pans. The effect of the pans is assumed to be cancelled by the differential measurement of the DSC. In this work this was ensured by using pans with the same weigh.

2.2.2.2   Calibration

The instrument was calibrated using sapphire as a reference material, since it has well known heat capacity values over a broad temperature range. The calibration values for the total heat capacity and reversing heat capacity were manually set to the default values of 1.0 before starting the calibration process. Two hermetically sealed Al pans with matched mass, one with a sapphire disc and the other left empty as a reference, were used to calibrate the instrument under different cooling rates and isothermally. At the end of the calibration process, the calibration constants KC_p were calculated as follows:

KC_p (Total) = Theoretical Value / Measured total heat capacity Value   [2-4]
KC_p (Reversing) = Theoretical Value / Measured reversing heat capacity Value   [2-5]

The default values were replaced by the values obtained from solving equations [2-4] and [2-5] respectively. For non-isothermal runs the following calibration procedure was performed as recommended by the manufacturer: 1) Sampling Interval 1.0 seconds/point;

50

2) Zero heat flow at the average of start and end temperatures; 3) Equilibrate at start temperature; 4) Modulated +/- 0.5°C every 100 seconds; 5) Isothermal for 5.0 minutes; 6) Ramp 5 °C/min to end temperature.

KC$_p$ values were calculated at the midpoint of the temperature range for non isothermal experiments. Quasi-isothermal experiments were also performed at different temperatures and hence the corresponding KC$_p$ values were also computed.

2.2.2.3 Procedure

All the conditions employed during the preparation for the DSC experiments were maintained constant; i.e., gas flow, cooling system, start and end temperature, etc. The binary mixtures were first crystallized following the same procedure as used in the DSC experiments. For the modulation investigations, different modulation combinations of amplitude (±1.5 - 2 °C) and period (30 - 120 s) were employed at different temperatures (-40, -30, -20, -10, 0, 70, 80 and 90 °C) where they were kept isothermally for 20 min. This was done to plot the C$_p$ (T) for each system. The specific heat capacity values, reversing heat capacity, for each temperature were subsequently extracted to an Excel file for further analyses. Each point measurement represents the average of reversing C$_p$ recordings during its modulation period.

2.2.3 Thermal relaxation measurements with Physical Properties Measurement System (PPMS®)

2.2.3.1 The instrument

Heat capacity measurements were carried out on a commercial relaxation calorimeter, a physical property measurement system (PPMS, from Quantum Design, US). This instrument is made available to researchers by the Facilities for Materials Characterization, managed by the Institute for Research in Materials at Dalhousie University. The PPMS is a fully-automated variable temperature and magnetic field system with numerous measurement applications such as thermal transport, heat capacity, DC magnetometry, AC susceptibility, and electro transport with an operational temperature range 1.8 to 395 K (Lashley *et al.*, 2003).
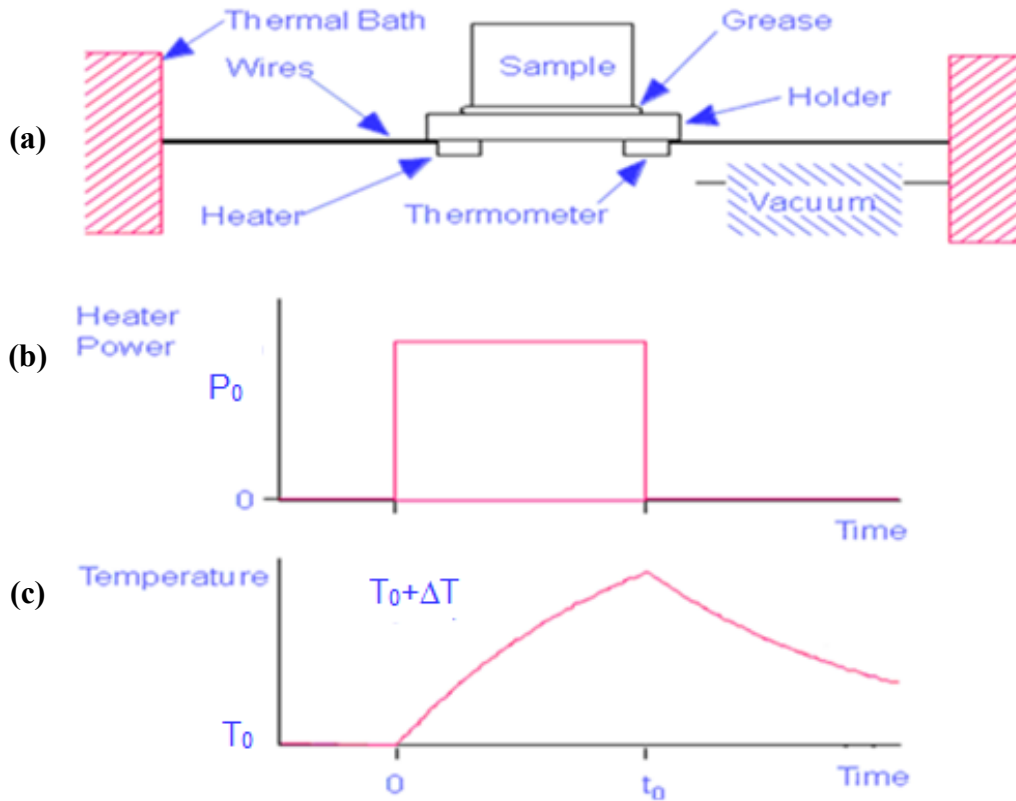
Figure 2-5: (a) depiction of the experimental set up of the platform; (b) the heating process; a square-pulse is applied to the platform (with or without the sample), (c) shows the consequent exponential temperature increase up to a temperature $T=T_0$ $+\Delta T$, where the input power is discontinued and the resultant temperature decay to T_0 is monitored (Dachs & Bertoldi, 2005).

A sample of unknown heat capacity is attached to a 3 mm x 3 mm alumina platform with high thermal conductive grease (Apiezon® N grease). The platform is linked to a copper heating bath through eight very thin wires, and is placed in a chamber under vacuum where the temperature is controlled by cryogens such as helium. These wires serve as electrical connections to the temperature sensor and heater and to isolate the sample from the surroundings.

The determination of a sample's heat capacity is performed by measuring the thermal response of a sample/calorimeter assembly. As shown in Figure 2-5, a predetermined amount of heat is added to the platform by applying a square-pulse of a

height P_0 and width t_0 to reach a temperature $T = T_0 + \Delta T$, where ΔT is the temperature difference between the system and thermal bath at T_0. Afterwards, the power input to the platform is discontinued and the system is allowed to relax back to T_0. The exponential decay in temperature can be described as: (Kennedy *et al.*, 2007)

$$T_p = T_0 + \Delta T e^{-t/\tau_1} \qquad\qquad [2\text{-}6]$$

where T_p is the platform temperature and the characteristic time constant τ_1 is directly related to the heat capacity by the following equation: (Kennedy *et al.*, 2007)

$$\tau_1 = C_{pl} / K_1 \qquad\qquad [2\text{-}7]$$

where K_1 is the thermal conductance between thermal bath and the system. With the use of τ_1, the heat capacity of a sample can be measured using the simple model, referred to sometimes as a one-τ model (Dachs & Bertoldi, 2005), assuming that the sample and the sample platform are in good thermal contact with each other and their temperature is unchanged following the equation:

$$C = -K_1(T - T_0) + P_0 \qquad\qquad [2\text{-}8]$$

In cases where the thermal contact between the sample and the sample platform is poor, thermal grease is added, and the heat flow through the sample-platform interface produces a temperature gradient that must be accounted for to accurately measure the heat capacity of the sample. Another characteristic time constant $\tau_2 = C_{sa} / K_2$ is therefore introduced; where C_{sa} is the heat capacity of the sample and K_2 is the thermal conductance between the sample and the platform.

Here, a more sophisticated model, called the two-τ model, is used (Dachs and Bertodli, 2005) using the following equations:

$$C_{pl} = P(t) - K_1\left(T_P(t) - T_0\right) + K_2\left(T_s(t) - T_P(t)\right) \qquad \text{[2-9]}$$

$$C_{sa} = -K_2\left(T_s(t) - T_P(t)\right) \qquad \text{[2-10]}$$

Eventually, the complete response records are analyzed and converted into heat capacity numbers by the application of a non-linear fitting technique described by Hwang *et al.* (1997). Note that both models assume that the sample is isothermal at any given time, i.e. that there are no thermal gradients inside the sample. This requires that the sample possesses a relatively high thermal conductivity, which is not quite the case for the TAG mixtures.

2.2.3.2 Sample Preparation

Four to eight mg of LLL, MMM and 3L7M were melted in an oven set at 100 °C for 5-10 min. The molten samples were transferred to pre-cleaned Perkin Elmer micro hermetic pans and lids before crimping using disposable capillary tubes with a wire plunger (Drummond Scientific Company, Wiretrol® II, 5 μL and 10 μL). All the weighing measurements were carried out using a Mettler M3 Micro Balance with accuracy ≤ 0.005 mg.

2.2.3.3 Procedure

The measurements of the heat capacity values of the samples were obtained at different temperatures in the solid state (-40, -30, -20, -10, 0, 10, 20 °C) and when the samples were re-melted in the liquid form (60, 70, 80, 100, 120 °C). Three measurements were taken at each temperature with accuracy ≤ 0.007 J/g°C. Only two cooling rates, 2.5 and 10 °C/min, were explored due to the instrument having a limited cooling rate of 10 °C/min.

Chapter 3   RESULTS AND DISCUSSION

3.1   Results and Discussion I: Enthalpy of crystallization

Though the determination of the melting enthalpy of a pure substance may not seem too difficult, the task is not so straightforward for the enthalpy of crystallization of a multicomponent phase. One reason is that the melting temperature of that phase needs to be found as well, and that is not an easy feat, because of the need to supercool the material. Another reason is that it is often impossible to obtain the phase on its own. It will usually appear mixed with at least another phase, or more. Thus, it is necessary to collect information on the different mixtures of phases formed, and from there try to elucidate the enthalpy corresponding to each phase formed. In this work, the enthalpy of crystallization of pure LLL, MMM and their binary mixtures cooled from the melt at seven cooling rates (20, 15, 10, 7.5, 5, 2.5 and 1 °C/min) was investigated.

3.1.1   Temperature and enthalpy calibration

In order to illustrate the dependency of the cell constant calibration values on different heating and cooling rates, approximately 2 mg of indium were used for calibration runs under the same temperature ramps used for the samples (20, 10, 15, 7.5, 5, 2.5 and 1 °C/min). The enthalpy of melting and crystallization were determined using the same method used to obtain the enthalpy of crystallization previously discussed in section 2.2.1.5. The produced heat flow peaks as a function of different cooling and heating rates as shown in Figure 3-1.
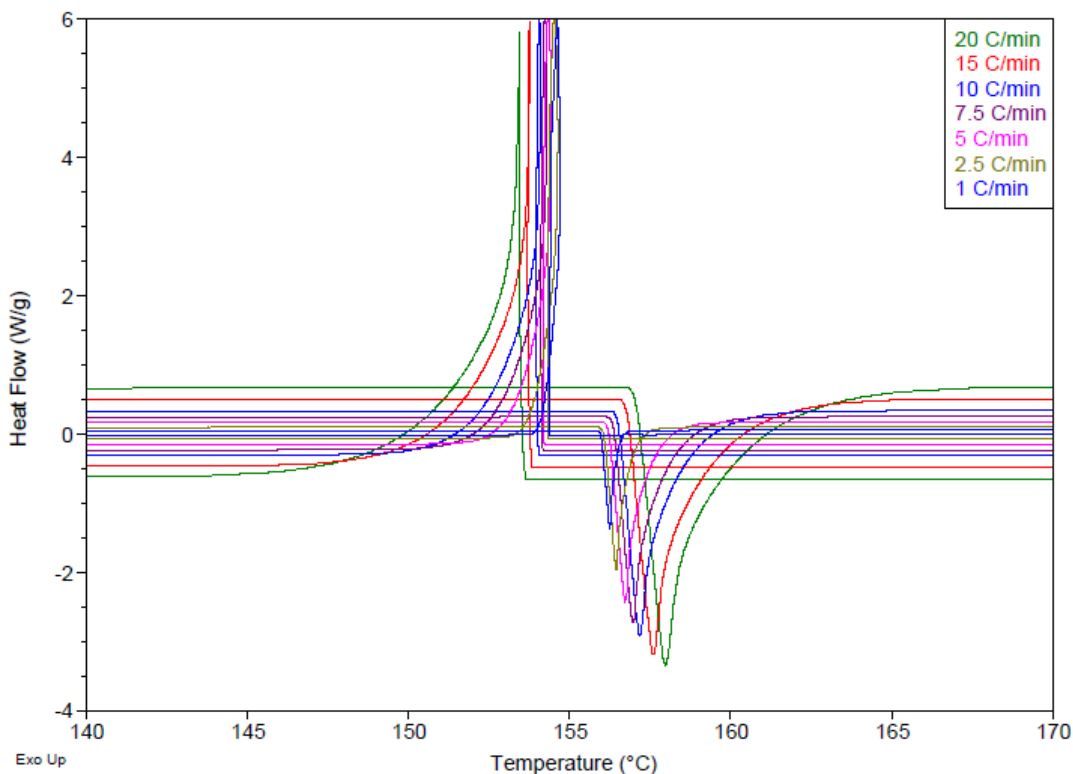
Figure 3-1: Heat flow vs. temperature for an indium sample under different heating and cooling rates.

The crystallization and melting peaks are shown as upward (exothermic) and downwards (endothermic) peaks respectively. A supercooling of about 2 or 3 °C at 10 and 20 °C/min, respectively, were found, which agrees with the reported values in the work done by Neuenfeld and Schick (2006). For the calculation of the enthalpy at different cooling and heating rates, the subtracted values between the extrapolated fitted lines for the solid and liquid were obtained at the theoretical melting temperature of indium. Figure 3-2 shows the calculation of the enthalpy values of melting and cooling using three temperature ramps; as an example, 20, 7.5 and 1 °C/min. The vertical dashed line represents the theoretical melting point of indium, 156.6 °C; the blue and the red curves represent the integrated heat flow during cooling and heating respectively; the dashed and the dotted lines represent the fitted lines for cooling and heating curves,

58

respectively, where the upper fitted lines represent the fitted lines for integrated heat flow values in the solid state. The integrated heat flow measurements were fitted to a second order polynomial with $R^2 \approx 1$.
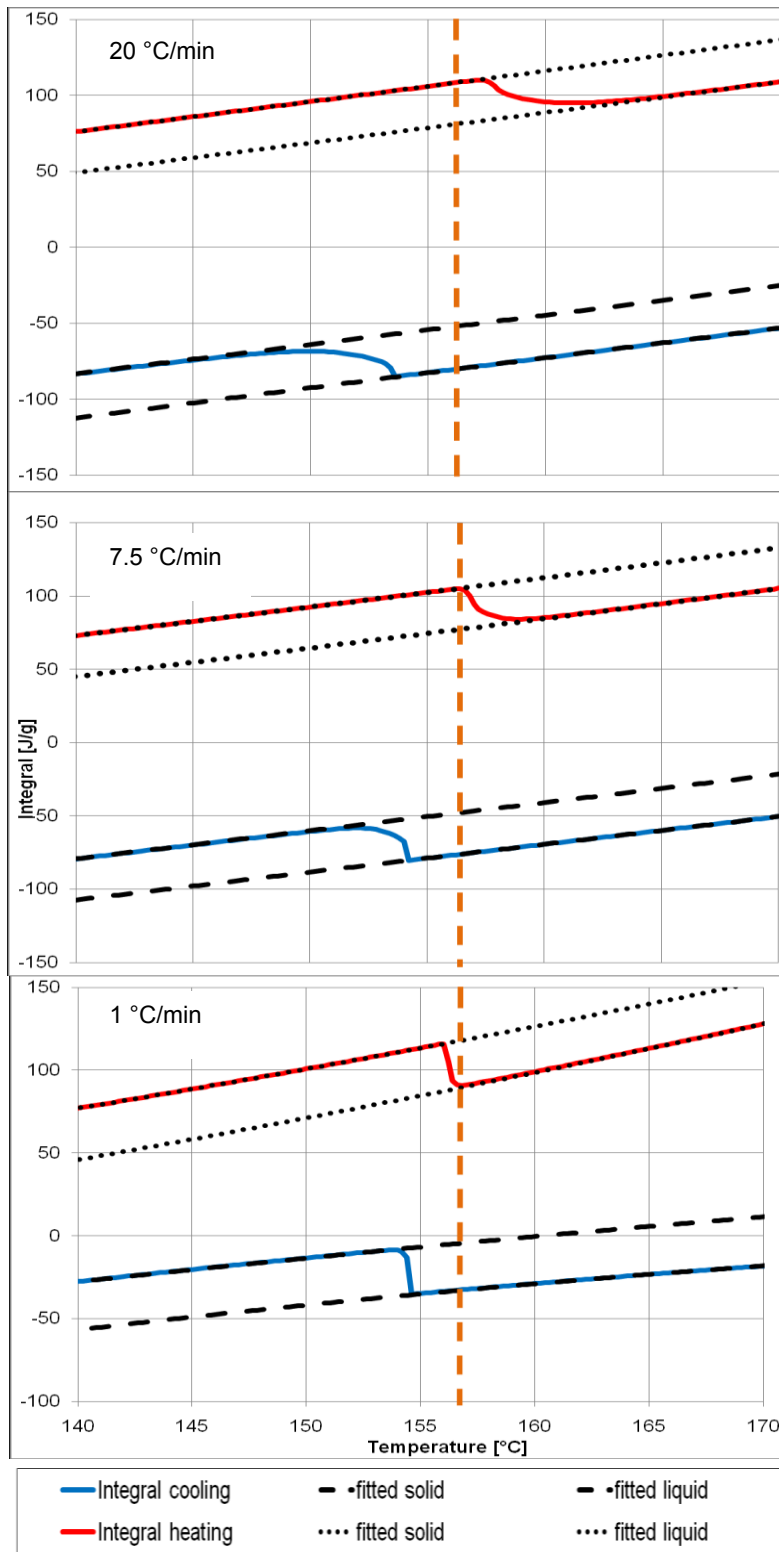
Figure 3-2: Integrated heat flow signals as a function of temperature during heating and cooling of indium using temperature ramps of 20, 7.5,1 °C/min; the upper fitted lines for each curve are for solid.

The effect of using different temperature ramps on the transition temperature of indium is shown in Figure 3-3. The transition temperature shows a linear dependence on the temperature ramp applied. During heating, the transition temperature increased with increasing temperature ramp while the opposite trend is observed for cooling.
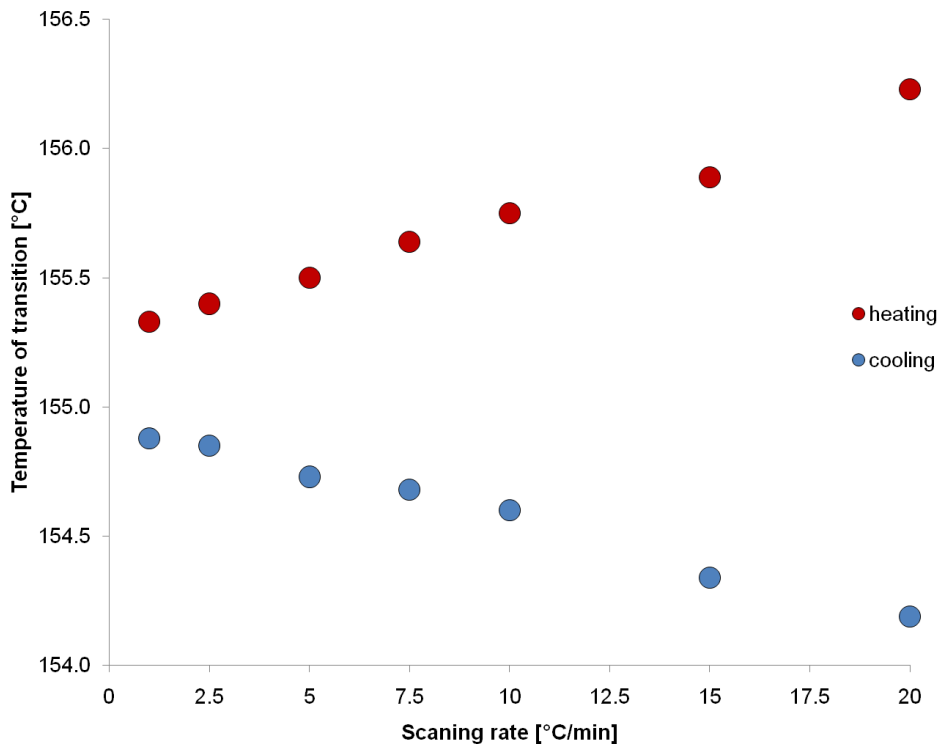
Figure 3-3: Temperature transition of indium at different heating and cooling rates (n=3).

The identification of the actual melting and crystallization temperatures needs a better consideration of the heat flow path between the sample and the bottom of the sample container, and the path between the sample container and the calorimeter. They change as a function of the temperature ramp, but this was not the objective of this study. Therefore the temperature correction for indium was applied based on the heating curve. The values were still rather far from 156.6 °C. The extrapolated value of the melting

temperatures upon heating is 155.3 °C. A very sensitive procedure was used to determine the onset of melting. It consists of using the derivatives of the heat flow signal that can detect any onset of melting, even at the depressed melting point surface of the material. More crude techniques, such as inflection point asymptotic extrapolation, are used routinely in most other studies.

The other property used for calibration is the enthalpy of a reference material, in this case indium. The enthalpy of crystallization and melting calculated at the theoretical melting temperature of indium are shown in Figure 3-4 at different cooling and heating rates.
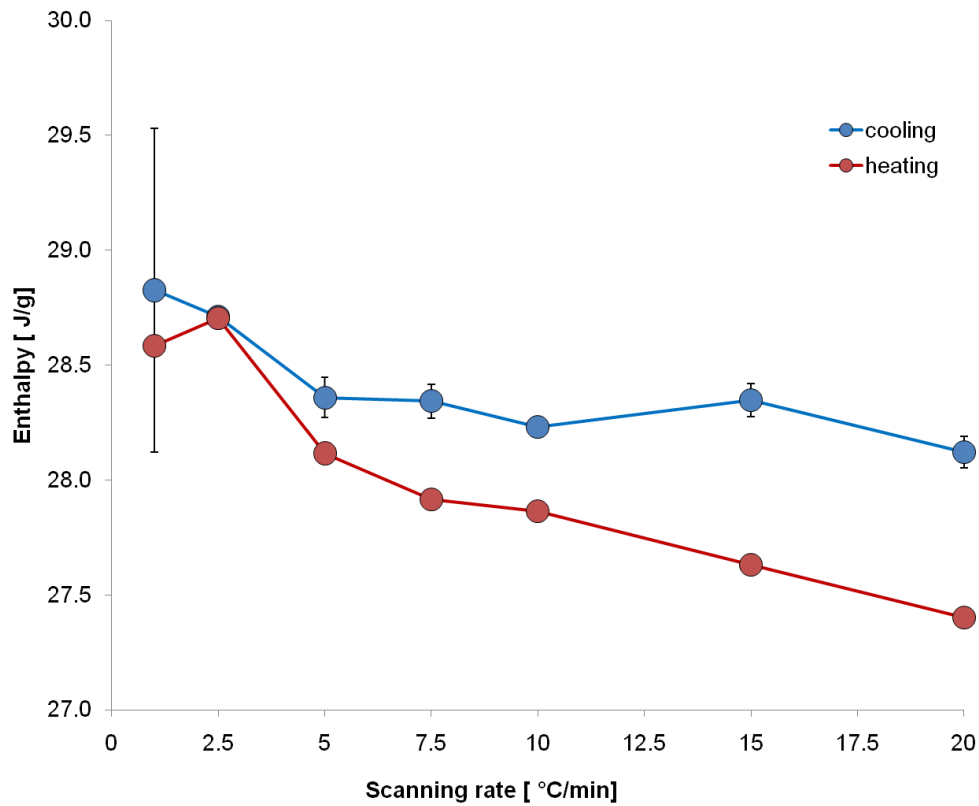
Figure 3-4: The influence of using different cooling and heating rates on the final enthalpy values of indium. Each measurement point is the average of three measurements. The error bars represent the standard error with n=3.

These values were obtained from experiments with the Q100 DSC with a predetermined calibration factor (cell constant) of 1.0412 using a heating rate of 15 °C/min. To get exactly an average of 28.1 J/g, the cell constant would have been 1.0502. Mean values of 28.23 ±0.14 and 28.25 ±0.18 J/g were obtained for the various cooling and heating rates applied, respectively. This shows that the difference in the calculated enthalpy for indium between cooling and heating is very small. This implies that the correction factors calculated during heating can be used for the cooling experiments performed at different cooling rates. This is important as the enthalpies under study are calculated during cooling and the instrument is calibrated during heating only.

The running integral method of calculating the melting enthalpy of indium, however, is not used by the TA Instruments software during the calibration of enthalpy (cell constant). The TA Instruments' software uses a sigmoidal integration procedure to calculate the melting peak area of indium with the capability of selecting the peak limits either manually or automatically. This method, as mentioned earlier in section 2.2.1.5, is not objective and the determination of the peak integration limits is dependent on the operator, which causes considerable variability in the resultant enthalpy (Foubert *et al.*, 2003). In order to assess the effect of using different sigmoidal integration limits on the calculated melting enthalpy of indium, the melting enthalpy of indium heated through its melting temperature at 10 °C/min was calculated using sigmoidal integration with the Universal Analysis software (TA Instruments) at different peak integration limits. Figure 3-5 is an example of a sigmoidal integration for indium heated at 10 °C/min with selected integration limits of 146.48 and 173.74 °C.
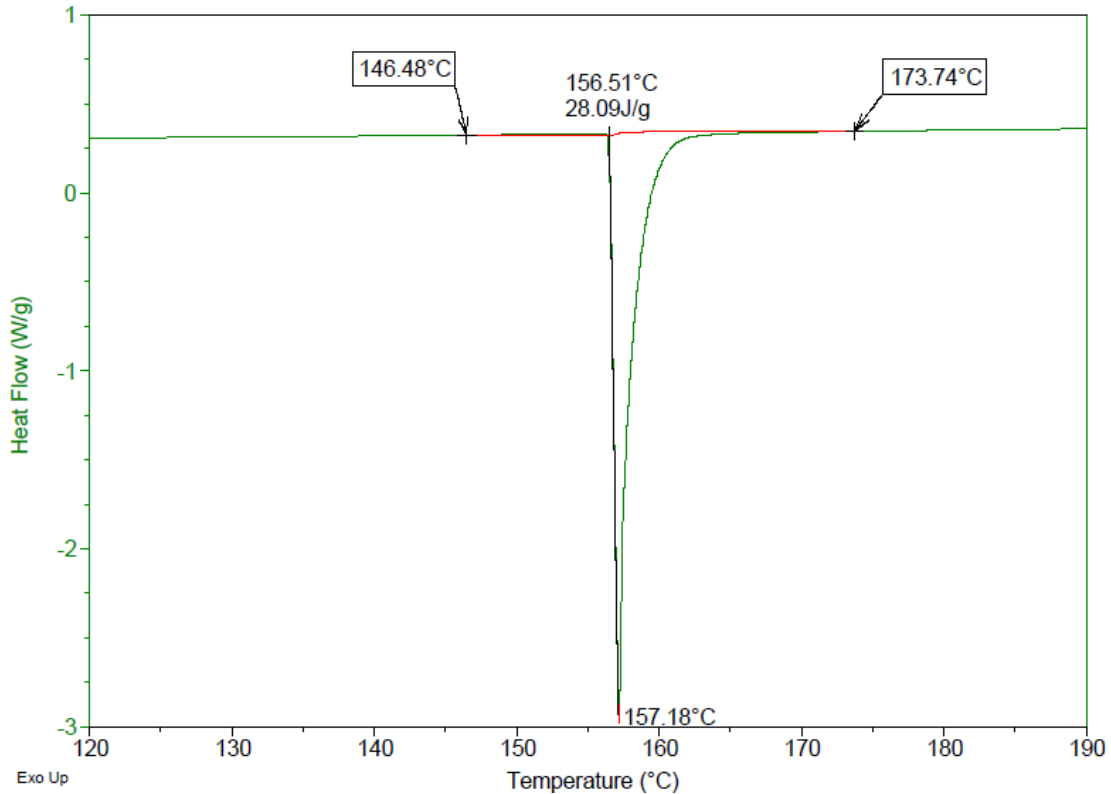
Figure 3-5: Plot of a sigmoidal peak integration of indium at 10 °C/min.

The sigmoidal peak integration provides three values which are, from top to bottom in Figure 3-5, the extrapolated peak onset temperature (156.51 °C), the calculated melting enthalpy (28.09 J/g), and the temperature at the peak maximum (157.18 °C). Many studies use this extrapolated value as the melting and the crystallization temperatures of the sample at a given heating and cooling rate. This is a rather rough estimate that is only approximately correct for very sharp peaks. For broader peaks, the onset needs to be directly determined, for instance using the derivatives method proposed by Foubert *et al*. (2003). The peak maximum indicates the temperature at which the melting process proceeds with the maximum rate (Menczel & Prime, 2009), and is always higher than the temperature at the onset of melting. The numbers in boxes represent the temperature limits, i.e., the peak limits used for integration chosen by the

operator. The red line is the interpolated sigmoidal line used as a base to perform the integration. Table 3-1 shows the calculated melting enthalpy of indium heated at 10 °C/min as a result of selecting different integration limits.

Table 3-1: Integrated melting enthalpy of indium at a heating rate of 10 °C/min as a result of varying integration limits using TA Instruments sigmoidal method.
.

Start °C	Stop °C	Area J/g
150	170	27.93
150	175	28.35
150	180	28.79
140	170	27.34
140	175	27.81
140	180	28.19
135	170	26.89
135	175	27.29
135	180	27.85

The mean value of the integrated enthalpies using the sigmoidal integration was found to be 27.83 ±0.59 (n=9) whereas it was 27.86 ±0.09 (n=3) using the subtraction method. If Bouzidi *et al.* (2005) method was to be used for the indium sample heated at 10 °C/min, then the resulted signal will look like the signals shown in Figure 3-6. Thus, the uncertainty in the calculated melting enthalpy of indium decreased considerably (about six times) with the use of the subtraction method of the fitting lines. It is however very important to have very good fitting lines of the data in the solid and liquid for the calculated enthalpies to be reliable and representative.
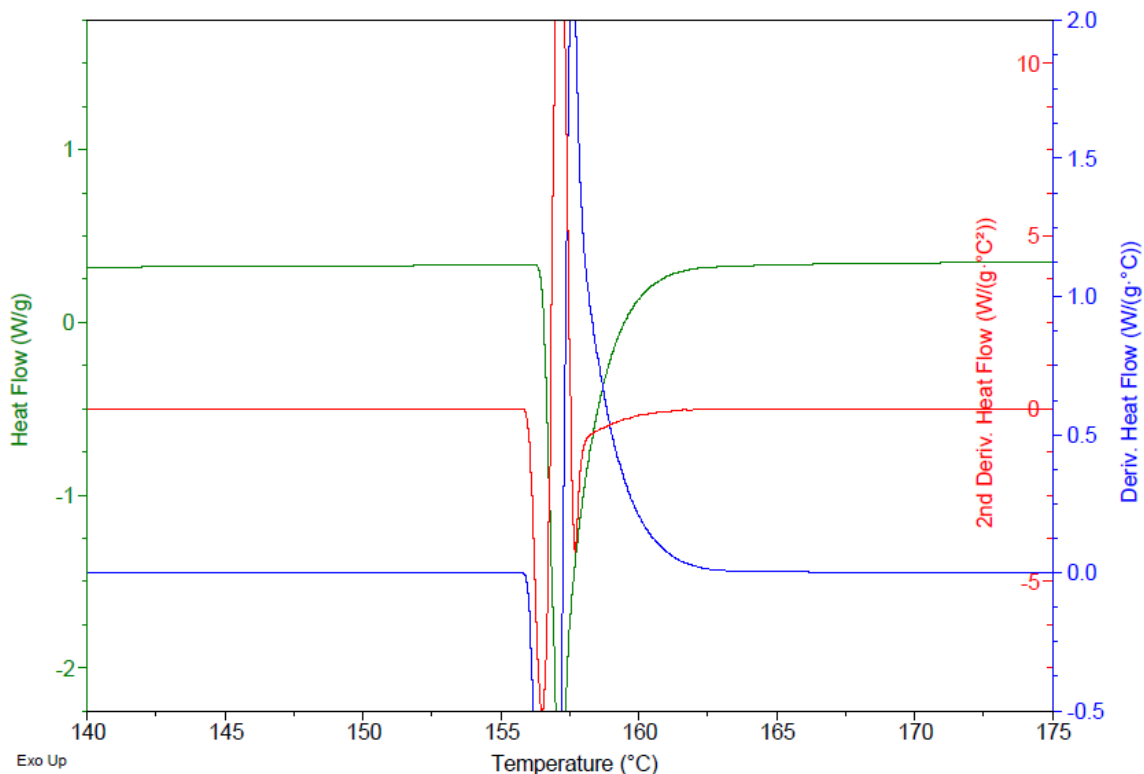
Figure 3-6: The first and the second derivative of the heat flow signal as a means to identify the proper integration limits of an indium sample heated at 10 °C/min as performed by Bouzidi *et al.* (2005) and Foubert *et al.* (2003).

To summarise, based on the results and observations of the present study it can be concluded that using DSC Q100 with Tzero[TM] calibrated with indium melting enthalpy at a reasonable heating rate (10 °C/min) allows for accurate measurements during cooling. The uncertainty due to calibration will be less than 0.7%. It was also shown that the subtraction method way of calculating enthalpy values gives rise to more precise data with less uncertainty, compared to the sigmoidal peak area integration method. In addition, the use of indium as a calibration material is adequate although its melting transition does not fall into the range of melting points of the samples under study.

3.1.2 Calculating the enthalpy of crystallization for the TAGs and their mixtures

Figure 3-7 shows the integrated relative heat flow (enthalpy difference, ΔH) for the binary mixture 5L5M at different cooling rates. The liquid state enthalpies are shown to equal 0 ±0.005 J/g (at 60 °C) after all the signals have been normalized and subtracted. Generally, lipids tend to crystallize at high cooling rates in the least stable phase, α-form, and in the most stable phase, β- form, at slow cooling rates. Since the crystallization process is a dynamic process, i.e., time –temperature dependent, least stable forms readily crystallize as the there is no sufficient time for more stable forms to crystallize at a relatively high cooling rate.
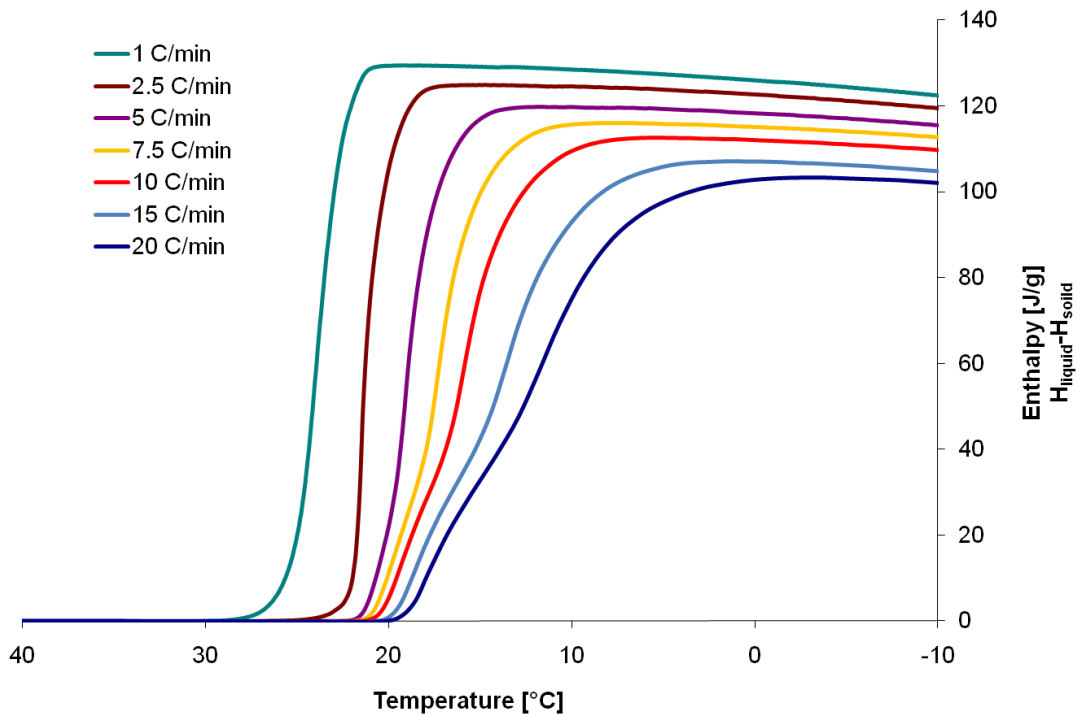
Figure 3-7: Integrated relative heat flow (enthalpy difference, ΔH) values for the binary mixture 5L5M determined by subtracting the integrated heat flow signals in the solid and liquid for different cooling rates.

Figure 3-8 shows the enthalpy difference, ΔH, values for LLL, MMM and their binary mixtures cooled at 10 °C/min. The mixtures follow a more or less consistent pattern, but the pure materials do not readily fit into it: MMM ends at a lower point than 3L7M and LLL cuts through the other curves and ends almost at the same value of MMM. This is due in part to the existence of polymorphism sub-modifications that are different in the mixtures than in the pure materials. Figure 3-10 shows the onset of crystallization temperatures obtained at the cooling rates explored for the three binary mixtures. It can be observed from these two figures that the onset of crystallization for the same binary mixture shifts to a higher temperature with decreasing cooling rate, about 10 °C as can be seen in Figure 3-8.
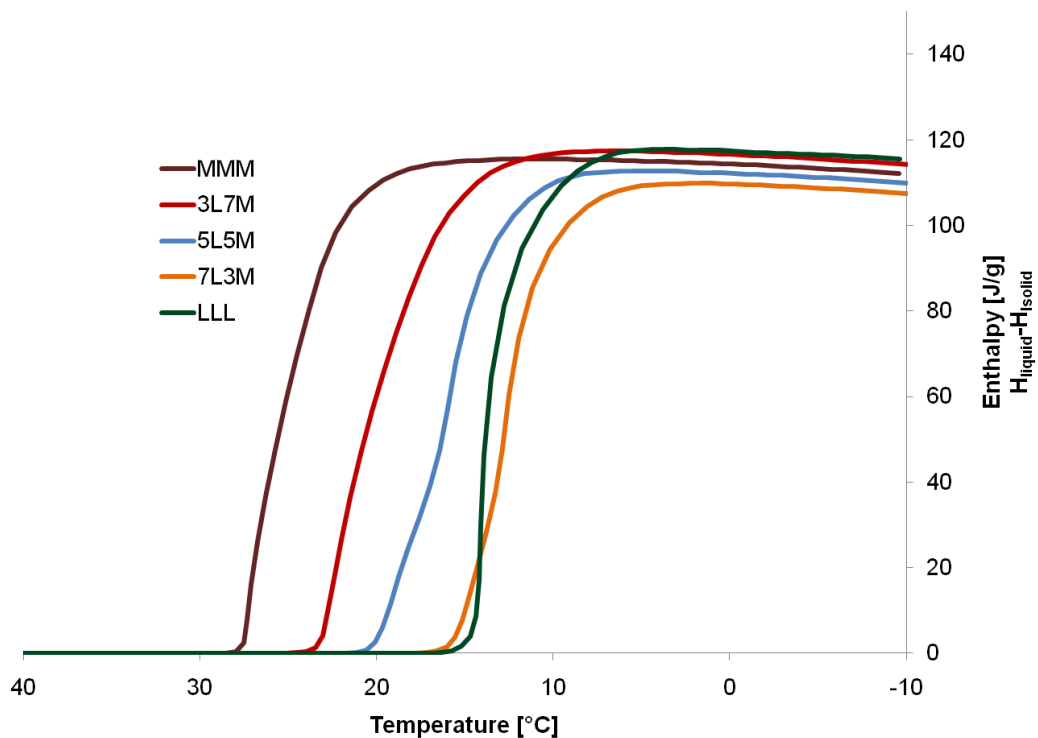
Figure 3-8: Integrated relative heat flow (enthalpy difference, ΔH) values for LLL, MMM and their binary mixtures at a cooling rate of 10 °C/min
.

In Figure 3-9, the enthalpy difference, ΔH, for three 5L5M runs cooled at 10 ºC/min and their average is shown. Some of the patterns are almost exactly on top of each other, whereas occasionally a slightly different path is followed. These differences could be due to many factors such as effective time-temperature profiles in samples of somewhat different size, pan positioning, etc.
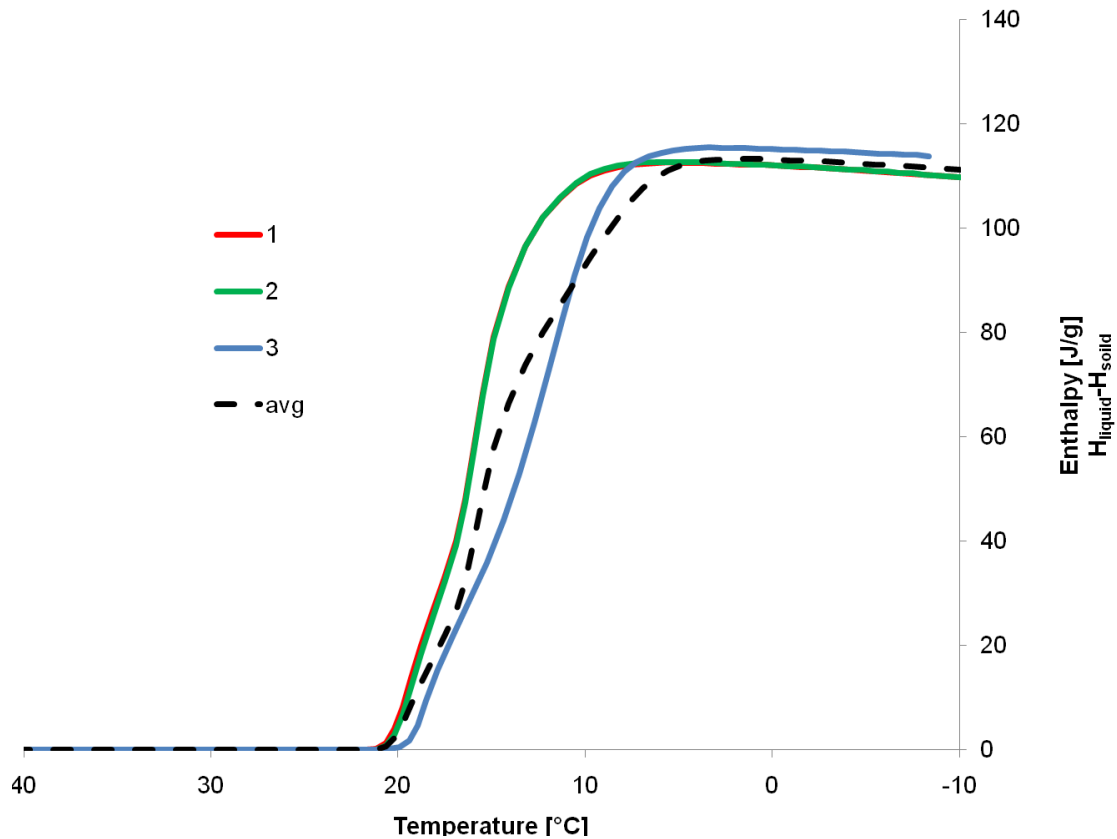
Figure 3-9: Relative heat flow (enthalpy difference, ΔH) values for three runs of 5L5M and their average cooled at 10 °C/min.

In addition, the onset of crystallization was also correlated to the sample composition, T_{onset} being higher in samples rich with MMM, higher melting component, and lower in samples rich with LLL, lower melting point, for every given cooling rate. Figure 3-10 shows the corresponding onset of crystallization temperatures as a function of varying MMM composition.
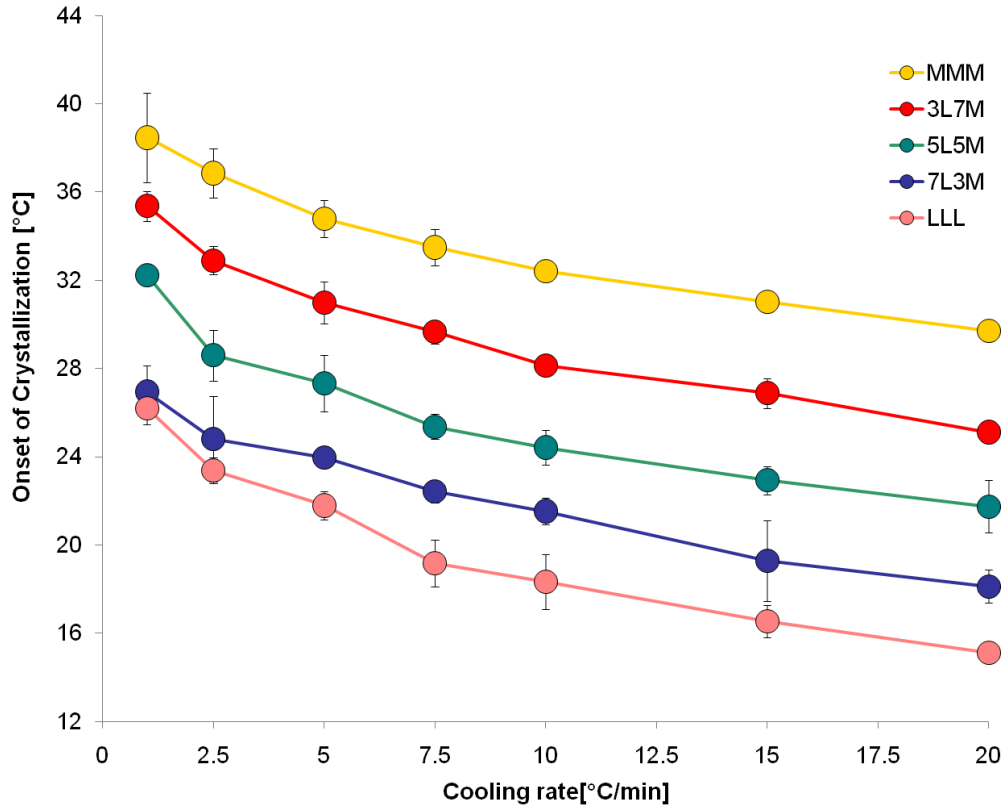
Figure 3-10: The onset of crystallization temperature as a function of cooling rate for MMM, LLL and their binary mixtures (n=6).

Figure 3-11 shows evidently the effect of the sample initial composition on the onset of crystallization at all cooling rates for MMM, LLL and their binary mixtures. Here all the samples are subjected to the same temperature versus time history and yet the onset of crystallization varied considerably. This is expected, since the undercooling is very different in each case. Figure 3-12 shows different possible undercooling conditions when a sample is cooled from the melt. The highlighted regions represent the possibility of creating the polymorph of the same colour. When the melt crosses the melting point of the α polymorph, all polymorphs will have a chance to crystallize.
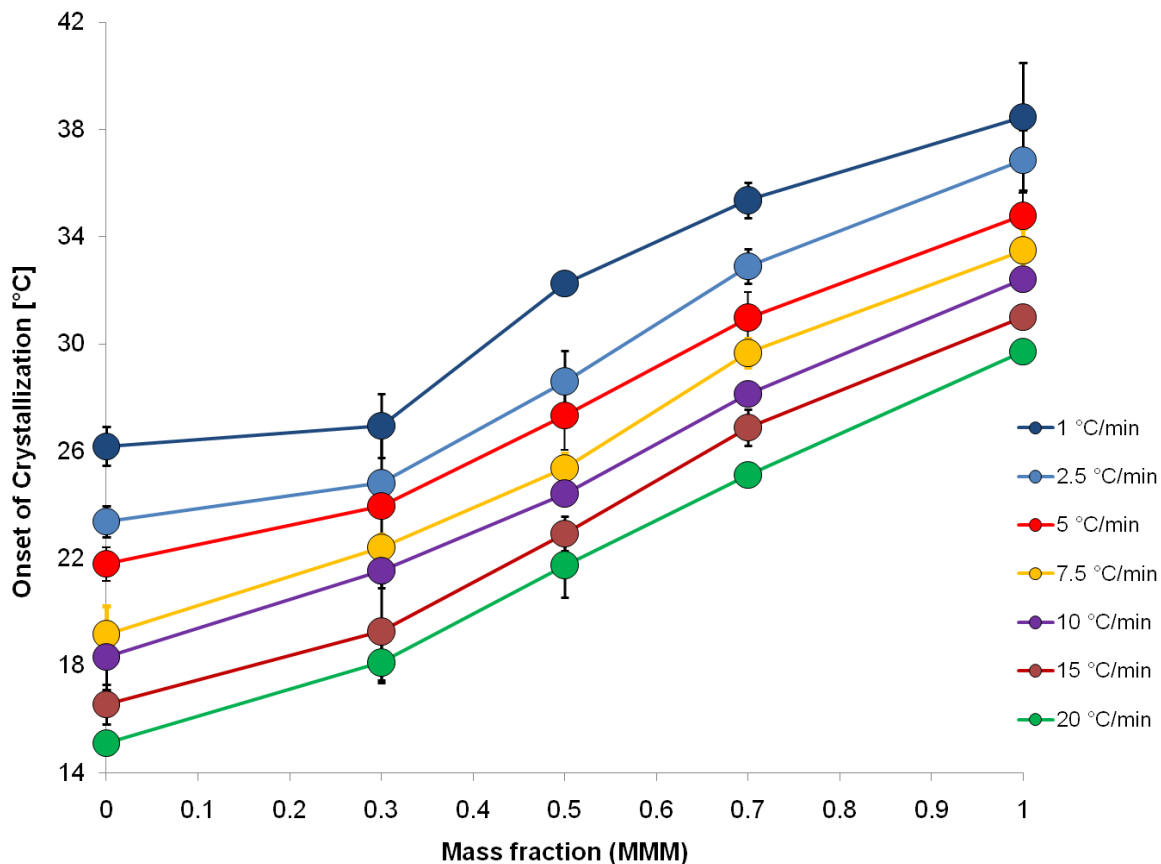
Figure 3-11: The onset of crystallization temperature as a function of different MMM mass fractions obtained at different cooling rates (n=3).

This means that the onset of crystallization that we observe in the DSC is governed by several factors. These factors include: 1) the tendency to form different crystalline phases of different polymorphic types and composition; 2) even if the same crystalline polymorph is obtained, the onset of crystallization will be lower at fast cooling rates; and 3) the onset temperature will vary with different sample sizes, different temperature ramps and the position of the pan on the sample post.
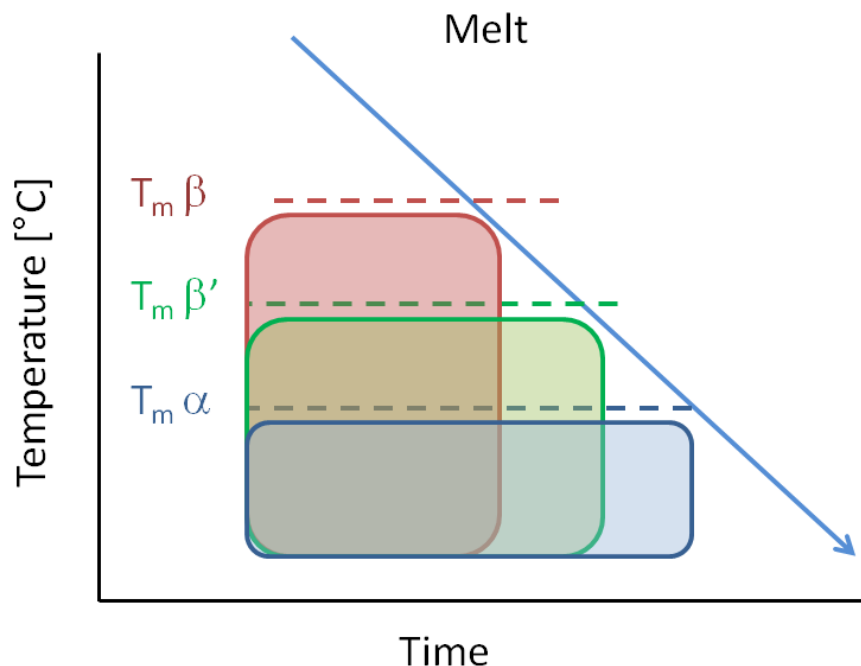
Figure 3-12: Different polymorphs that are expected to crystallize (represented as coloured regions) as their corresponding melting points are crossed by a molten sample being cooled (represented as a blue line)

In Figure 3-11, the onset of the crystallization decreased by about 12 °C in the case of cooling a 1 °C/min as the MMM concentration ratios decreased to reach the lowest in pure LLL. This is in perfect agreement with the results in the literature (Himawan *et al.*, 2007; Takeuchi *et al.*, 2002).

The enthalpy of crystallization values calculated at -10 °C for the three binary mixtures at different cooling rates were determined using the procedure above and are shown in Figure 3-13. In Figure 3-14, the enthalpy of crystallization of LLL and MMM are included. In the case of mixtures, it is necessary to define a common temperature or procedure for the comparison of enthalpies, since there is no common melting point.
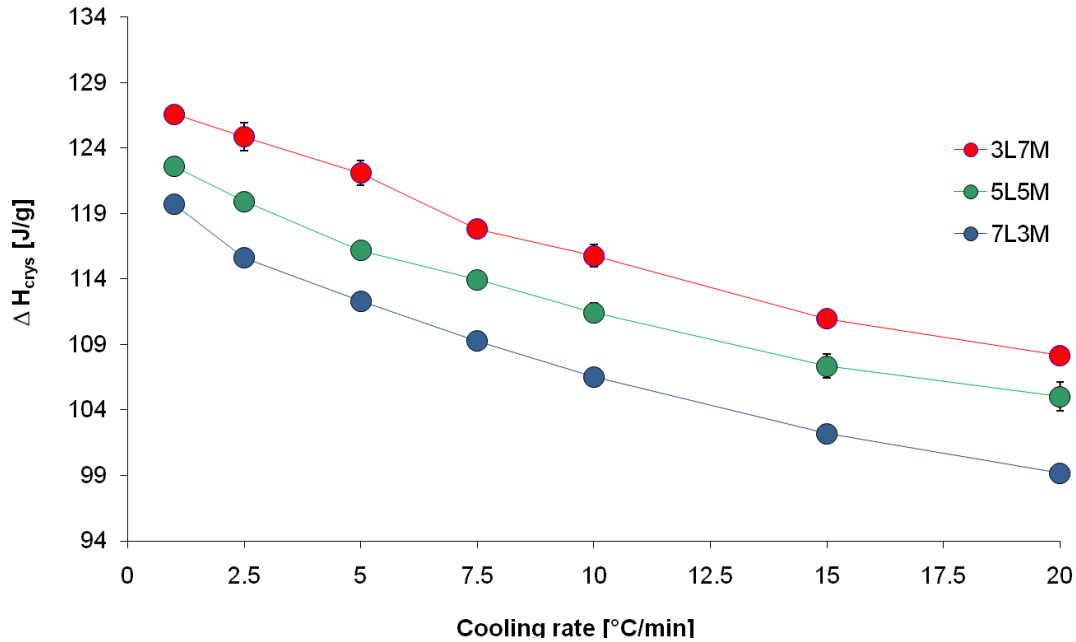
Figure 3-13: Enthalpy of crystallization values at -10 °C for the three binary mixtures at seven cooling rates.

For the binary mixtures, ΔH_{crys} increased with decreasing cooling rate and with higher MMM composition. The increase in enthalpy associated with the increase in MMM concentration is likely due to the fact that MMM has a higher ΔH_{crys} than LLL. The increase with slower cooling rates can be the result of a combination of factors. First of all, it could result from a higher proportion of β' to α. This would have become evident from XRD observations. Though in many cases the α phase appeared at the onset of crystallization, in most cases it actually transformed into β' by the time the sample had reached -10 °C (Anom, 2009). For the blends studied here, the α phase only remained for 3L7M cooled at 20 °C/min. If the polymorphic behaviour is the same, then the differences in enthalpy could only be accounted-for by some energy of mixing. However, the values of enthalpy of mixing a far too large, about 10 % of the enthalpy. The distortion of the phase diagram that would result from this energy does not seem

consistent with the smooth liquidus curve in the work of Takeuchi (2003). Thus, the question was raised if a more precise method should be developed for the measurement of the enthalpies, and if the trend was partially caused by the DSC instrument upon changing the cooling rates. As a result, a very rigorous method was developed, as is described later in this section. The increase in precision from this method allowed to establish that the increase in enthalpy was due in fact to the samples, not to an artefact of the cooling rates. Fortunately, more detailed recent X-ray diffraction observations from this research group have shown that there are two types of β' sub-forms in the mixtures. It is thus likely that the large change in enthalpy is due to different proportions between those two sub-polymorphs. There are no literature values for the enthalpy of crystallization of the sub-forms. The determination of these values is certainly a very important follow-up study to this Thesis.
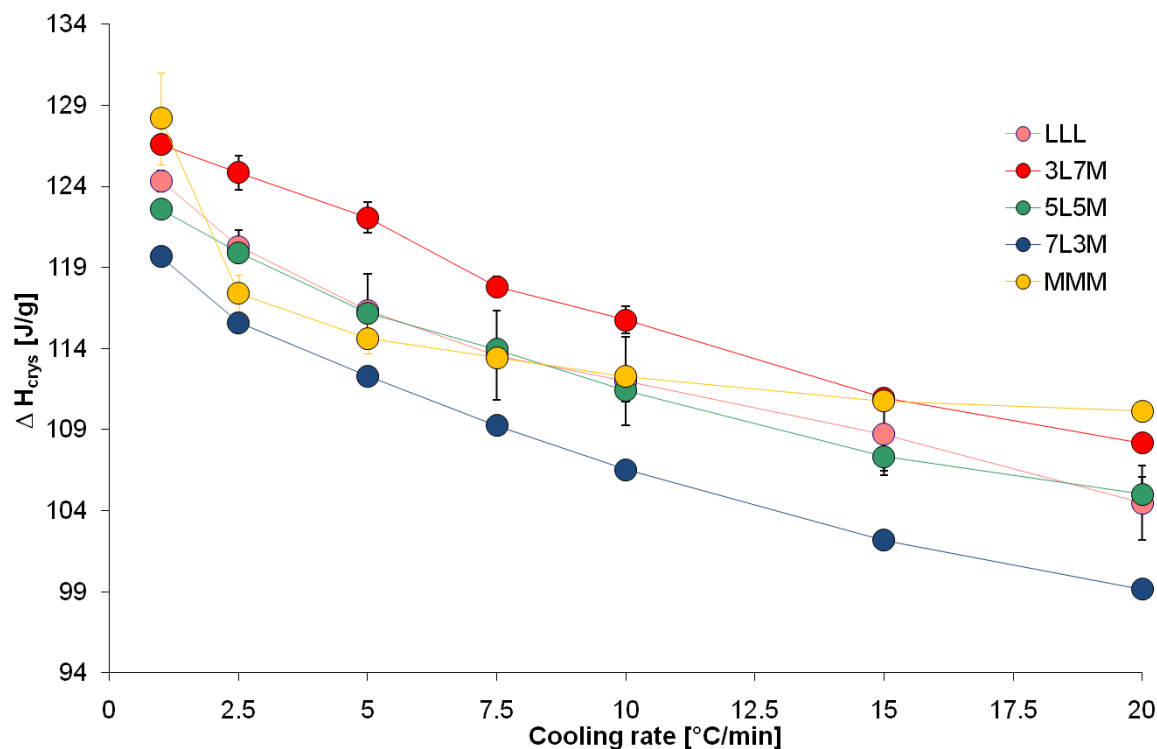
Figure 3-14: Enthalpy of crystallization at -10 °C for all samples at seven cooling rates. (n and SE are in table 3-2).

The pure LLL and MMM did not quite follow the trend of the blends at a fixed rate. While MMM was expected to have the highest ΔH_{crys} values, yet lower values were obtained when cooling rates of 15, 10, 7.5, 5 and 2.5 °C/min were used., On the other hand, ΔH_{crys} values for LLL were surprisingly higher than most of the binary mixtures. In principle, since LLL has a lower carbon number C_n it should exhibit lower thermal values of melting/crystallization points and enthalpies for the same polymorphic form. From the XRD data (Anom, 2009), it was learned that the polymorphs formed by the pure substances were not always the same as those formed by the blends. This was seen by observing the wide angle diffraction patterns. Recent observations by this research group showed that there were at least three distinct variations in the wide angle X-ray diffraction patterns of the β' polymorph, one of them only existed for the pure material,

the other two appeared in the blends. Thus the β' polymorph formed by pure LLL must have a particularly high ΔH_{crys} value. The identification of these sub-forms is now under study.

The values plotted in Figure 3-14 are presented in Table 3-2. Each value is an average of a multiple number, indicated in the table, of measurements for different pans used. The standard error of the mean, SE= $\dfrac{\sigma}{\sqrt{n}}$, for the measurements is also included.

A further test of the reproducibility of the method was conducted with three TAG blends of unknown composition. Two sample pans were prepared from each blend, and the following optimized procedure was employed:

Two pans were prepared with 5-10 mg of sample in each pan. These pans were mass matched to an empty reference pan to within 0.005 mg, and the same reference pan was to be used for all samples. Four measurements were conducted for each sample by performing the scans of the two pans alternately to ensure that all sources of variation to the measurements were taken into account. To account for the variability introduced by using different temperature ramps and placements, pre- and post isothermal periods were used and brought to a heat flow value of 0 W/g using a linear transformation discussed later in section 3.2.2.3. The data analysis to compute the enthalpy of crystallization at a given temperature was done using the running integral method explained above.

The ΔH_{crys} values obtained were between 100 and 129 J/g, one with less than 2 % SE. This confirmed the reproducibility of the results that can be obtained from a DSCQ100 instrument when the adequate protocol is followed.

Table 3-2: The average ΔH_{crys} and corresponding SE for each system at different cooling rates.

Sample	Cooling rate (°C/min)	Number of pans used	Number of runs	Avg. ΔH_{crys} (J/g)	SE (J/g)
MMM	20			110.15	0.4
	15			110.75	0.3
	10			112.28	0.5
	7.5	2	4	113.45	0.5
	5			114.62	0.9
	2.5			117.42	1.1
	1			128.2	2.8
3L7M	20			108.17	0.5
	15			110.96	0.4
	10			115.77	0.8
	7.5	2	6*	117.82	0.6
	5			122.08	1
	2.5			124.86	1.1
	1			126.58	0.6
5L5M	20			105.02	1.1
	15			107.34	0.9
	10			111.42	0.7
	7.5	2	6	113.95	0.6
	5			116.19	0.5
	2.5			119.91	0.6
	1			122.59	0.6
7L3M	20			99.16	0.2
	15			102.17	0.3
	10			106.52	0.3
	7.5	3	9	109.26	0.3
	5			112.32	0.4
	2.5			115.6	0.2
	1			119.68	0.6
LLL	20			104.48	2.5
	15			108.65	2.9
	10			111.62	3.1
	7.5	3	8	113.21	3.1
	5			116.09	2.6
	2.5			120.24	1.2
	1			124.45	0.7

*At 20 ºC/min the number of runs was 4.

The standard error for each mean was lowest for binary mixtures and highest for pure mixtures. The data presented in Table 3-2 included conducting different repetitions using the same pan for a sample in order to assess the repeatability of the sample measurement (instrumental and operator reproducibility) as well as the reproducibility of the measurements when different samples were run. The repeatability of a measurement is defined as "the closeness of the agreement between the results of successive measurements ... carried out under the same conditions of measurements"; (Hohne *et al.*, 2003) and the reproducibility is "the closeness of the agreement between the results of measurements ... carried out under changed conditions of measurements" (Hohne *et al.*, 2003). Measurement conditions comprise the instrument, the observer, the method of measurement and the evaluation procedure. The repeatability and reproducibility of the measurements will be discussed in later sections in more detail.

In the study of physico-chemical properties of lipids, many accounts in the literature are replete with DSC experimental data but not much attention has been paid to describing the DSC thermograms quantitatively or discuss the validity and meaning of the values derived from such thermograms. The DSC signal is an unavoidable product of the combination of different thermal phenomena including the contribution of the instrument and the sample, which makes its interpretation difficult. It is more so in the case of lipids even for simple TAGs, where phase transformations complicate the thermal behaviour under study. It is, therefore, essential to understand and separate these two effects based on, firstly, understanding the kinetics and thermodynamics of the samples and, secondly, understanding the fundamental operational aspect of DSC. For this

reason, the statistical analyses of repeatability and reproducibility of the measurements should be taken into account.

3.1.3 The effect of "take-out-put-back" of the sample pan

The effect of taking the pan out and return it back to the cell, referred to as "take-out-put-back" on the enthalpy values was investigated. ΔH_{crys} values of an MMM sample cooled at 15 °C/min with a mass of 6.049 mg were determined 19 times using the method explained in section 2.2.1.5. Two isothermal segments were performed before and after the crystallization peak at the initial and final temperature, respectively. These isothermal segments were used to account for the variations in the heat flow signals introduced by "take-out-put-back" of the pan. The normalization process used in the three step method, discussed later in section 3.2.2.3, and explained in Appendix B using the "Rotate" function in the Universal Analysis software (TA Instruments) was utilized. Figure 3-15 shows an overlay of 10 runs of MMM (the software does not allow overlaying more runs) as a result of the "take-out-put-back effect". The normalized isothermal periods before and after the crystallization are also shown. The procedure program is given in Appendix D.
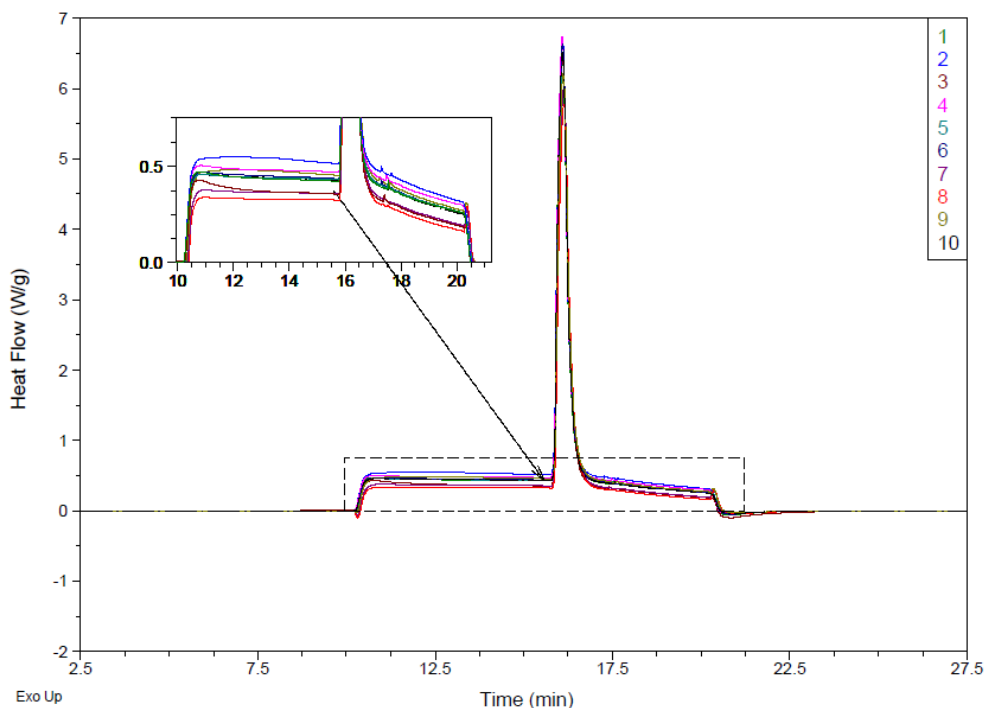
Figure 3-15: An overlay of 10 runs of the crystallization of MMM at 15 °C/min normalized to the isothermal heat flow segments before and after the crystallization event.

The calculated enthalpy of crystallization values are given in Table 3-3. The average enthalpy of crystallization value at -10 °C was found to be 116.70 J/g, with SD=1.32, SE= 0.31, and the calculated $SD/\overline{X}*100$ =1.13 %. The variation in the enthalpy of crystallization as a result of "take-out-put-back" provides the smaller limit for the uncertainty of the values determined. As will be discussed later on in the section about specific heat, these variations are small compared to the variation in the C_p values. This is because the large heat released during the crystallization process, i.e., enthalpy of crystallization, is such that it overrides the small variation in the C_p values caused by the different placement of the pan.

Table 3-3: The enthalpy of crystallization values of MMM calculated at -10 °C using a cooling rate of 15 °C/min with the "take-out-put-back" procedure.

	ΔH_{crys} [J/g]
1	118.24
2	118.26
3	117.88
4	118.89
5	117.02
6	117.19
7	114.61
8	113.26
9	116.73
10	116.78
11	116.26
12	115.92
13	116.30
14	115.91
15	116.58
16	117.18
17	117.13
18	116.51
Average	116.70
SD	1.32 (1.3%)
SE	0.31

If one was to perform four experiments, then the expected standard error of the mean would be 1.32/2 = 0.66, which is 0.5 % of the mean. Hence this seems to be a reasonable number of reproductions to recommend, so that the effect of two pans and two placements can be averaged out.

3.2 Results and Discussion II: Specific Heat

3.2.1 Determining the specific heat using DSC

The strong interest in determining the specific heat capacity, C_p, values for the samples under study emerged as a means to distinguish between different crystalline forms created after having a sample crystallized at different cooling rates. It was also important to know the C_p values in cases where the undercooling of the material was to be larger than 10 °C (Los & Floter, 1999). The C_p is needed in those cases to estimate changes in enthalpy due to temperature. It was observed that the material had different heat flow measurements under a fixed heating rate, after cooling to form it at different rates. Figure 3-16 shows the crystallization traces of 3L7M at different cooling rates with subsequent heating at 5 °C/min up to 80 °C, following an isothermal period of 10 min at - 15 °C. The obviously different melting profiles show that the final phase distribution is different for different cooling rates, but is very difficult to interpret.
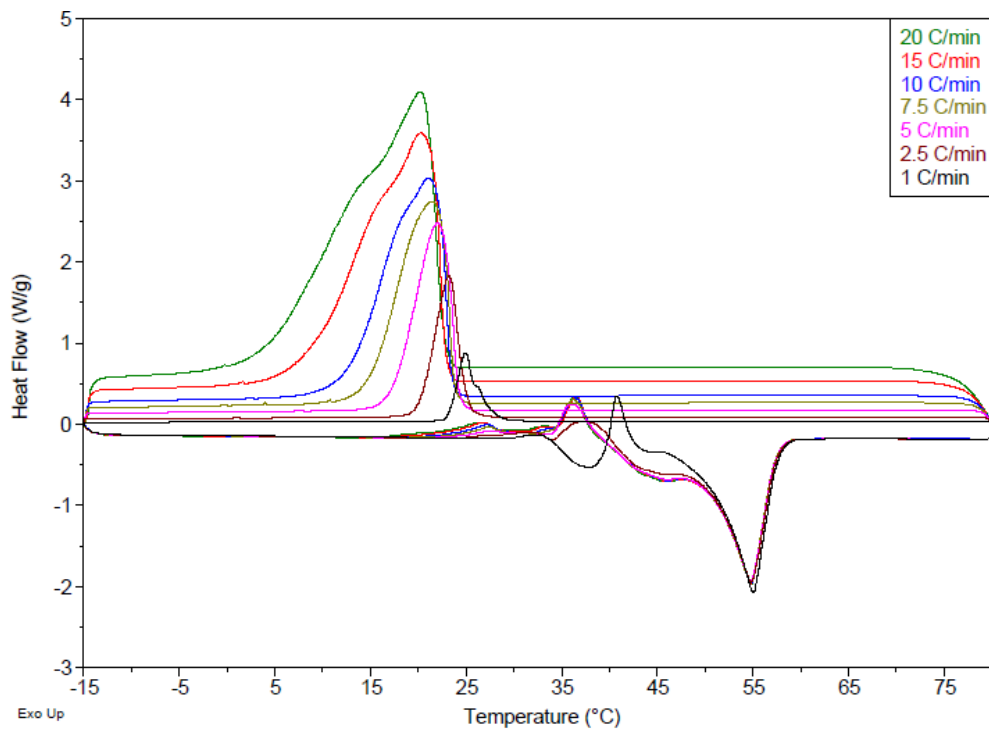
Figure 3-16: The crystallization of 3L7M from the melt using different cooling rates, and the subsequent melting traces at 5 °C/min.

Figure 3-17 shows the magnified heating traces at °5 C/min of the crystalline phases produced with different cooling rates. The different heat flow values indicate the presence of crystalline phases with different C_p values, and thus with different crystalline structure.
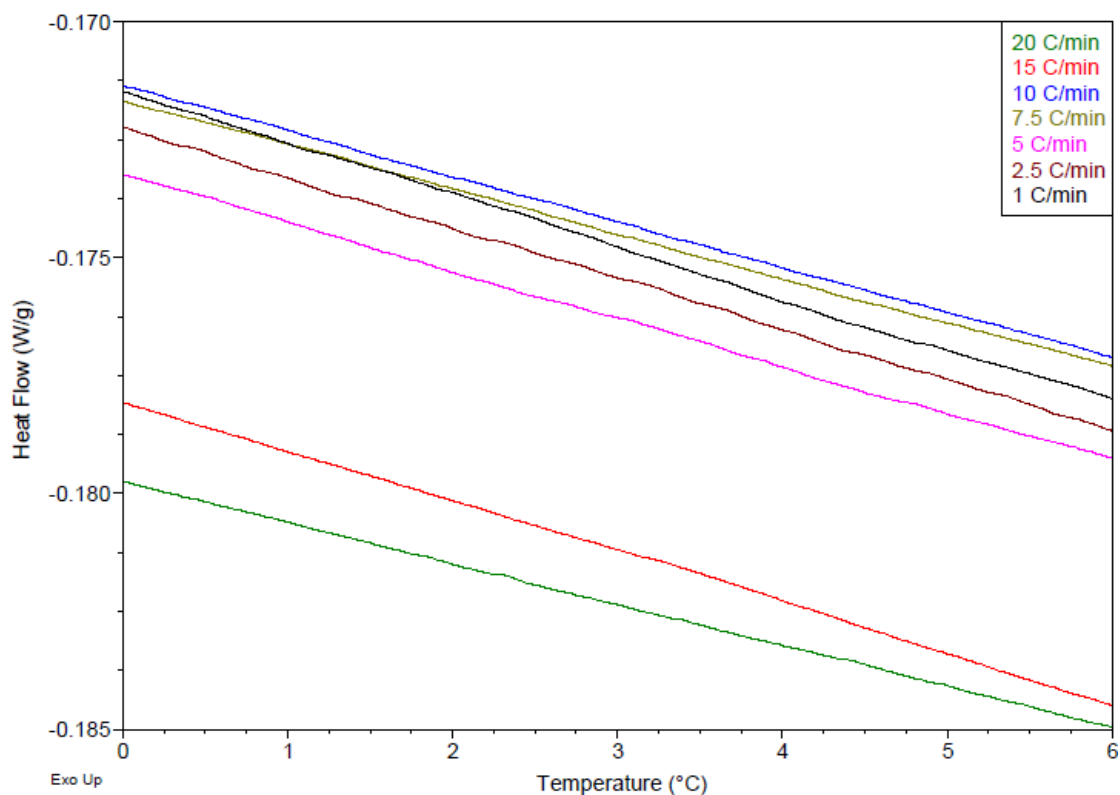
Figure 3-17: Magnified heat flow traces of 3L7M during subsequent heating at 5 °C/min shown in Figure 3-16.

Figure 3-17 shows that the crystalline phases produced using cooling rates of 20 and 15 °C/min are quite different from those obtained at slower cooling rates. The negative values for the heat flow come from the sign of ΔT used in the four-term heat flow equation, i.e., equation [2-1]. ΔT is the measurement signal used in equation [2-1] is an instantaneous consequence of the C_p difference between the sample and the reference pan at a given temperature.

When the furnace is heated at a fixed rate, the reference pan heats faster than the sample. The difference is proportional to the heat capacity difference between the two, since the heat capacity of the sample is larger than the heat capacity of the reference pan. For this reason, heat flow measurements generated during heating are reported as negative (negative ΔT) whereas it becomes positive (positive ΔT) on cooling since the

sample will build up a temperature gradient and hence the sample temperature will always be higher than the reference. If the instrument was absolutely symmetrical, the heat flow value produced on heating should be the same as that on cooling but of opposite sign, at a given temperature and rate. This means that the larger the negative values, the larger the heat capacity value in absolute terms.

The different phases formed at different cooling rates could be, for example, different proportions of two polymorphic forms. In this case one could attribute the higher and lower C_p values obtained at high and low cooling rates to a higher content of α phase and higher content of β' phase respectively.

In an ideal DSC the C_p values would be directly calculated through the following equation:

$$\frac{dQ}{dT} = C_p \frac{dT}{dt}$$
[3-1]

where $\frac{dQ}{dT}$ is the heat flow and $\frac{dT}{dt}$ is the underlying heating or cooling rate. However, in a real DSC other factors are included, and a better equation would be equation [2-1]. Yet, as has been discussed so far, even equation [2-1], provides at best a "pseudo C_p" for the samples, calculated in units of J/g°C since the heat flow signals are already normalized to the sample mass. The values obtained are pseudo C_p as these values do not actually correspond to the actual C_p values of the sample, but rather to values that are dependent on other factors such as thermal lag. Therefore, a more elaborate data treatment is necessary to obtain the real C_p values. Since the pseudo C_p values of the samples were calculated from regions where there is no phase transition, having a smooth, flat baseline is crucial to obtaining reliable data. This is because the signal is

small compared to the background, whereas during first order phase transitions the signal is much larger.

In order to test the confidence in the C_p values obtained for different crystalline phases at the end of cooling, it was a prerequisite to be able to precisely measure the C_p in the liquid state. The knowledge of liquid heat capacity values is important for the following reasons:

1) The measurement of the C_p in the liquid state is much simpler because the liquid is a single phase of homogenous composition. In other words, there are no different crystalline phases that could be of different polymorphic type and/or different compositions. In heating it is more likely that, through natural convection, the temperature gradient through the sample is smaller than in a solid TAG. ; 2) The literature is rich with reports of C_p values in the liquid state, obtained either directly from calorimetric experiments or indirectly through estimations and modeling based on composition and structure (Morad *et al.*, 2000; Phillips & Mattamal, 1976). It is well known that the C_p values are linearly proportional with temperature in the liquid state (Morad *et al.*, 1995b; Santos *et al.*, 2005; Zabransky *et al.*, 2001); 3) It is much easier to examine the effect of varying operational parameters on the samples such as heating and cooling rates, samples mass, pan type ,etc., and thus any necessary correction to account for these effects can be calculated and could possibly be used as a reference for the C_p values obtained in the solid state; and 4) since the enthalpy values were calculated by subtracting the integrated heat flow values in the solid state from the extrapolated line fitted to the data in the liquid state, the knowledge of the actual C_p values in the liquid is crucial since it is the reference in this calculation.

For these reasons the determination of C_p values in the liquid state was intensively studied and different experimental effects on the final C_p measurements were also investigated in detail.

Since the numerical value of heat flow as a function of temperature is the main experimental measurement for the calculation of pseudo C_p according to equation [3-1], it will be used as the determining measurement for the following comparisons, for simplicity. Schick (2009) was not, however, in favour of presenting the sample measurements in units of heat flow rate. It could be argued that the reasons listed in that work could be applicable for the instrument used (Perkin Elmer DSC) and not to TA DSC Q1000 with Tzero^{TM}. With a DSC Q1000 instrument the heat flow rate measurements are dealt with as absolute signals from which supposedly absolute C_p values are directly obtained (Cassel, 2001). However, the only difference between that instrument and the Q100 used in this Thesis is a software feature. The Q1000 allows for the input of the mass of the reference and sample pans, and compensates for that difference. In this Thesis it was painstakingly ensured that the pans, which usually weigh about 56 mg, where within 0.005 mg of each other, thus rendering that correction unnecessary.

3.2.2   Factors affecting the measurements

The only signals that are actually measured in the DSC instrument used in this Thesis are the voltages across the thermocouples, used to calculate the temperatures at their junctions. These temperatures are converted into heat flow signals using equation [2-1]. Therefore, the effects of experimental factors on the measured temperatures are discussed below.

3.2.2.1   Sample size

In order to elucidate the dependency of heat flow values in the liquid state on the sample size, four different sample sizes of OOO were measured and sealed hermetically in Al pans. The sample masses were chosen to be 2.5, 5, 7.5 and 10 mg ±0.005 mg. OOO was chosen for this investigation because its melting temperature, i.e., the β polymorph at 5 °C (Ferguson & Lutton, 1947), is much lower than those for MMM and LLL and hence allows for a longer operational temperature range in the liquid state to perform the investigation. Its reported C_p values in the liquid state are, furthermore, not too different from those of MMM and LLL. Figure 3-18 shows the heat flow signals during heating and cooling of OOO at a temperature ramp of 10 °C/min for four OOO samples with different masses as indicated by different colors. As can be observed, the sample mass of 2.5 mg shows a significant decrease in the heat flow per unit mass measurement compared with the other samples. For example, the measured heat flow values at 50 °C for a heating rate of 10 °C/min were found to be -0.189 ±0.002, -0.321 ±0.001, -0.333 ±0.002 and 0.314 ±0.001 J/g for 2.5, 5, 7.5 and 10 mg samples ,respectively. If C_p values were calculated using these values, in relation to the values obtained by Morad *et al.*

88

(2000), the 2.5 mg sample would yield a difference in pseudo C_p of about 45%. However, the 5, 7.5 and 10 mg sample would produce variations of about 6.7, 3.1 and 8.7 %, respectively.
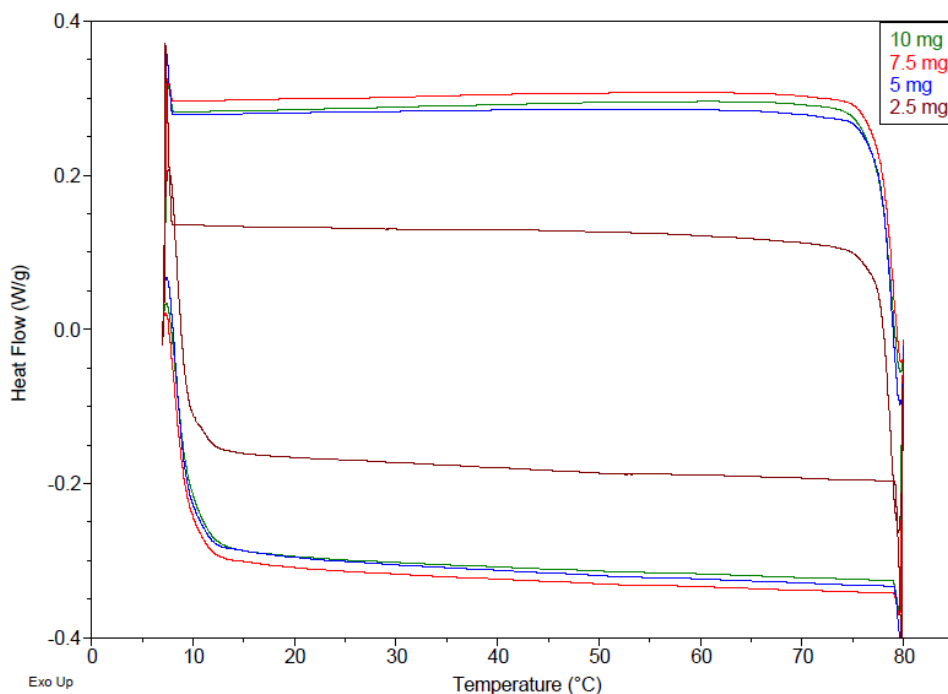
Figure 3-18: Heat flow traces of OOO of different masses in the liquid state using a heating and cooling rate of 10 °C/min in the liquid state. Each trace was conducted three times.

Figure 3-19 shows the heat flow values measured upon both heating and cooling at 10 °C/min obtained at 50 °C for OOO. The difference between the heat flow measurements during cooling and heating decreased as the sample mass increased.
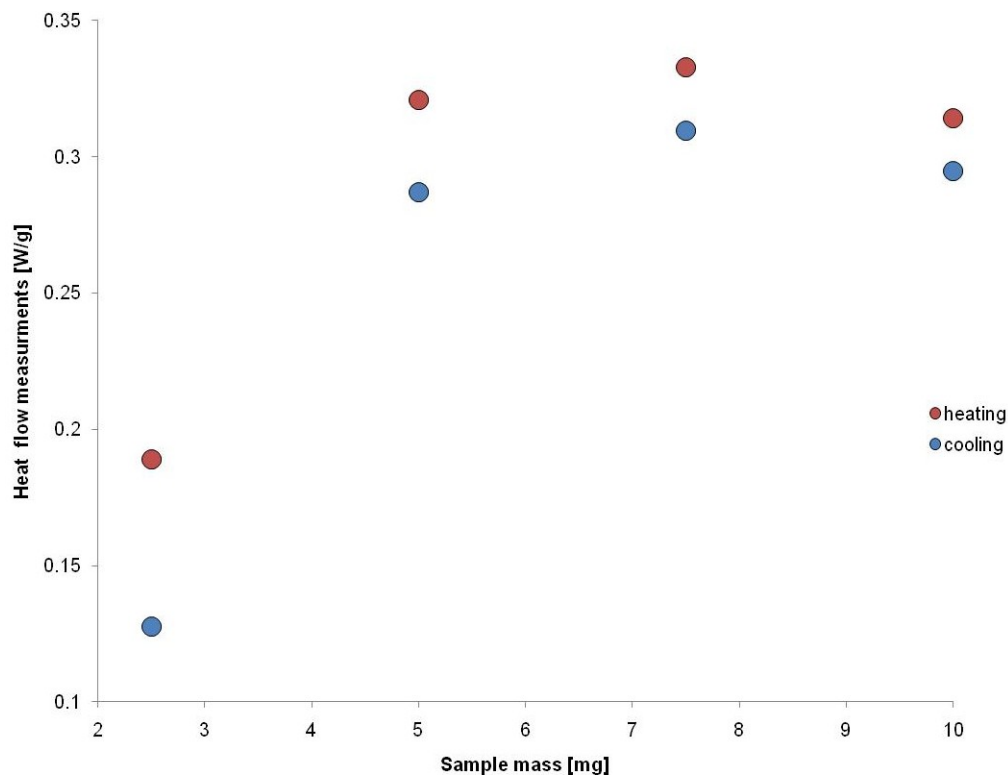
Figure 3-19: The measured heat flow signals (absolute values) of OOO sample at 50 °C during heating and cooling at 10 °C/min for different sample masses.

This effect of low sample mass yielding low heat flow measurements was observed for all heating and cooling rates. Figure 3-20 shows a comparison between using two different sample sizes, 10 and 2.5 mg, on the final heat flow measurement at all cooling and heating rates explored. The heat flow per unit mass was lower in the 2.5 mg sample than that of the 10 mg sample at all cooling and heating rates. The difference decreased considerably as the temperature ramp used was reduced.
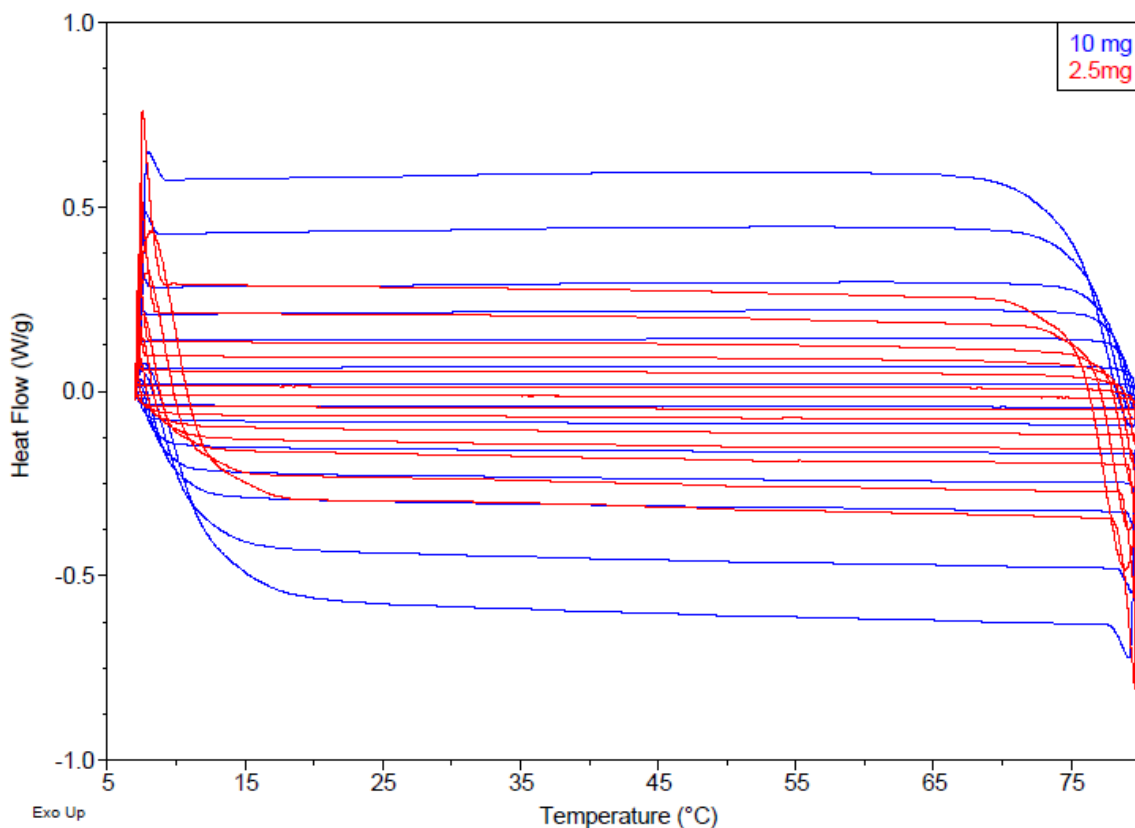
Figure 3-20: Heat flow measurements of two different sizes of OOO in the liquid state during heating and cooling at different temperature ramps. Each trace was conducted three times.

The heating and cooling traces can be distinguished from each other from the transient temperature responses occurring at the beginning of the temperature ramps. The cooling and heating heat flow traces have different transient responses to the underlying cooling and heating rates at about 80 and 7 °C, respectively. The faster the temperature ramp the longer it takes to reach stable heat flow so it is necessary to start from temperatures beyond the thermal event of interest, especially when using rapid temperature ramps.

Figure 3-21 shows the corresponding heat flow measurements at different heating and cooling rates for two sample sizes of OOO taken at 50 °C.
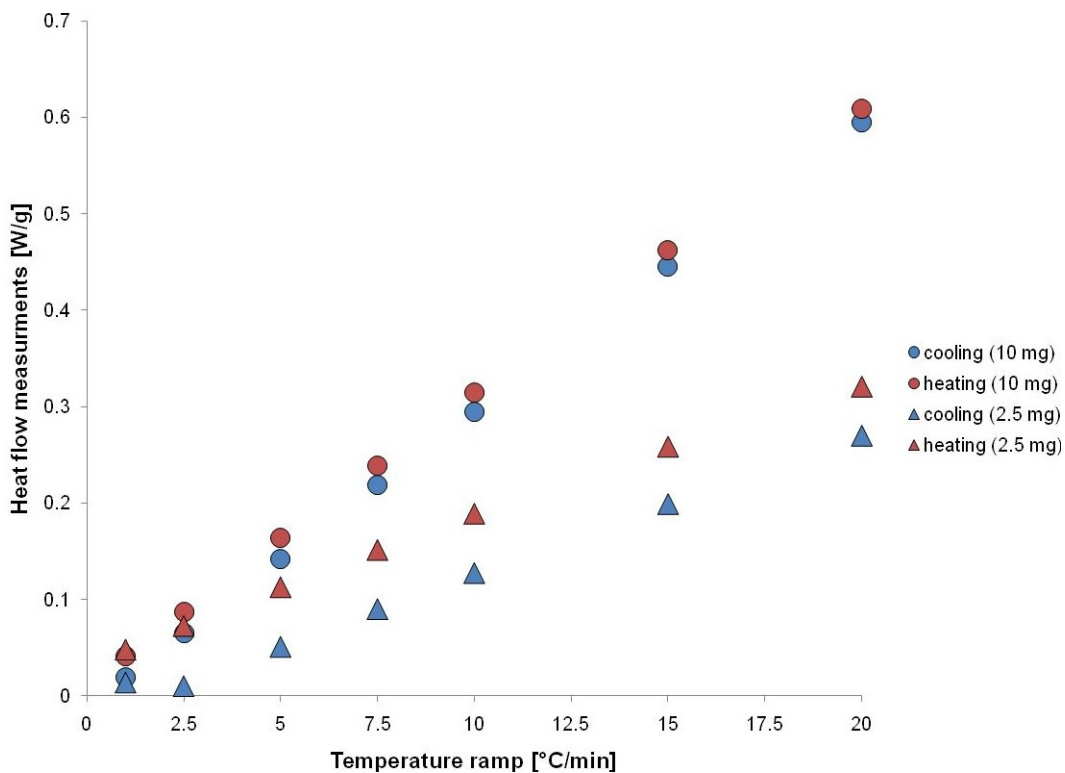
Figure 3-21: The measured heat flow (absolute values) of OOO sample at 50 °C during several heating and cooling rates for two sample masses (n=3).

The difference between the heating and cooling signal decreased as the sample mass increased. Probably the larger absolute signal from the large samples is less sensitive to the small variation introduced by the cooling and heating baselines. Additionally, some of the smaller samples were not even able to cover the whole surface of the pan as observed during sample preparation, though the ratio of sample to contact area is still unknown.

Other studies recommend that the sample mass should scale inversely with temperature ramp (Schick, 2009). For low rates, it is recommended to use higher sample masses to get a good signal-to noise ratio whereas a small amount of sample should be

used at higher rates to minimize the thermal lag effect (Schick, 2009). However, the data in Figure 3-21 show that for samples that are too small this does not apply. The type of the sample container used in the present study was an Al hermetic pan with maximum capacity allowance of 20 µL. The sample size recommended by TA Instruments for the determination of C_p is from 10 to 70 mg at a heating rate of 20 ºC/min. These conditions must, however, take into consideration the thermal conductivity and thermal diffusivity of the sample to be studied as heat flows differently with different samples even under the same experimental conditions. Metallic materials have good heat conducting capabilities and hence have almost uniform temperature distribution within the sample. In the case of materials with low thermal diffusivity, on the other hand, the heat capacity values will be greatly affected by the sample size since there will be an extra thermal resistance introduced by the sample itself. Consider, for instance, that the heat conductivity of Al is one thousand times larger than that of the organic thermoplastic polymer PET (Xu *et al.*, 2000).

3.2.2.2 Temperature ramp

It is important to have the heat flow measurements normalized for their respective heating and cooling rates in order to elucidate the rate effects and make the measurements comparable. Having done so, the signals produced will be pseudo C_p in units of J/g °C as a function of temperature. Figure 3-22 shows the heat flow signals as a function of temperature for different heating and cooling rates with 10 mg of OOO sample in the liquid state.
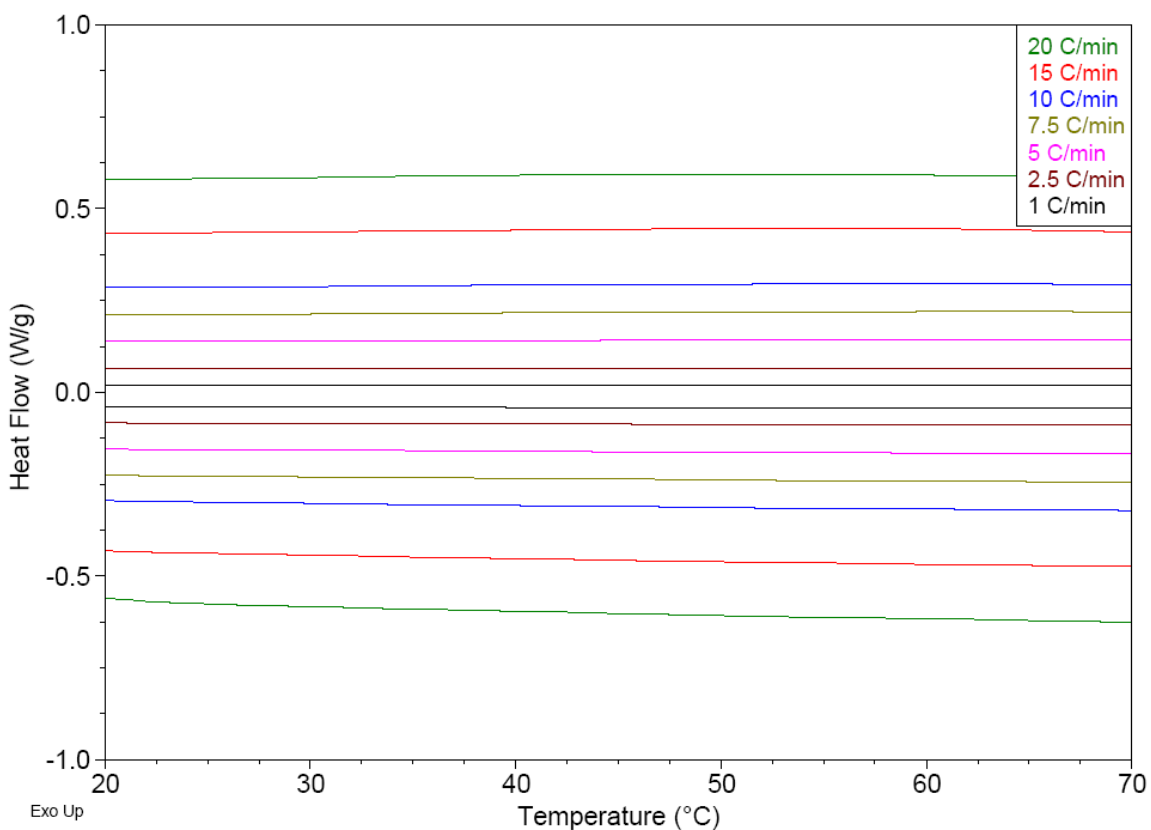
Figure 3-22: Heat flow measurements as a function of temperature using different temperature ramps with 10 mg OOO sample in the liquid state.

In Figure 3-23, the corresponding pseudo C_p values as a function of temperature at different heating and cooling rates are shown whereas in Figure 3-24, the pseudo C_p values as a function of different cooling and heating rates at 50 °C is shown.
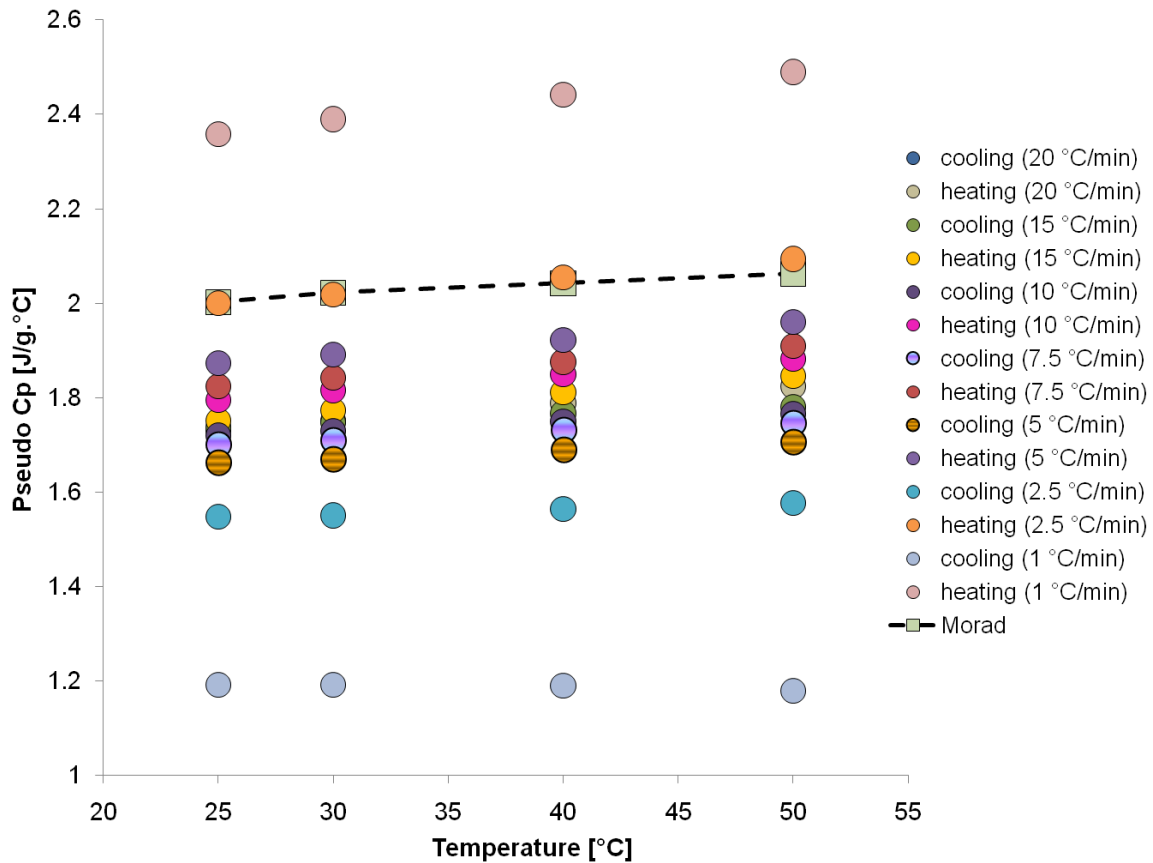
Figure 3-23: Pseudo C_p values as a function of temperature at different heating and cooling rates for OOO with a sample mass of 10 mg (n=3), compared to values obtained by Morad *et al*. (2000).
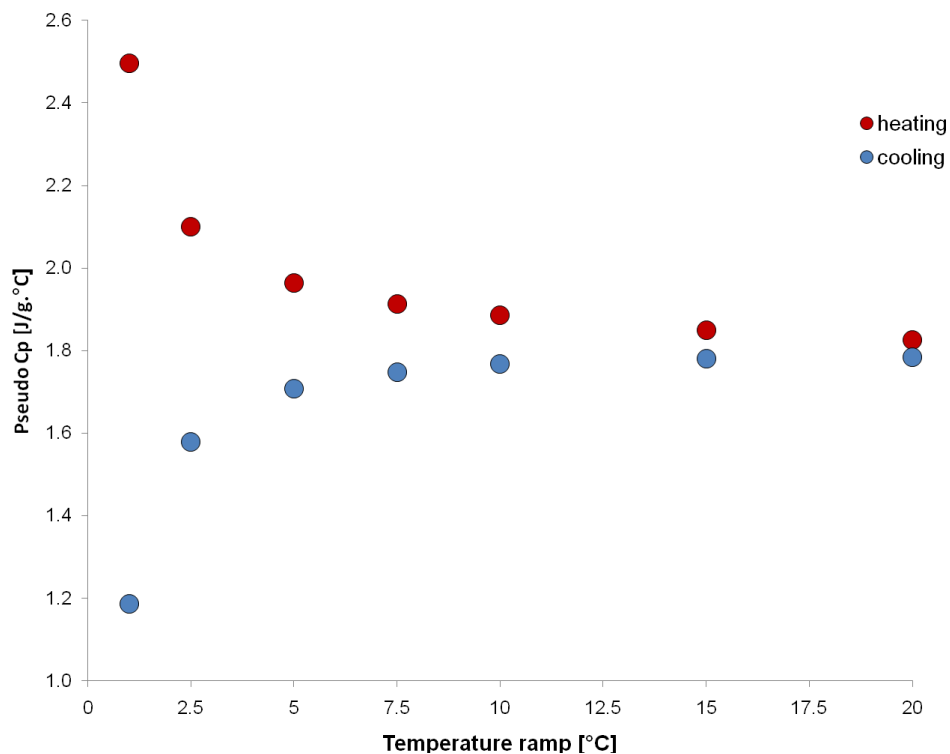
Figure 3-24: Pseudo C_p values taken at 50 °C as a function of different temperature ramps for OOO with a sample mass of 10 mg (n=3).

As shown in Figure 3-24, the highest pseudo C_p values were produced when heating rates of 2.5 and 1 °C/min were employed, whereas the lowest values were found during cooling under the same temperature ramps. Another observation is that the variability in pseudo C_p values produced during heating was a little larger than that obtained on cooling for temperature ramps between 5 and 20 ºC/min. The values during heating regimes were also found to be slightly larger than those during cooling. The pseudo C_p values obtained at different cooling and heating rates are given in Table 3-4.

Table 3-4: Pseudo C_p values for 10 mg of OOO sample (n= 3) at different heating and cooling rates at different temperatures.

T [°C]	Temperature ramp [°C/min]	Pseudo C_p [J/g°C] Heating	Cooling
20	20	1.685 ±0.004	1.739 ±0.003
30		1.753 ±0.003	1.758 ±0.003
40		1.791 ±0.003	1.776 ±0.002
50		1.826 ±0.002	1.784 ±0.002
20	15	1.732 ±0.003	1.731 ±0.002
30		1.778 ±0.003	1.749 ±0.002
40		1.816 ±0.004	1.769 ±0.002
50		1.850 ±0.004	1.781 ±0.002
20	10	1.771 ±0.003	1.713 ±0.003
30		1.819 ±0.003	1.731 ±0.002
40		1.853 ±0.003	1.752 ±0.002
50		1.886 ±0.004	1.768 ±0.002
20	7.5	1.807 ±0.005	1.695 ±0.002
30		1.847 ±0.005	1.712 ±0.002
40		1.880 ±0.004	1.733 ±0.002
50		1.913 ±0.004	1.749 ±0.002
20	5	1.862 ±0.005	1.657 ±0.002
30		1.897 ±0.005	1.672 ±0.003
40		1.929 ±0.005	1.691 ±0.002
50		1.963 ±0.005	1.708 ±0.002
20	2.5	1.988 ±0.004	1.542 ±0.002
30		2.025 ±0.005	1.552 ±0.002
40		2.061 ±0.006	1.566 ±0.003
50		2.100 ±0.006	1.579 ±0.001
20	1	2.342 ±0.004	1.199 ±0.010
30		2.392 ±0.003	1.195 ±0.004
40		2.446 ±0.002	1.190 ±0.002
50		2.497 ±0.007	1.186 ±0.009

All comparisons of C_p values for OOO samples were made against the values reported by

Morad *et al.* (2000) as shown in Table 3-5.

Table 3-5: C_p values as a function of temperature for OOO samples as reported by Morad *et al.* (2000).

T[°C]	C_p [J/g°C]
50	*2.0627*
60	2.0827
80	2.1227
100	2.1627
120	2.2027
140	2.2427
160	2.2827
180	2.3227

These values were obtained using improved conditions mentioned in an earlier work (Morad *et al.*, 1995a), i.e., heating rate of 17 °C/min, a sample mass of 21 mg and a N_2 flow rate of 50 mL/min using a Seiko 220 heat flux DSC. It should be noted that the C_p value at 50 °C was not reported but was calculated using a linear relation fitted to the other data with $R^2=1$, the linear relation used was:

C_p (J/g.°C) = 0.002*T (°C) + 1.9627

One of the observations on the C_p values given in Table 3-4 and plotted in Figures 3-23 and 3-24 is that all the values increased as the heating rate decreased while the opposite trend is observed on cooling at all temperatures. This observation could raise the question of why almost always the C_p values reported in the literature using DSC are given during heating and not on cooling. Is it possible to draw a conclusion that the best heating rate to obtain the "accurate C_p" value is to use a heating rate of 2.5 °C/min and a mass of 10 mg since it is the closest to the reported value? In the work of Morad *et al.* (1995a) it was mentioned that "The sample mass is implicitly related to the temperature ramp. Perhaps each temperature ramp has an optimum sample mass". This creates a sort of circular

problem, yet to be solved, as is often the case when discussing accuracy of measurements and generation of reference values.

In Morad's (1995a) work, five LLL samples with masses of 10, 16, 21, 25 and 35 mg were used with a heating rate of 17 °C/min. This heating rate was selected amongst others investigated (6, 10, 15, 17, 20 and 23 °C/min). Similarly, a sample mass of 21 mg was concluded to be the optimum as it produced the lowest standard deviation value among the other runs. It was found that a sample mass of 21 mg was the same as recommended by the manufacturer, when different samples masses were examined. However, it was not mentioned in their work why these sets of sample masses and heating rates were selected and not others. One can argue that different results may be obtained if the sample masses and heating ramps were different from the ones investigated, or if the instrument used was different from Seiko 220 heat flux DSC (Japan) but the same improved conditions were used. In spite of that, their work seem to provide the most trustworthy data in the literature since they used Round-Robin test where the measurements are done in different places using different instruments (Morad *et al.*, 1995a). Unfortunately it was not reported if the instruments were all the same model or not. Another point to consider here is that when materials with low thermal conductivity, such as TAGs, are investigated using calorimeters, it is expected to have results that are precise but inaccurate (Kennedy *et al.*, 2007). This effect is even more pronounced when large sample sizes are selected for their self-insulating properties (Martin *et al.*, 1992). Thus having a known and defined heat capacity value of the same material in internationally recognised standards is important to assess the accuracy of the measurements. Sadly, there are no standards for TAGs yet.

In the work of de Barros *et al.* (1995), the effect of using different combinations of sample masses of sapphire and heating rates on the accuracy and precision of resultant C_p values were investigated using a Setaram DSC 121 (France). Four heating rates were investigated, 1, 2, 5 and 10 °C/min. It was found that for heating rates more than 2 °C/min the accuracy decreased significantly as the heating rate increased, however the precision of the results did not show a significant variation except at 10 °C/min. Also, for the three different sample sizes investigated, it was reported that accuracy and precision decreased with decreasing sample mass. TAGs have much less thermal conductivity (ca. 0.2 W/m.K) than sapphire (ca. 20 to 17 W/m.K between 20 and 70 °C) and hence they are expected to exhibit a stronger effect on the accuracy and precision of the final heat capacity values. In the work of Morad *et al.* (1995a) in determining the improved conditions to acquire reproducible C_p values for TAGs using heat flux DSC, it was reported that values with precision of ±1% up to 220 °C can be obtained. However, there was no mention of the accuracy of the values.

All the aforementioned experiments were performed during heating. Upon cooling the determination of Cp would be even more difficult since most DSC instruments are not equipped for cooling calibration, though for the sake of this research it is important since the relevant experiments are precisely done on cooling. During heating the phases of the materials undergo several transformations, and we are interested in measuring the phases as they are, rather than try to elucidate what they were as we destroy them by heating.

3.2.2.3 Reduction of temperature ramp effects by using the three step method

The determination of the absolute C_p values using DSC of different materials has been mostly performed with reported accuracies around 3-5% (Bernardes *et al.*, 2006). The measurement involves three consecutive runs under an identical thermal regime. The first run is recorded using two empty pans. The second run is carried out with a material (usually a sapphire disc) with a known C_p value in a wide temperature range. The sapphire disc is placed in the sample pan and the temperature program is repeated. Finally, the sapphire sample is replaced by a known amount of a sample with unknown C_p and the same temperature program is run again. During this procedure, the same two pans should be used throughout the procedure. This procedure is known in the literature as the classical three step method (Hohne *et al.*, 2003). The procedure is described and illustrated in detail by ASTM (ASTM-E1269, 2005).

The C_p values for the OOO samples were measured at different cooling and heating rates using this method enhanced by a signal normalization procedure. It was ensured that the reference and the sample pans were weight-matched to within ±0.005 mg. All the sample masses were chosen to be about 4 - 6 mg ±0.005 and the pans were not crimped throughout the procedure. Attention was also paid to place the sample pans on a centered position on the post while the reference pan remained unchanged. The C_p calculations were made manually since it was not possible to perform them automatically using the specialty library in the Universal Analysis software (TA Instruments) software. It was ensured that stable isothermal segments were obtained before and after the heating ramp. When the three data files (baseline, sapphire, and sample) were collected, it was necessary to make the signals comparable to perform the calculation. This was done by

applying a normalization process over the isothermal periods. This step, unfortunately, was not very clear in the ASTM method and is more clarified in the technical note by Hesse (2010) who is a TA Instruments engineer. The normalization procedure for the data is described in detail in Appendix B (Hesse, 2010).

The three traces (baseline, sapphire, and sample) from which heat flow values were extracted for MMM are shown in Figure 3-25. The C_p values were calculated with the following equation using the three step method (Diedrichs & Gmehling, 2006; Hohne *et al.*, 2003):

$$C_{P\,sample} = \frac{\dot{Q}_{sample} - \dot{Q}_{empty}}{\dot{Q}_{reference} - \dot{Q}_{empty}} \frac{m_{reference}}{m_{sample}} C_{P\,reference} \qquad [3\text{-}2]$$

where $\dot{Q}$ and m represent the heat flow and the sample mass respectively.
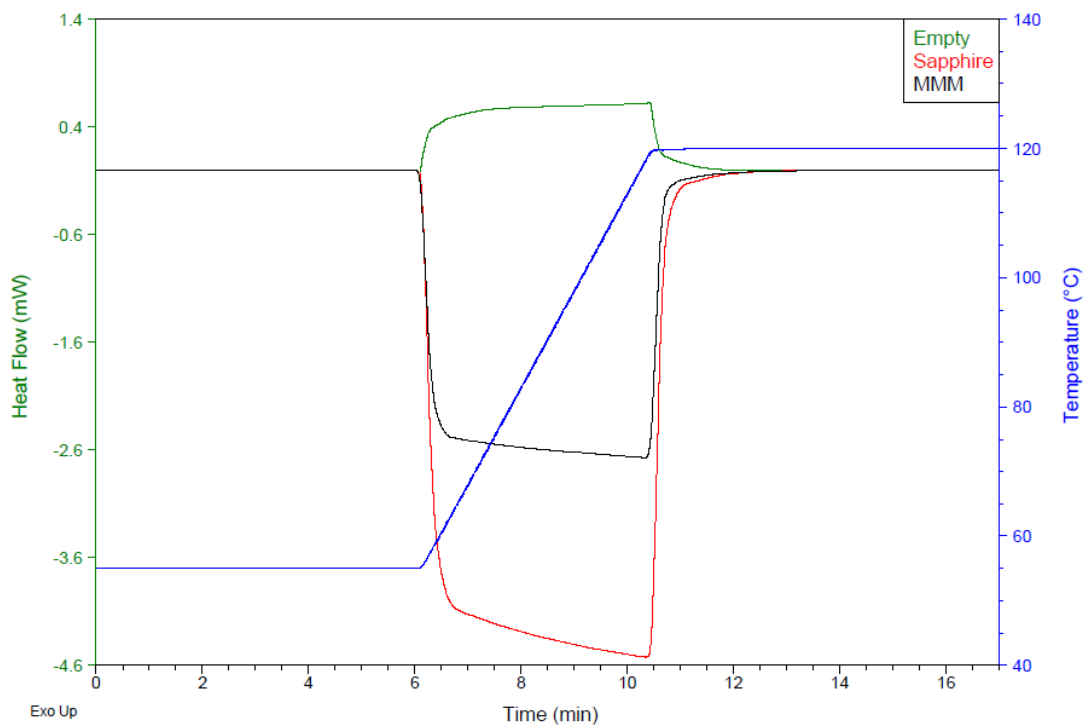
Figure 3-25: Normalized heat flow traces of empty pans (baseline), sapphire, and MMM sample using a heating rate of 15 °C/min.

All the measurements were carried out in the liquid state over a temperature range from 55 to 120 °C. For each experiment, three heating and cooling runs were carried out alternatively using the same temperature ramp. The temperature ramp was chosen to be 15 °C/min because the instrument was calibrated at this temperature ramp. Furthermore, when the three step method was utilized at different heating and cooling rates all the results showed a very small dependence on the temperature ramp for the OOO sample as shown in Figure 3-26. The pan was not removed from the furnace and the equipment was not disturbed in any way.
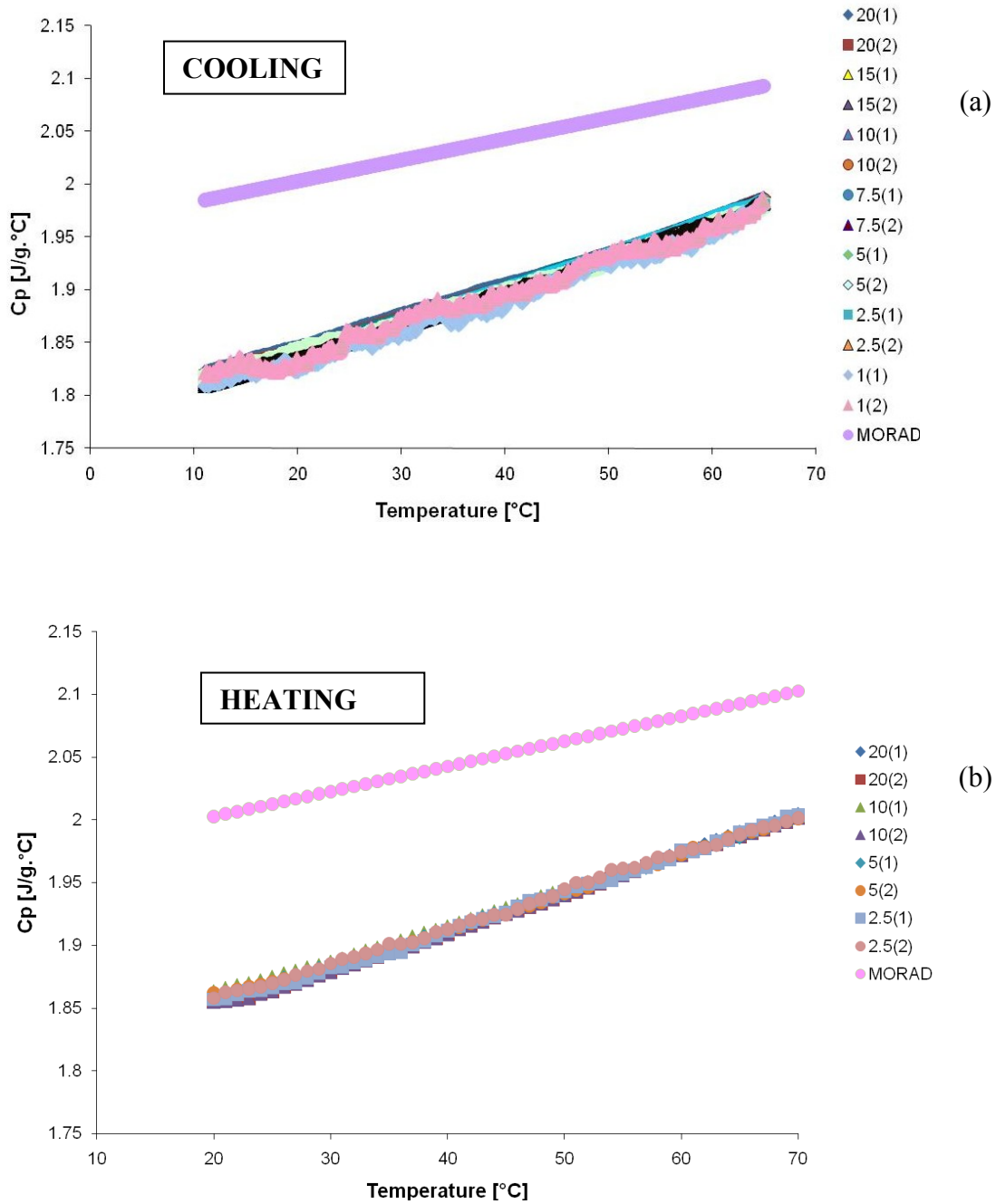
Figure 3-26: C_p values vs. temperature for OOO samples during (a) cooling and (b) heating at different temperature ramps. Each measurement was performed thrice. The values by Morad *et al.* (2000) are also included for comparison.

The values found for the OOO sample were obtained with a sample mass of 6.361 ±0.005 mg using the same experimental conditions. The C_p values were expected to be

larger if larger samples had been used. The objective here was to test the hypothesis that with the use of the three step method, no apparent influence of the temperature ramps would be found, and this was confirmed. The temperature ranges for Figure 3-26 displayed in the heating plot start and end at higher temperatures than the cooling plot. This is because there is a transient segment at the beginning of the cooling ramp (high temperature) and of the heating ramp (low temperature). The data clearly lie on the same line, showing the effectiveness of the three step plus normalization method to remove the effect of cooling rates. They both show a clear linear dependency on temperature. However, the values themselves are not only different from Morad's *et al.* (2000), but also differ in their slope and intercept, which describe their temperature dependence. The difference is likely due to the effect described in the next section.

3.2.2.4 Effect of "take-out-put-back" the sample pan

Further experiments were conducted to evaluate the reproducibility of the measurements of the C_p values obtained for the liquid state of MMM, LLL and 5L5M. All the conditions used before were used during cooling and heating with a temperature ramp of 15 °C/min. The results of a first run are shown in Figure 3-27. Very small variations in the C_p values were observed between heating and cooling. C_p values were the highest for MMM, lowest for LLL, and intermediate for 5L5M, which makes sense. This trend was to be expected since MMM has higher carbon number than LLL, and 5L5M is a mixture of both. The experiment was done in the temperature range 55-120 °C where no crystallization could possibly take place. Each sample was run once with three heating and cooling regimes performed alternatively during the same experiment. The conditions used with the OOO sample were also employed for LLL, MMM and 5L5M, i.e., pan masses, pan positioning and non crimped pans. The sample masses were 5.400, 4.345 and 4.758 mg ±0.005 mg for MMM, LLL and 5L5M, respectively. The C_p values were much larger for MMM and much lower for LLL, when compared to values obtained by Morad *et al.* (2000).
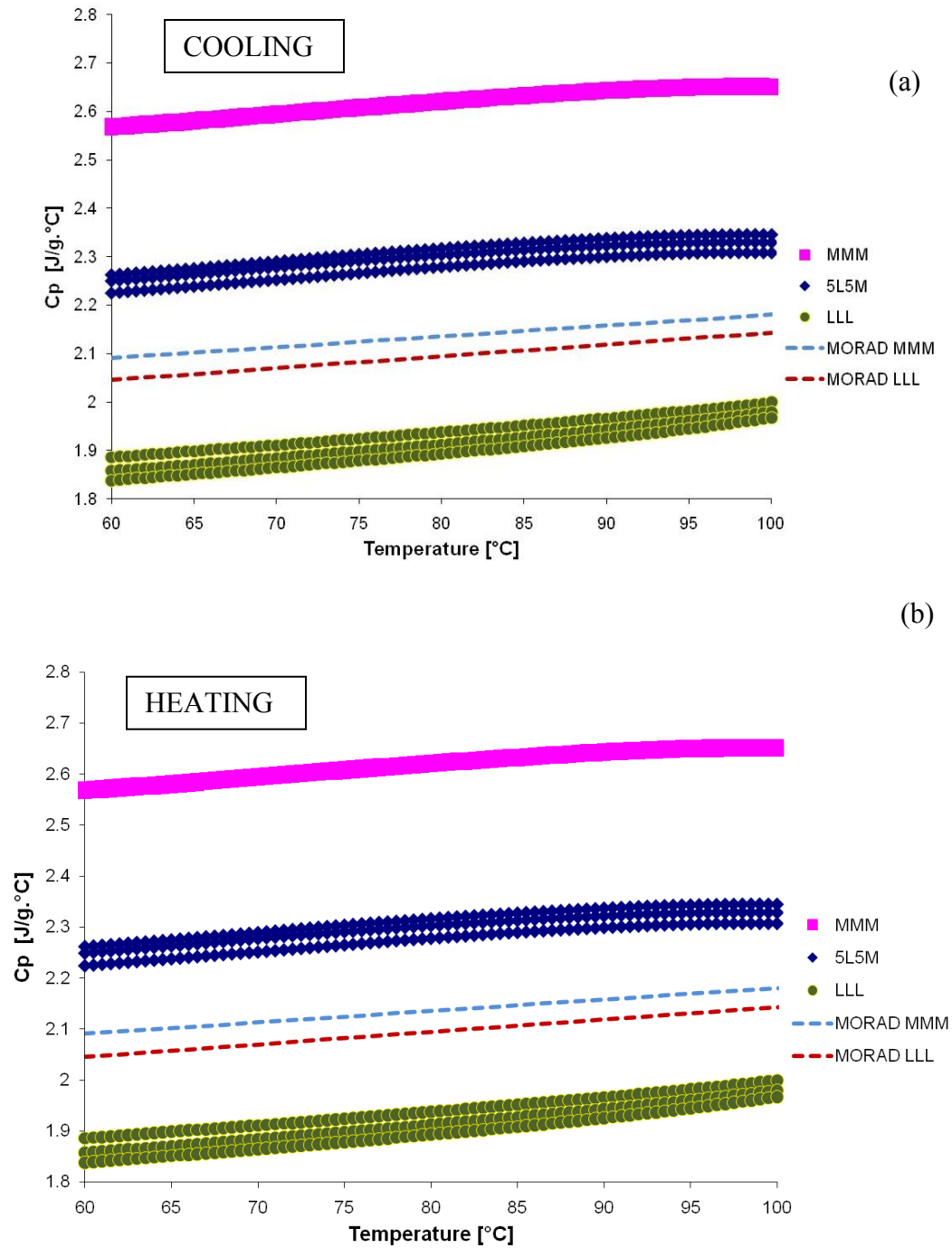
Figure 3-27: C$_p$ values vs. temperature for MMM, 5L5M and LLL samples during (a) cooling and (b) heating using a temperature ramp of 15 °C/min. Each measurement was performed thrice. The values by Morad *et al.* (2000) for MMM and LLL are also included for comparison.

The C_p values for MMM were about 18% larger than the values obtained by Morad *et al.* (2000) although the sample mass for MMM was about 4 times less than the sample mass reported by Morad *et al.* (2000). Thus the difference did not seem to be attributable to the sample mass.

The same MMM, LLL and 5L5M pans were loaded again into the cell and the same thermal procedure to obtain the heat flow signals was repeated for baseline, sapphire and sample. The results obtained are shown in Figure 3-28. The values in Figures 3-27 and 3-28 showed clearly that C_p values for all samples showed small variability between repetitions of the thermal profile without moving the sample pan. However, it was found that taking the sample pan out and placing it back again into the furnace considerably influenced the C_p values despite that the same thermal treatment was being used. The operator tried in all cases to place the sample pan as centered as possible. For example, it can be seen in Figure 3-28 that 5L5M had higher C_p values than MMM, which is extremely unlikely. Moreover, LLL showed an increase in C_p values of about 11.3% whereas MMM and 5L5M showed a decrease of about 15.7 and 1.4% ,respectively, for the values obtained during heating at 90 °C.

These findings prompted us to examine the influence of loading the sample several times into the cell on the heat flow signals from which C_p values are obtained. This will be discussed in the following pages.
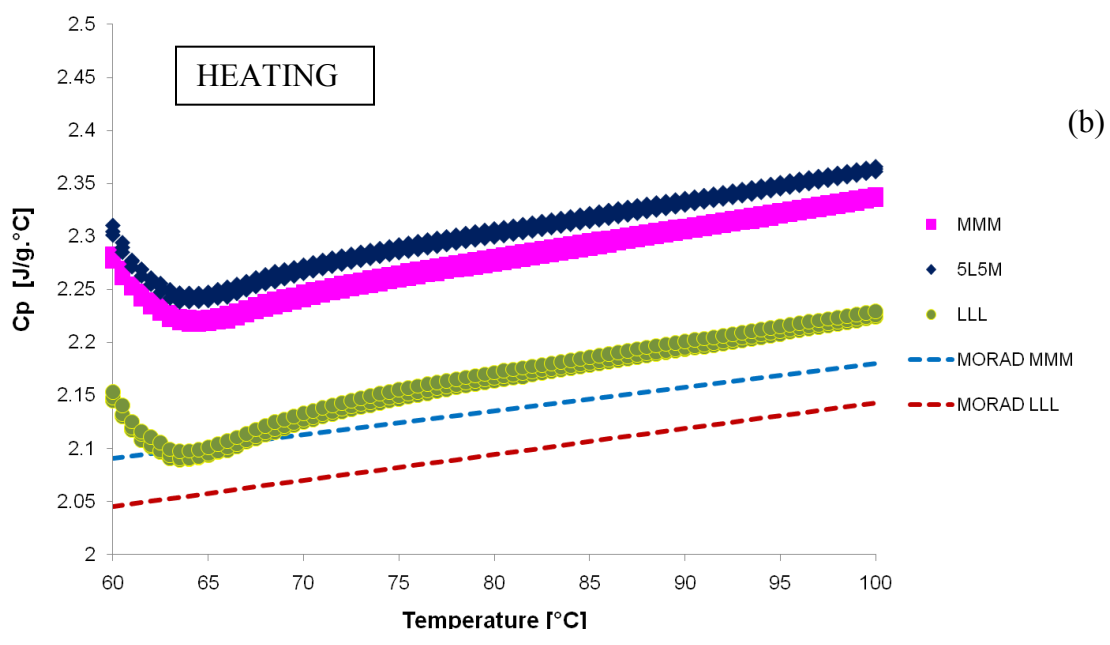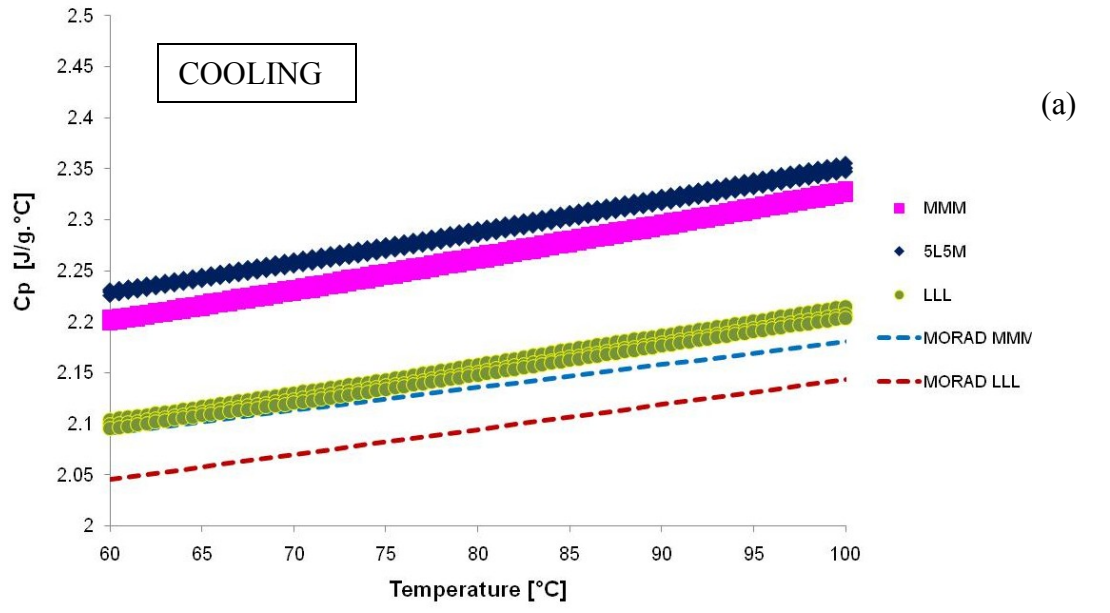
Figure 3-28: C_p values vs. temperature for MMM, 5L5M and LLL samples in the second run during (a) cooling and (b) heating using a temperature ramp of 15 °C/min. Each measurement was performed thrice. The values by Morad *et al.* (2000) for MMM and LLL are also included.

109

The following experiments were done to evaluate the effect on C_p values of the placement of the sample pan on its post, while keeping other factors unchanged. This was carried out by taking the sample pan out and then loading it back again on the sample post, always trying to center it as best as possible. The C_p values of the MMM sample with a mass of 6.049 mg were determined 19 times using the three step method during cooling and heating at 15 °C/min. Unlike other experiments, the MMM sample here was crimped to prevent its loss, and the reference pan was untouched during the whole procedure. Figure 3-29 shows the C_p values of the MMM sample in the liquid state during heating and cooling. The measured C_p values changed dramatically upon both cooling and heating. To evaluate the deviation of the C_p values, the slopes and the intercepts for each curve in the figure were determined using a linear fit to the data and then compared. Table 3-6 shows the average values of the slopes and intercepts during heating and cooling. One can observe the large standard deviation (SD) of the slope for heating. More modest, though still too large, SD values were observed for cooling. These large SD values clearly show that the position of the pan greatly influenced the function describing the measured C_p values. The reduction of the values for cooling may perhaps be due to the asymmetric convection heat transfer between heating and cooling.

Table 3-6: The average values of slopes and intercepts (n=19) obtained by performing a linear fit to each curve in Figure 3-29.

	Heating			Cooling		
	average	SD	(SD/average)%	average	SD	(SD/average)%
slopes $J/(g°C^2)$	0.001	0.001	222.068	0.010	0.002	17.378
Intercepts $J/(g°C)$	1.560	0.127	8.159	0.736	0.236	32.034
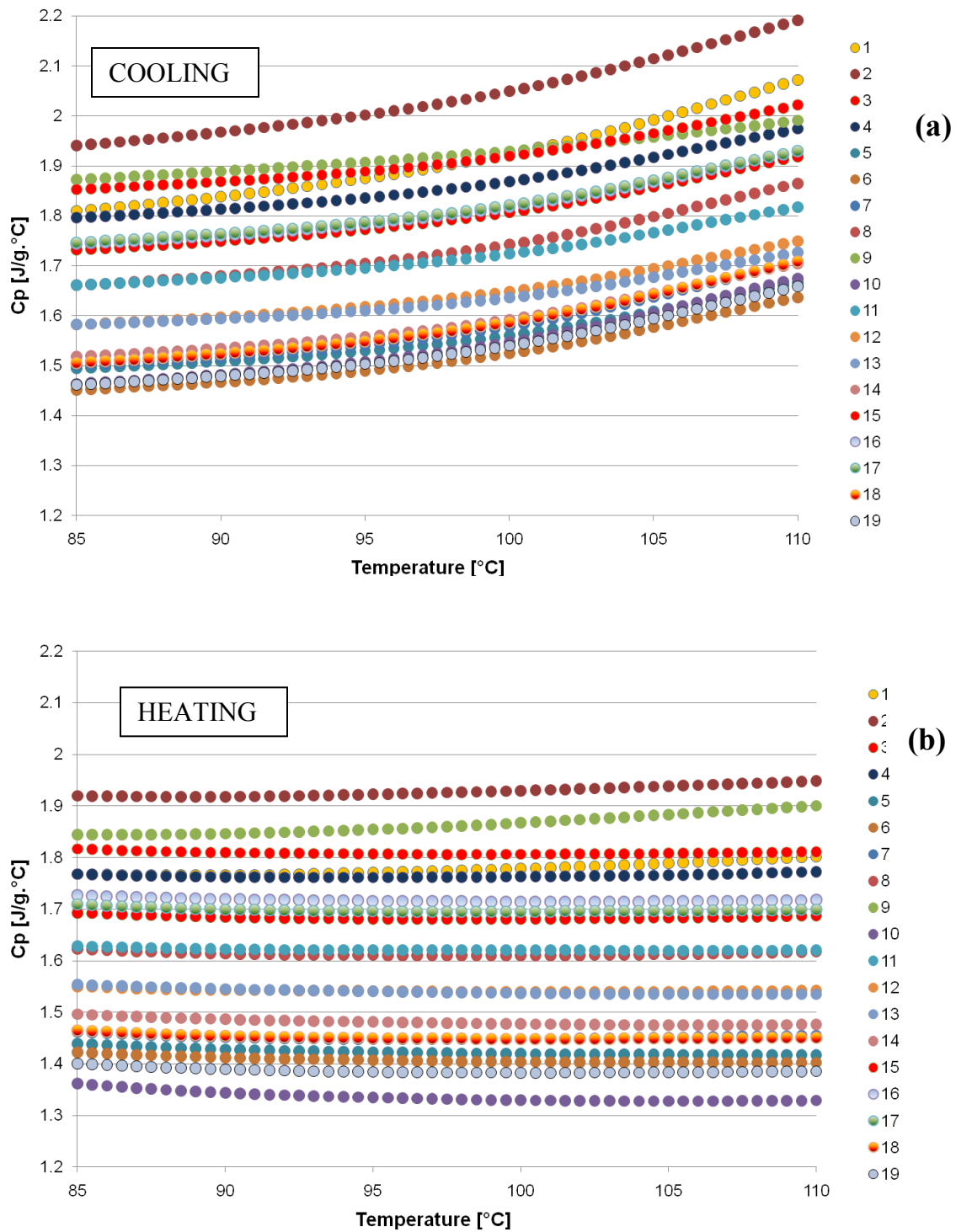
Figure 3-29: C_p values vs. temperature for MMM performed 19 times to investigated the effect of "take-out-put-back" of the sample pan during (a) cooling and (b) heating using a temperature ramp of 15 °C/min.

3.2.3   Determining the specific heat capacity using MDSC®

In the chronological order of the attempts to determine the C_p for the materials under study, MDSC® was the first to be used. This is because of its reputation in the literature in determining the C_p values directly and accurately, and more importantly, for its claimed capabilities in deconvoluting simultaneous thermal events that occur during a phase transition. The aim here was to investigate the validity of MDSC® capabilities in finding the C_p for the samples under study. Also, the precision and reproducibility of the measurements were tested under different experimental conditions, i.e., modulation periods and amplitudes.

To explore the influence of using different combinations of modulation periods and amplitudes, a quasi-isothermal experiment on a LLL sample with a mass of 8.254 ±0.005 mg was carried out using modulation periods of 30, 60, 90, 120, 150 and 180 s. In this case there is no temperature ramp, only sinusoidal variation around an average temperature. For each modulation period explored, amplitudes of ±0.1, ±0.3 and ±0.5°C were applied. The measurements were taken around a midpoint of 80 °C while it was ensured that all other experimental parameters were kept invariant. The results are shown in Figure 3-30. Each measurement represents the average of the data collected within a 10-minute isothermal hold. The SD for the measurements ranged from ±0.001 to ±0.008 J/g°C for C_p values that were between 1.4 and 1.9 J/g°C.

It is clear from Figure 3-30 that for the selected modulation amplitudes, there was no effect on the C_p values. However, the C_p values showed a significant dependence on the modulation periods applied, being highest and lowest in the modulation periods of 120 and 30 s, respectively. Since there were no phase transitions present, it is clear that

so-called non-reversing or transient thermal phenomena were present. These are most likely associated with variations in thermal lag in the sample due to formation of different temperature gradients inside the sample under different periods.
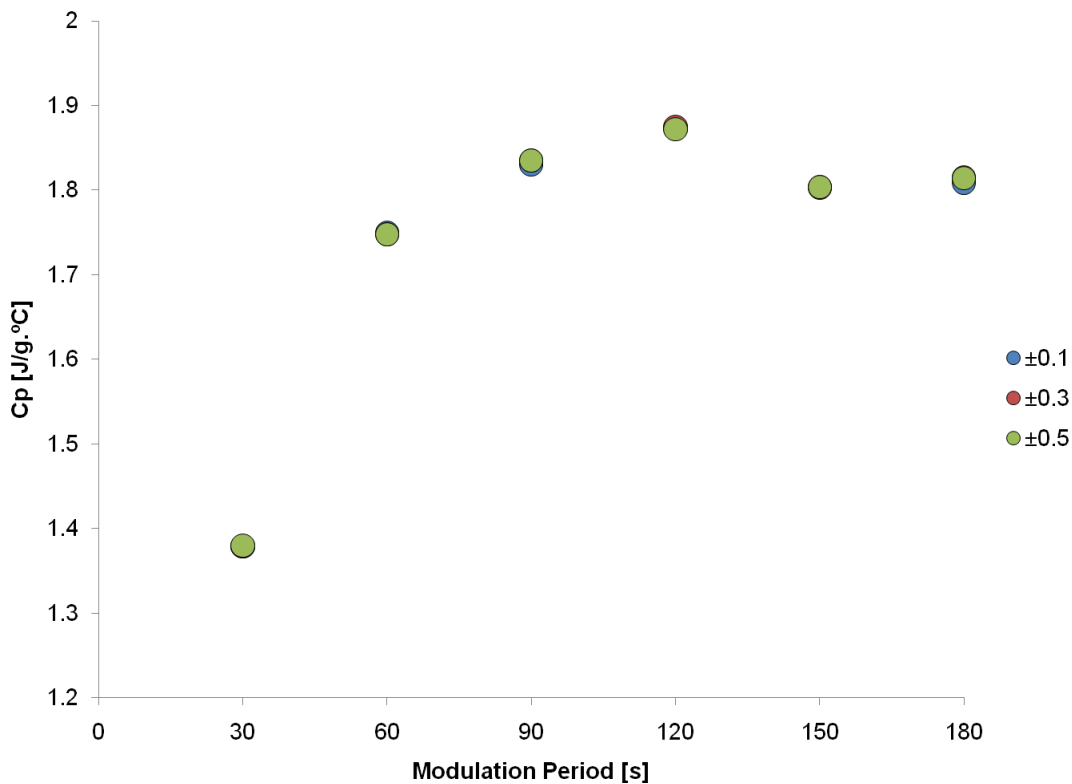
Figure 3-30: The effect of using different combinations of periods and amplitudes on the C_p values obtained by MDSC for a LLL sample in the liquid state at 80 °C.

It was therefore attempted to decrease the resistances introduced by the sample container and the transient temperature profiles in the sample as much as possible. In order to do this, new pans with low masses ($\approx$ 25 mg), about half the conventional ones, with a new way of crimping were used. The way of creating these pans is explained in detail in appendix C. One of the advantages of these pans is the enhancement of the heat transfer between the sample and the sample measuring platform with reduced thermal

113

resistance. With the use of these pans, the C_p values of sapphire at different temperatures were determined using a period of 120 s and amplitude of ±1.5 ˚C. The experimental results and the literature values (Ditamars *et al.,* 1982) for sapphire are shown in Figure 3-31.
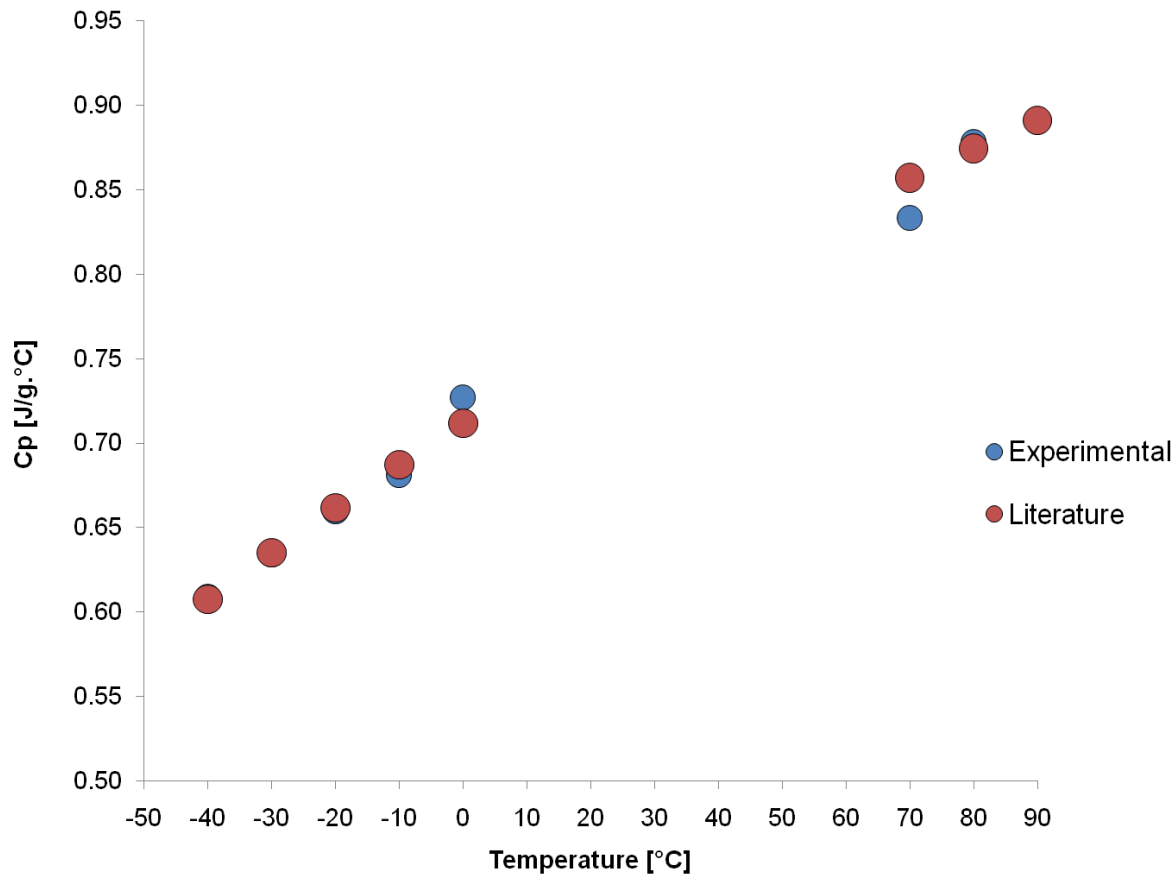
Figure 3-31: The experimental C_p values obtained by MDSC for a sapphire sample (26.808 mg) obtained using a period of 120 s and amplitude of ±1.5 °C, compared with the the literature C_p values at selected temperatures (Ditamars *et al.*, 1982)

Each measurement was obtained by averaging all the C_p values acquired within a10-minute isothermal hold. The SD for the measurements ranged from ±0.0001 to 0.0010 J/g°C (n=2856) indicating high precision of the measurements. These temperatures were selected since they represent the solid and the liquid state for the TAG

samples. The correction factors applied in the subsequent samples were calculated from values in Figure 3-31 by dividing the theoretical values by the experimental values. An example of a typical MDSC signals with sapphire in the new pans is shown in Figure 3-32.
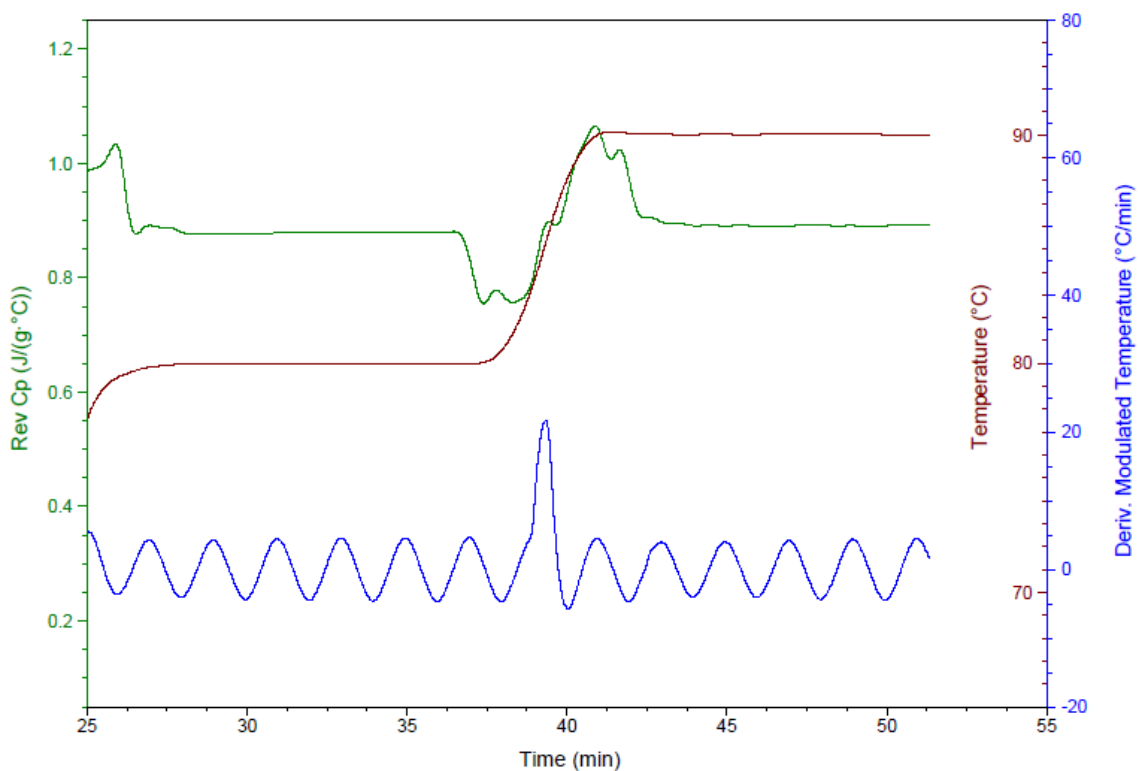
Figure 3-32: Plot showing the Reversing C_p (Rev. C_p), the modulation signal generated using a period of 120 s and amplitude of ±1.5 °C at 80 and 90 °C, for a sapphire sample. (Deriv. = Derivative)

Since such a good result was obtained with sapphire, the C_p values for the binary mixtures 3L7M, 5L5M and 7L3M having masses of 10.930, 8.920 and 6.674 mg ±0.005 mg were determined using the same procedure and the same type of pans. These pans had two punctured holes in the lid. The holes were made to reduce the deformation from the expansion of the gas in the sample containers. It had been observed that the unpunctured pans fell off the sample platform concurrently with the crystallization process of the samples; and this was attributed to some mechanical movements that resulted from the

expansion of the sample containers. The issue, however, persisted. The C_p values for 3L7M, 5L5M and 7L3M are presented in Figures 3-33, 3-34 and 3-35, respectively.
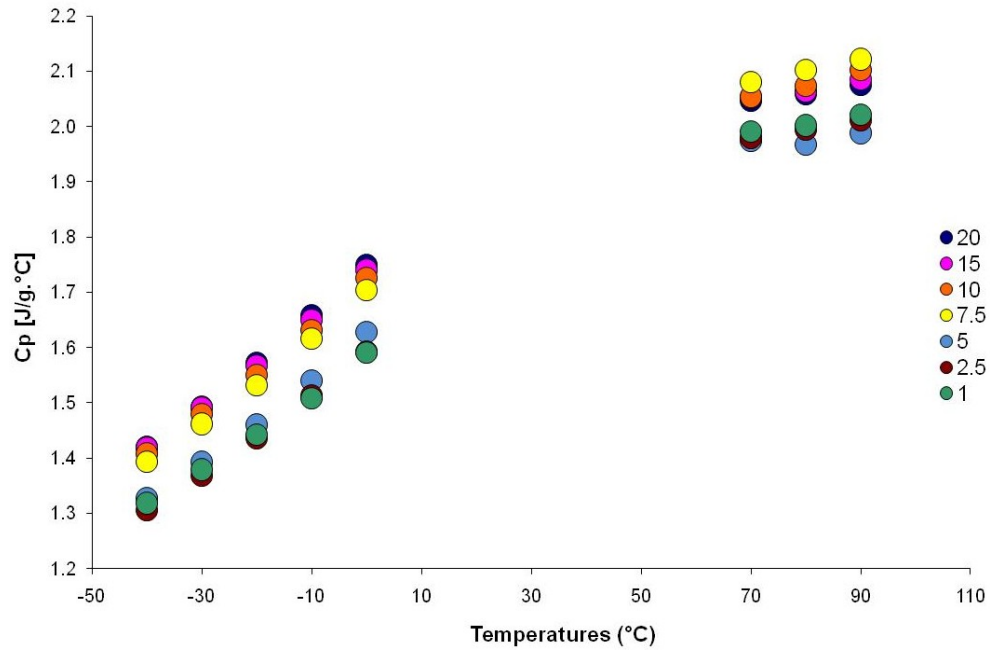
Figure 3-33: The C_p values, obtained by MDSC, at different temperatures for 3L7M cooled using different cooling rates. The values obtained using a modulation period of 120 s and amplitude of ±1.5 °C.
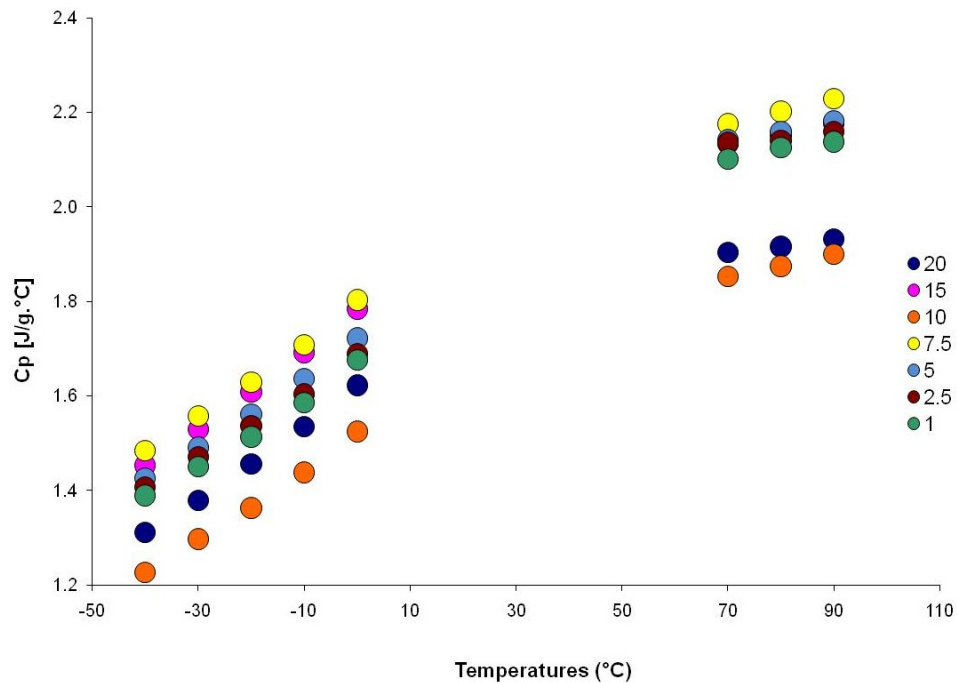
Figure 3-34: The C_p values, obtained by MDSC, at different temperatures for 5L5M cooled using different cooling rates. The values were obtained using a modulation period of 120 s and amplitude of ±1.5 °C.
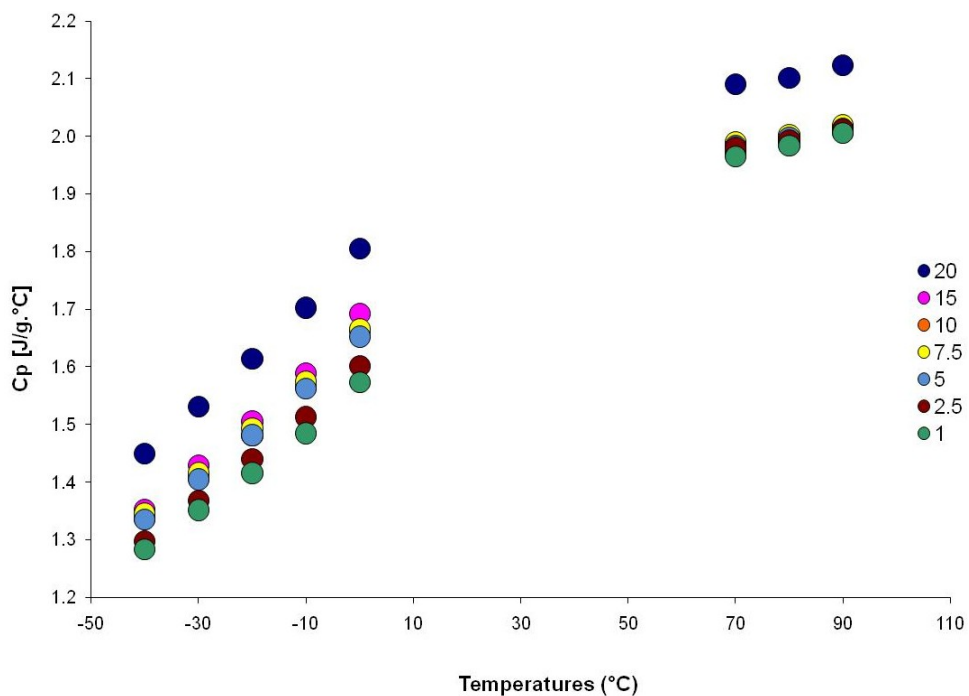
Figure 3-35: The C_p values, obtained by MDSC, at different temperatures for 3L7M cooled using different cooling rates. The values were obtained using a modulation period of 120 s and amplitude of ±1.5 °C.

117

The first observation is that the C_p values for the liquid state for the three binary mixtures fell into two sets. This was because of the discontinuity in acquiring measurements in cases when the sample pan fell from the post. After the sample pan was returned to its position and the experiment was resumed for the remaining cooling rates, different values for the liquid state were obtained. This is clearly an effect of pan "take-output-back" previously discussed in section 3.2.2.4. The comprehensive study on "take-output-back" had not been yet conducted when performing the MDSC experiments. The strange behaviour remained unexplained until investigating later the effect of "take-out-put-back" of the sample pan on the C_p values.

The second point observed is the consistency of the C_p values when the experiment was not mechanically disturbed. The DSC instrument has been shown to be capable of producing precise, yet not necessarily accurate measurements, so long as there is no change in the experimental setting of the sample, particularly its position on the sample post. This was also found when a LLL sample (8.712 mg) was run and, fortunately, the problem of the pan falling from the past did not occur. The results are shown in Figure 3-36.
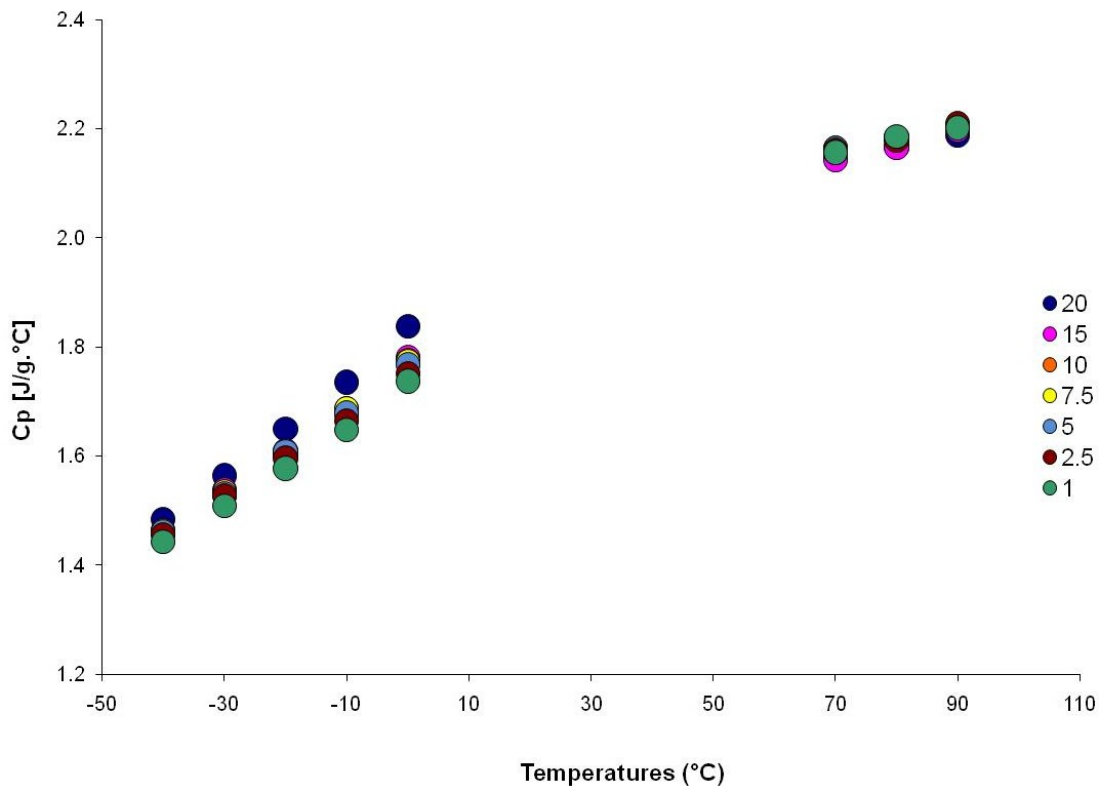
Figure 3-36: C_p values using MDSC at different temperatures for LLL cooled using different cooling rates. The values were obtained using a modulation period of 120 s and amplitude of ±1.5 °C.

In the case of LLL, the C_p values in the liquid state at 70, 80 and 90 °C were found to be 2.156±0.008, 2.178±0.008, and 2.201±0.007 J/g °C, respectively, for the different cooling rates applied. These values are lower by 4 % than the values obtained by Morad (2000). Given the changes observed in the involuntary "take-out put-back" cases when the pan fell, these small differences in the values seem to be a mere coincidence for this particular run. It is very likely that the MDSC values will change if the position of the pan is changed as discussed earlier in section 3.2.2.4. The use of thermal grease as in the PPMS experiments was considered, but this was not recommended by TA Instruments since, according to them, the performance of the cell could be degraded.

119

Seems, thus, that unless there is a way to remove the effect of the period-amplitude choice on the values, MDSC is a worse choice than straight DSC to attempt determination of C_p. Both methods, however, are flawed by the problem of the sample pan positioning.

3.2.4   Determining the specific heat capacity using PPMS®

During the initial stages of using PPMS, several samples of LLL, 7L3M and MMM were run so that the operational capabilities of the technique and its limitations could be better understood. The instrument was incapable of reaching cooling rates faster than 12 °C/min. In order to investigate the effect of using different cooling rates on the resultant crystalline phases, cooling rates of 10 and 2.5 °C/min were applied to a 5.2 ±0.05 mg MMM sample contained in a micro Perkin Elmer aluminum pan. In each experiment, six cooling rates were performed in the following order 10, 2.5, 2.5, 10, 10, 2.5 °C/min and the measurements were taken at different temperatures where the sample was in the solid state, i.e. from -40 to 40 °C, and in the liquid state, i.e. 60, 70, 80, 100 and 120 °C. The results obtained are plotted in Figure 3-37. The experiment was performed in triplicates with excellent reproducibility despite the cooling rates being applied in a random order as shown in Table 3-7. The C_p values for the α and β' polymorphs as reported by Hampson and Rothbart (1983) were also plotted in Figure 3-37 for comparison. The XRD data reported by Anom (2009) showed that only the α and β' polymorphs of MMM appeared at the end of cooling using both cooling rates of 10 and 2.5 °C/min, respectively. The PPMS value at 15 °C was lower by about 5% than that

reported by Hampson and Rothbart (1983) for the α polymorph. However, the PPMS value for the β' polymorph was lower by about 1 % at 5 °C. One can consider the values obtained by PPMS as reference values since thermal relaxation is a well established technique, but is limited to cooling rates faster than 12 °C/min.
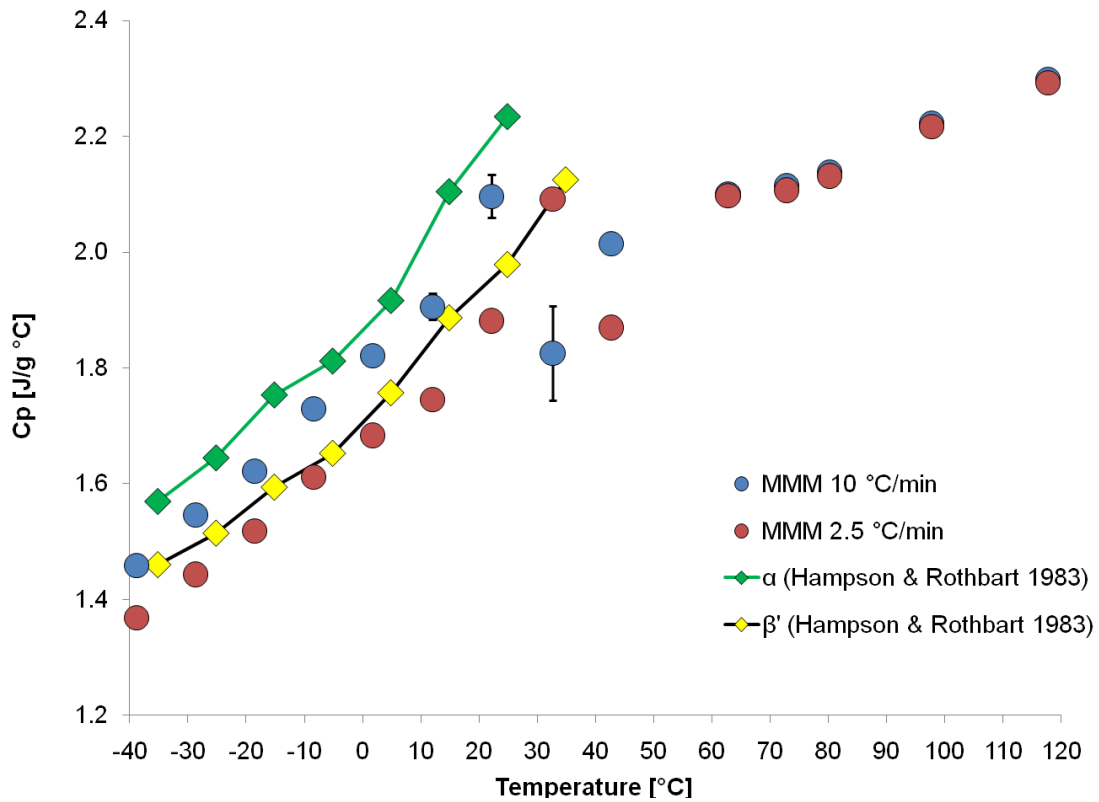
Figure 3-37: The C_p values obtained for a MMM sample at different temperatures at 10 and 2.5 °C/min using PPMS. Each measurement point represents the average of three determinations.

Table 3-7: The C_p values for MMM obtained at different temperatures using cooling rates of 10 and 2.5 °C/min. Three measurements were taken at each temperature.

Temp [°C]	10 °C/min		2.5 °C/min	
	C_p [J/g °C]	SE	C_p [J/g °C]	SE
-38.8	1.455	0.002	1.372	0.003
-28.7	1.708	0.009	1.599	0.001
-18.5	2.324	0.009	1.979	0.001
-8.5	2.194	0.010	1.993	0.001
1.8	2.180	0.010	2.159	0.003
12.0	2.723	0.013	2.716	0.002
22.1	3.165	0.021	4.041	0.002
32.7	6.397	0.047	6.521	0.003
42.7	4.745	0.005	5.086	0.007
53.0	1.913	0.966	1.821	0.038
62.8	1.921	0.006	1.841	0.002
72.8	1.955	0.003	1.864	0.003
80.2	1.963	0.012	1.899	0.003
97.7	2.012	0.005	1.955	0.002
117.7	2.069	0.006	2.000	0.003

The C_p values for the crystalline phases obtained at 10 °C/min were higher than those at 2.5 °C/min, except for the values at 30 °C.

Figure 3-38 shows the values obtained using PPMS and the values reported in the literature for the samples in the liquid state (Charbonnet & Singleton, 1947; Hampson & Rothbart, 1983; Morad *et al.*, 2000; Phillips & Mattamal, 1976). As shown in Figure 3-38, the C_p values obtained by PPMS showed a linear relationship with temperature as reported in the literature (Morad *et al.*, 1995b). The PPMS values are within the literature values and can be used to assess the accuracy and precision of the C_p values obtained elsewhere.
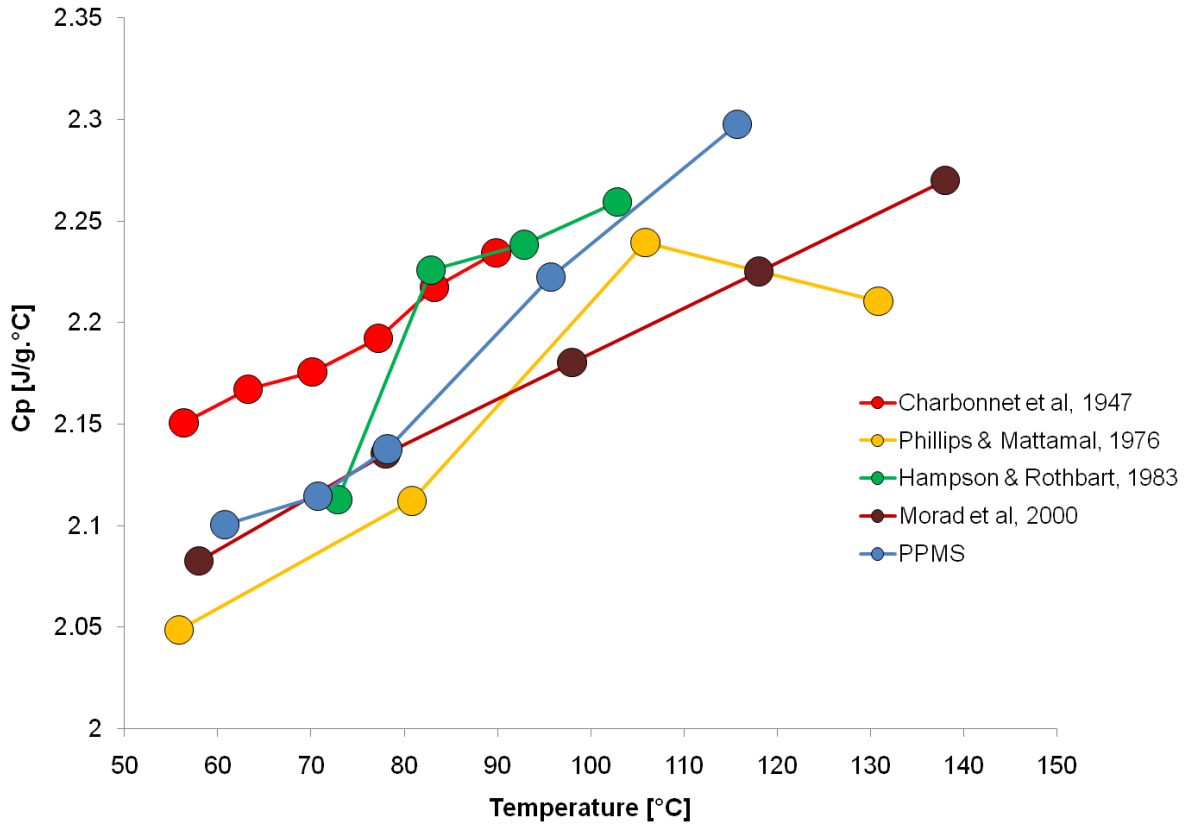
Figure 3-38: C_p values as a function of temperature for MMM in the liquid state using PPMS as compared to data reported in the literature (Charbonnet & Singleton, 1947; Hampson & Rothbart, 1983; Morad *et al.*, 2000; Phillips & Mattamal, 1976).

Since these were only exploratory experiments, no measurements were conducted with different sample sizes to improve accuracy. The method, however, seems very promising, compared to DSC and MDSC.

Chapter 4   Conclusions

The determination of precise enthalpies is necessary for the determination of the free excess energy of interaction parameters of mixing two TAGs, trilaurin and trimyristin, crystallized at different cooling rates. These parameters are part of a theoretical model proposed by Los & Flöter (1999) to estimate the kinetic composition of a crystal that is growing from a solution. For this reason, it was the purpose of this work to determine if it was possible to obtain accurate and precise heat capacity and enthalpy of crystallization values for the different crystalline phases at the end of cooling.

A method was thus developed to obtain enthalpy of crystallization values with a precision of ≤ 2% (SE) using a DSC Q100.

The method to obtain precise enthalpy values includes an experimental procedure and a data analysis procedure. The experimental procedure requires a sample mass of 5-10 mg in each sample pan. Two sample pans should be prepared for each blend and the experiments should be in this order: Pan 1, Pan 2, Pan 1 and Pan 2. In this way two sources of variability to the measurements could be averaged: pan position and sample mass. The reference pan should be prepared such that its mass is matched to the sample pans to within 0.005 mg, and used in all experiments without moving it or taking it out of the DSC cell. By so doing, any possible variations in the measurements introduced by the mass imbalance of the reference and the sample pans will be minimised. Two isothermal periods before and after the crystallization transition must be used.

The data analysis procedure to compute the enthalpy of crystallization at a given temperature requires bringing the heat flow during the isothermal periods to 0 W/g with the use of a linear transformation (also called signal rotation), to minimise the variability

in the measurements produced by using different temperature ramps and, to some small extent, pan placement. Then the whole heat flow signal is integrated from a common liquid temperature point onwards. Subsequently, a quadratic function is fitted to the liquid integrated signal. Then a liquid signal is computed as a function of temperature and extrapolated using this quadratic function. The computed liquid signal is then subtracted from the total integrated signal over the span of the temperature range. The resulting curve is the enthalpy difference between the liquid and the solid phases at any given temperature.

The specific heat capacity values obtained were significantly influenced by the experimental conditions, especially by the sample pan position. Thus, it is not possible to measure accurate C_p values for TAGs using a DSC Q100 instrument. Under different heating rates the C_p values were larger than those obtained under cooling. The differences between the values obtained at different cooling and heating rates increased for slower temperatures ramps. In addition, these differences were larger when smaller sample sizes were used. Moreover, the effect of taking the sample pan and put it back again was found to have an enormous effect on the final measurements, even though the same experimental procedures were used. MDSC in this instrument was not able to determine reproducible heat capacity values either. The heat capacity values were also affected by the selection of the MDSC modulation period and to a lesser extent by the amplitude. The placement of the pan was, however, the factor that impaired the reproducibility the most.

The preliminary thermal relaxation measurements with the PPMS instrument yielded heat capacity values that were within the literature values. More experiments are needed to evaluate properly its reproducibility for these materials. Perhaps its cooling rate

125

capacity can be enhanced since it is only needed to prepare the sample, but not to conduct the C_p measurements.

A factor that plays a significant role in the discrepancies in the heat capacity values obtained is the low thermal conductivity of TAGs, which also determines the low thermal diffusivity. Low thermal diffusivity means that the rates of heat transfer and local temperature change in the solid are low. This means that the solid will develop large temperature gradients inside, when compared to a similar solid that has a large thermal diffusivity. This kind of delay is reflected in the signals from the DSC.

The heat flow signals in the case of C_p determination for the fats are typically in the order of 2.15 mW, compared to 0.371 mW for the empty pans. As can be seen, the signal is not too large compared to the background. Thus, the pan position affects the C_p determination very much, especially if the material does not reach an isothermal distribution easily. In the case of enthalpy determination, the signal is typically 50 mW, and thus the relative error is very small. Consequently, determining accurate and reproducible heat capacity values was not possible with the Q100 DSC, but it was possible to determine reasonably accurate enthalpy values. Determining the thermal conductivity of the materials should be considered as a future objective of this research field.

BIBLIOGRAPHY:

Anom, E. Y. (2009). *Comparison of the theoretical and experimental composition of crystallizing lipid mixtures.* Dalhousie University, Halifax.

ASTM-E1269. (2005). Standard test method for determining specific heat capacity by differential scanning calorimetry: ASTM International, West Conshohocken, PA.

Belitz, H., Grosch, W., & Schieberle, P. (2009). *Food Chemistry* (4th ed.). Heidelberg: Springer.

Bernardes, C., Santos, L., & da Piedade, M. (2006). A new calorimetric system to measure heat capacities of solids by the drop method. *Measurement Science & Technology, 17*(6), 1405-1408.

Biliaderis, C. G. (1983). Differential scanning calorimetry in food research - a Review. *Food Chemistry, 10*(4), 239-265.

Bloor, R. (1920). Outline of a classification of the lipids. *Proc. Soc. Exp. Biol. Med, 17*, 138-140.

Boistelle, R. (1988). Fundamentals of nucleation and crystal growth. In N. Garti & K. Sato (Eds.), *Crystallization and polymorphism of fats and fatty acids* (pp. 189-226). New York: Marcel Dekker.

Cao, J. N. (2007). Numerical simulation of DSC and TMDSC curves as well as reversing and nonreversing curve separation. *Journal of Applied Polymer Science, 106*(5), 3063-3069.

Cassel, R. B. (2001). *How Tzero(TM) Technology Improves DSC Performance Part III: The Measurement of Specific Heat Capacity* (No. TA279). New Castle, DE: TA Instruments.

Cassel, R. B. (2002). *How Tzero™ Technology Improves DSC Performance Part VI: Simplifying Temperature Calibration for Cooling Experiments* (No. TA285). New Castle, DE: TA Instruments.

Cassel, R. B. (2005). *Tzero(TM) technology and linearity* (No. TA325). New Castle, DE: TA Instruments.

Chapman, D. (1962). The Polymorphism of Glycerides. *Chem. Rev., 62*(5), 433-456.

Charbonnet, G. H., & Singleton, W. S. (1947). Thermal properties of fats and oils VI. Heat capacity, heats of fusion and transition, and entropy of trilaurin, trimyristin, tripalmitin, and tristearin. *Journal of the American Oil Chemists' Society, 24*(5), 140-142.

Christie, W. W. (1987). *High-performance liquid chromatography and lipids: A practical guide* (1st ed.). NewYork: Pergamon Press.

Clarkson, C. E., & Malkin, T. (1934). Alternation in long-chain compounds Part II An x-ray and thermal investigation of the triglycerides. *Journal of the Chemical Society*, 666-671.

Coupland , J. (2002). Crystallization in emulsions. *Current Opinion in Colloids and Interface Science, 7*(4-5), 445-450.

Dachs, E., & Bertoldi, C. (2005). Precision and accuracy of the heat-pulse calorimetric technique: low-temperature heat capacities of milligram-sized synthetic mineral samples. *European Journal of Mineralogy, 17*(2), 251-259.

Danley, R. L. (2003). New heat flux DSC measurement technique. *Thermochimica Acta, 395*(1-2), 201-208.

deMan, J. M., deMan, L., & Blackman, B. (1983). Melting-Point Determination of Fat Products. *Journal of the American Oil Chemists' Society, 60*(1), 91-94.

Diedrichs, A., & Gmehling, J. (2006). Measurement of heat capacities of ionic liquids by differential scanning calorimetry. *Fluid Phase Equilibria, 244*(1), 68-77.

Duffy, P. (1853). XVIII.—On certain isomeric transformations of fats. *Quarterly Journal of the Chemical Society of London, 5*(3), 197-210.

Eiteman, M. A., & Goodrum, J. W. (1994). Heat-Capacity of the Triglycerides - Tricaproin, Tricaprylin and Tricaprin. *Journal of the American Oil Chemists' Society, 71*(5), 549-550.

Ferguson, R. H., & Lutton, E. S. (1947). The Polymorphism of Triolein. *Journal of the American Chemical Society, 69*(6), 1445-1448.

Garti, N., & Sato, K. (1988). *Crystallization and polymorphism of fats and fatty acids* (Vol. 31). New York: Marcel Dekker.

Garti, N., & Sato, K. (2001). *Crystallization processes in fats and lipid systems*. New York: Marcel Dekker.

Ghotra, B. S., Dyal, S. D., & Narine, S. S. (2002). Lipid shortenings: a review. *Food Research International, 35*(10), 1015-1048.

Gmelin, E., & Sarge, S. M. (1995). Calibration of Differential Scanning Calorimeters. *Pure and Applied Chemistry, 67*(11), 1789-1800.

Hagemann, J. W. (1988). Thermal behaviour and polymorphism of acylglyceride. In N. Garti & K. Sato (Eds.), *Crystallization and Polymorphism of Fats and Fatiy Acids* (pp. 9-95). New York: Marcel Dekker.

Hagemann, J. W., & Rothfus, J. A. (1983). Polymorphism and Transformation Energetics of Saturated Monoacid Triglycerides from Differential Scanning Calorimetry and Theoretical Modeling. *Journal of the American Oil Chemists' Society, 60*(6), 1123-1131.

Hagemann, J. W., & Tallent, W. H. (1972). Differential Scanning Calorimetry of Single Acid Triglycerides - Effect of Chain-Length and Unsaturation. *Journal of the American Oil Chemists' Society, 49*(2), 118-123.

Hampson, J. W., & Rothbart, H. L. (1969). Heats of Fusion for Some Triglycerides by Differential Scanning Calorimetry. *Journal of the American Oil Chemists' Society, 46*(3), 143-144.

Hampson, J. W., & Rothbart, H. L. (1983). Triglyceride specific heat determined by differential scanning calorimetry. *Journal of the American Oil Chemists' Society, vol. 60, no. 6*, 1102-1104.

Hartel, R. W. (2001). *Crystallization in Foods*. Maryland: Aspen Publishers, Inc.

Hartel, R. W., & Kaylegian , K. E. (2001). Advances in milk fat fractionation: Technology and Applications. In K. Sato & N. Garti (Eds.), *Crystallization processes in fats and lipid systems* (pp. 381-427). New York: Marcel Dekker.

Hesse, N. (2010). *Heat Capacity Determination at High Temperatures by Using Simultaneous DSC-TGA*. New Castle: TA instruments.

Himawan, C., MacNaughtan, W., Farhat, I. A., & Stapley, A. G. F. (2007). Polymorphic occurrence and crystallization rates of tristearin/tripalmitin mixtures under non-isothermal conditions. *European Journal of Lipid Science and Technology, 109*(1), 49-60.

Himawan, C., Starov, V. M., & Stapley, A. G. F. (2006). Thermodynamic and kinetic aspects of fat crystallization. *Advances in Colloid and Interface Science, 122*, 3–33.

Hohne, G. W. H. (1991). Remarks on the Calibration of Differential Scanning Calorimeters. *Journal of Thermal Analysis, 37*(8), 1987-2000.

Hohne, G. W. H., Hemminger, W. F., & Flammersheim, H., -J. (2003). *Differential Scanning Calorimetry* (2nd ed.). Heidelberg: Springer.

Hutchinson, J. M. (1998). Characterising the glass transition and relaxation kinetics by conventional and temperature-modulated differential scanning calorimetry. *Thermochimica Acta, 324*(1-2), 165-174.

Kasap, S. O., & Capper, P. (2006). *Springer handbook of electronic and photonic materials*. New York: Springer.

Keller, G., Lavigne, F., Loisel, C., Ollivon, M., & Bourgaux, C. (1996). Investigation of the complex thermal behavior of fats - Combined DSC and X-ray diffraction techniques. *Journal of Thermal Analysis, 47*(5), 1545-1565.

Kennedy, C. A., Stancescu, M., Marriott, R. A., & White, M. A. (2007). Recommendations for accurate heat capacity measurements using a Quantum Design physical property measurement system. *Cryogenics, 47*(2), 107-112.

Larsson, K. (1966). Classification of Glyceride Crystal Forms. *Acta Chemica Scandinavica, 20*(8), 2255-2260.

Lashley, J. C., Hundley, M. F., Migliori, A., Sarrao, J. L., Pagliuso, P. G., Darling, T. W., et al. (2003). Critical examination of heat capacity measurements made on a Quantum Design physical property measurement system. *Cryogenics, 43*(6), 369-378.

Lavigne, F., Bourgaux, C., & Ollivon, M. (1993). Phase-Transitions of Saturated Triglycerides. *Journal De Physique Iv, 3*(C8), 137-140.

Lawler, P., & Dimick, P. (2002). Crystallization and Polymorphism of Fats. In C. Akoh & D. Min (Eds.), *Food Lipids Chemistry, Nutrition, and Biotechnology* (2nd ed., pp. 293-318). New York: Marcel Dekker.

Los, J., & Floter, E. (1999). Construction of kinetic phase diagrams. *Physical Chemistry Chemical Physics, 1*(18), 4251-4257.

Lutton, E. S. (1945). The Polymorphism of Tristearin and Some of its Homologs. *J. Am. Chem. Soc, 67*, 524-527.

MacNaughtan, W., Farhat, I. A., Himawan, C., Starov, V. M., & Stapley, A. G. F. (2006). A differential scanning calorimetry study of the crystallization kinetics of tristearin-tripalmitin mixtures. *Journal of the American Oil Chemists' Society, 83*(1), 1-9.

Marangoni, A. G. (2005a). Crystallization kinetics. In A. G. Marangoni (Ed.), *Fat crystal networks* (pp. 21-82). New York: Marcel Dekkar.

Marangoni, A. G. (2005b). Crystallography. In A. G. Marangoni (Ed.), *Fat crystal networks* (pp. 1-20). New York: Marcel Dekkar.

Marangoni, A. G., & Narine, S. (2002). *Physical Properties of Lipids* New York: Marcel Dekker.

Marriott, R. A., Stancescu, M., Kennedy, C. A., & White, M. A. (2006). Technique for determination of accurate heat capacities of volatile, powdered, or air-sensitive samples using relaxation calorimetry. *Review of Scientific Instruments, 77*(9), -.

Martin, J. L., Salla, J. M., Cadenato, A., & Ramis, X. (1992). Effects of Experimental Sample Mass on the Calorimetric Study of Thermoset Resins. *Journal of Thermal Analysis, 38*(4), 917-927.

Martins, J. A., & Cruz-Pinto, J. J. C. (1999). The temperature calibration on cooling of differential scanning calorimeters. *Thermochimica Acta, 332*(2), 179-188.

Matovic, M., Miltenburg, J. C. v., & Los, J. (2005). Metastability in solid solution growth. *Journal of Crystal Growth, 275*, e211–e217.

McClements, D. J. (2005). *Food emulsions: principles, practices, and techniques* (2nd ed.). Boca Raton: CRC Press.

Menczel, J. D. (1997). Temperature calibration of heat flux DSC's on cooling. *Journal of Thermal Analysis, 49*(1), 193-199.

Metin, S., & Hartel, R. W. (2005). Crystallization of fats and oils. In F. Shahidi (Ed.), *Bailey's Industrial Oil and Fat Products* (6th ed., Vol. 6, pp. 45-76): John Wiley & Sons.

Morad, N. A., Idrees, M., & Hasan, A. A. (1995a). Improved conditions for measurement of the specific-heat capacities of pure triglycerides by dfferential scanning calorimetry. *Journal of Thermal Analysis, 44*(4), 823-835.

Morad, N. A., Idrees, M., & Hasan, A. A. (1995b). Specific heat capacities of pure triglycerides by heat-flux differential scanning calorimetry. *Journal of Thermal Analysis, 45*(6), 1449-1461.

Morad, N. A., Kamal, A. A. M., Panau, F., & Yew, T. W. (2000). Liquid specific heat capacity estimation for fatty acids, triacylglycerols, and vegetable oils based on their fatty acid composition. *Journal of the American Oil Chemists' Society, 77*(9), 1001-1005.

Nettleton, J. A. (1995). *Omega-3 fatty acids and health*. NewYork: Springer.

Ollivon, M., & Perron, R. (1982). Measurements of Enthalpies and Entropies of Unstable Crystalline Forms of Saturated Even Monoacid Triglycerides. *Thermochimica Acta, 53*(2), 183-194.

Oneill, M. J. (1966). Measurement of Specific Heat Functions by Differential Scanning Calorimetry. *Analytical Chemistry, 38*(10), 1331-&.

Perron, R. R. (1984). Some Comments About the Heat Behavior of Triglycerides - Role of Insaturation. *Revue Francaise Des Corps Gras, 31*(4-5), 171-179.

Phillips, J. C., & Mattamal, M. M. (1976). Correlation of Liquid Heat-Capacities for Carboxylic Esters. *Journal of Chemical and Engineering Data, 21*(2), 228-232.

Phipps, L. W. (1964). Heterogeneous and homogeneous nucleation in supercooled triglycerides and n-paraffins. *Transactions of the Faraday Society, 60*, 1873-1883.

Reading, M., & Hourston, D. J. (2006). *Modulated temperature differential scanning calorimetry: theoretical and practical applications in polymer characterisation*. Dordrecht: Springer.

Reading, M., Luget, A., & Wilson, R. (1994). Modulated Differential Scanning Calorimetry. *Thermochimica Acta, 238*, 295-307.

Santos, J. C. O., Santos, M. G. O., Dantas, J. P., Conceicao, M. M., Athaide-Filho, P. F., & Souza, A. G. (2005). Comparative study of specific heat capacities of some vegetable oils obtained by DSC and microwave oven. *Journal of Thermal Analysis and Calorimetry, 79*(2), 283-287.

Sarge, S. M., Hohne, G. W. H., Cammenga, H. K., Eysel, W., & Gmelin, E. (2000). Temperature, heat and heat flow rate calibration of scanning calorimeters in the cooling mode. *Thermochimica Acta, 361*(1-2), 1-20.

Sato, K. (2001a). Crystallization behaviour of fats and lipids - a review. *Chemical Engineering Science, 56*(7), 2255-2265.

Sato, K. (2001b). Molecular Aspect in Fat Polymorphism

In N. Widlak, R. W. Hartel & S. Narine (Eds.), *Crystallization and Solidification Properties of Lipids* (pp. 1-16). Champaign, Illinois: AOCS Press.

Sato, K. (2001c). Molecular Aspect in Fat Polymorphism. In R. W. Hartel & S. Narine (Eds.), *Crystallization and Solidification Properties of Lipids* (pp. 1-16). Champaign, Illinois: AOCS press.

Sato, K., & Garti, N. (1988). Crystallization and polymorphic transformation: An introduction. In N. Garti & K. Sato (Eds.), *Crystallization and polymorphism of fats and fatty acids* (Vol. 31, pp. 3-9). New York: Marcel Dekker.

Sato, K., & Ueno, S. (2005). Polymorphism in Fats and Oils. In F. Shahidi (Ed.), *Bailey's Industrial Oil and Fat Products* (6th ed., Vol. 6, pp. 77-120): John Wiley & Sons.

Sato, K., Yoshimoto, N., & Arishima, T. (1989). Crystallization Phenomena in Fats and Lipids. *Journal of Dispersion Science and Technology, 10*(4-5), 363-392.

Schick, C. (2009). Differential scanning calorimetry (DSC) of semicrystalline polymers. *Analytical and Bioanalytical Chemistry, 395*(6), 1589-1611.

Simpson, T. D., Hockett, D. P., & Harris, L. (1984). Specific-Heats of the Solid-State Phases of Trimargarin and Tristearin. *Journal of the American Oil Chemists' Society, 61*(5), 883-886.

Singh, S. K., Jalali, A. F., & Alden, M. (1999). Modulated temperature differential scanning calorimetry for examination of tristearin polymorphism: I. Effect of operational parameters. *Journal of the American Oil Chemists' Society, 76*(4), 499-505.

Swenson, C. A. (1999). Specific heat (Cp) of Apiezon N grease, (1 to 108 K) and calorimetry: Cp of copper below 30 K. *Review of Scientific Instruments, 70*(6), 2728-2731.

Takeuchi, M., Ueno, S., Floter, E., & Sato, K. (2002). Binary phase behavior of 1,3-distearoyl-2-oleoyl-sn-glycerol (SOS) and 1,3-distearoyl-2-linoleoyl-sn-glycerol (SLS). *Journal of the American Oil Chemists' Society, 79*(7), 627-632.

Takeuchi, M., Ueno, S., & Sato, K. (2003). Synchrotron radiation SAXS/WAXS study of polymorph-dependent phase behavior of binary mixtures of saturated monoacid triacylglycerols. *Crystal Growth & Design, 3*(3), 369-374.

Thomas, L. C. (2005). *Modulated DSC® Paper #1 Why Modulated DSC®? ; An Overview and Summary of Advantages and Disadvantages Relative to Traditional DSC*. New Castle, USA: TA Instruments.

Timms, R. E. (1978). Heats of Fusion of Glycerides. *Chemistry and Physics of Lipids, 21*(1-2), 113-129.

Timms, R. E. (1985). Physical-Properties of Oils and Mixtures of Oils. *Journal of the American Oil Chemists' Society, 62*(2), 241-249.

Timms, R. E. (1991). Crystallisation of fats [Electronic Version]. *BNET*. Retrieved 27-March-2011 from http://findarticles.com/p/articles/mi_hb5255/is_n10/ai_n28601842/?tag=content;col1.

Tomasi, C., Mustarelli, P., Hawkins, N. A., & Hill, V. (1996). Characterisation of amorphous materials by modulated differential scanning calorimetry. *Thermochimica Acta, 278*, 9-18.

Toro-Vazquez, J., Rangel-Vargas, E., Dibildox-Alvarado, E., & Charó-Alonso, M. (2005). Crystallization of cocoa butter with and without polar lipids evaluated by rheometry, calorimetry and polarized light microscopy. *European Journal of Lipid Science and Technology, 107*(9), 641–655.

Ueno, S., Minato, A., Seto, H., Amemiya, Y., & Sato, K. (1997). Synchrotron radiation X-ray diffraction study of liquid crystal formation and polymorphic crystallization of SOS (sn-1,3-distearoyl-2-oleoyl glycerol). *Journal of Physical Chemistry B, 101*(35), 6847-6854.

Van Durme, K., Van Assche, G., & Van Mele, B. (2004). Kinetics of demixing and remixing in poly(N-isopropylacrylamide)/water studied by modulated temperature DSC. *Macromolecules, 37*(25), 9596-9605.

van Miltenburg, J. C., van Ekeren, P. J., Gandolfo, F. G., & Floter, E. (2003). Investigation of the thermal behavior of trielaidin between 10 K and 360 K. *Journal of Chemical and Engineering Data, 48*(5), 1245-1250.

Van Oort, M. J. M., & White, M. A. (1987). Automated, Small Sample-Size Adiabatic Calorimeter. *Review of Scientific Instruments, 58*(7), 1239-1241.

Verdonck, E., Schaap, K., & Thomas, L. C. (1999). A discussion of the principles and applications of Modulated Temperature DSC (MTDSC). *International Journal of Pharmaceutics, 192*(1), 3-20.

Wesdorp, L. H., Van Meeteren, J. A., de Jong, S., Giessen, R. V. D., Overbosch, P., Grootscholten, P. A. M., et al. (2005). Liquid-Multiple solid phase equilibria in fats: theory and experiments. In A. G. Marangoni (Ed.), *Fat Crystal Networks* (pp. 481-709). New York: Marcel Dekker.

White, M. A. (1999). *Properties of Materials*: Oxford University Press

White, M. A., & Johnson, M. (2009). Physical Properties Measurement System (PPMS). Retrieved 3-April-2011, from http://irm.dal.ca/Files/PPMS.pdf

Widlak, N., Hartel, R. W., & Narine, S. (2001). *Crystallization and Solidification Properties of Lipids* Champaign, Illinois: AOCS Press.

Wunderlich, B., Jin, Y. M., & Boller, A. (1994). Mathematical-Description of Differential Scanning Calorimetry Based on Periodic Temperature Modulation. *Thermochimica Acta, 238*, 277-293.

Xie, F. W., Liu, W. C., Liu, P., Wang, J., Halley, P. J., & Yu, L. (2010). Starch thermal transitions comparatively studied by DSC and MTDSC. *Starch-Starke, 62*(7), 350-357.

Xu, S. X., Li, Y., & Feng, Y. P. (2000). Study of temperature profile and specific heat capacity in temperature modulated DSC with a low sample heat diffusivity. *Thermochimica Acta, 360*(2), 131-140.

Yeaman, S. J. (2004). Hormone-sensitive lipase - New roles for an old enzyme. *Biochemical Journal, 379*, 11-22.

Zabransky, M., Ruzicka, V., & Domalski, E. S. (2001). Heat capacity of liquids: Critical review and recommended values. Supplement 1. *Journal of Physical and Chemical Reference Data, 30*(5), 1199-1689.

Zéberg-Mikkelsen, C. K., & Stenby, E. H. (1999). Predicting the melting points and the enthalpies of fusion of saturated triglycerides by a group contribution method. *Fluid Phase Equilibria, 162*(1-2), 7-17.

Zhao, J., Hoogenboom, R., Van Assche, G., & Van Mele, B. (2010). Demixing and Remixing Kinetics of Poly(2-isopropyl-2-oxazoline) (PIPOZ) Aqueous Solutions Studied by Modulated Temperature Differential Scanning Calorimetry. *Macromolecules, 43*(16), 6853-6860.

APPENDICES

Appendix A: Enthalpy and baseline calibration.

In order to perform thermal properties measurements (phase transition enthalpies, melting points, heat capacity, etc.) with low uncertainty, proper instrument calibration is needed and thus should be performed carefully (Hohne *et al.*, 2003). The quality of the measured data depends heavily on the operation and the calibration procedures and to a lesser extent on the calibration material. The accuracy of the results are intimately correlated with how much the operator is knowledgeable and skilful with the instrument (Hohne, 1991).

DSC measurements are obtained from the heat flow rate, which is derived from temperature measurements at the sample and reference positions. The heat flow is in turn influenced by the sample behaviour, sample history, temperature ramp, sample mass, type of purge gas, type of sample container, position of the sample and the lid on the measuring post, chemical reactivity of the sample, flatness of the pans base and thermal resistances. So, what is observed as a phase transition peak, usually heat flow rate as a function of time or temperature, is the result of the interaction of all these parameters. Furthermore, the results obtained during heating and cooling experiments do not generally yield identical results even when undercooling does not occur. (Gmelin & Sarge, 1995).

According to the German Society for Thermal Analysis GEFTA, one of the fundamental rules applied to any DSC measurements is that the experimental conditions for the calibration and sample measurements should vary as little as possible.

Based on all of the above, it was necessary to closely examine and understand how the calibration of the DSC used in this research is calibrated.

Baseline calibration with Tzero^{TM} Technology in DSC Q100

The instrument used in this study was a DSC Q100 from TA Instruments with the heat flow measurement technology Tzero^{TM}. This technique developed by Danley (2003) significantly minimizes the instrument baseline defects (offset, slope, curvature) resulting from asymmetry of the sensors during manufacturing giving rise to improved resolution and dynamic response. This is achieved by accounting for the slight imbalances between the sample and the reference sensors independently, so this technique does not assume that the two calorimeters are identical, unlike other DSC calorimeters. With the use of a four-term heat flow equation, the sensors thermal parameters of capacitances and resistances are included, as follows:

$$q = -\frac{\Delta T}{R_r} + \Delta T_0 \left(\frac{1}{R_s} - \frac{1}{R_r} \right) + (C_r - C_s)\frac{dT_s}{dt} - C_r \frac{d\Delta T_s}{dt} \qquad \text{[A-1]}$$

The first term is the conventional DSC heat flow; the second and the third term reflect the imbalances between thermal resistances and capacitances of the sample and reference calorimeters. The fourth term accounts for the heat flow resulting from the difference in heating rate between the two calorimeters, which is usually zero except during the occurrence of transition or during modulation. In the latter case the instantaneous rate is shifted by a phase difference with respect to the driving temperature sinusoidal function.

There are four temperature terms in the above equation which determine the resultant heat flow measurement and are consequently used to calculate the other thermal properties of the sample (heat capacity, enthalpy). These measuring temperatures include

Ts, T_0 and differential temperatures ΔT and ΔT_0, the measured temperature of the sample calorimeter, the temperature of the DSC enclosure, the temperature difference between the reference calorimeter and between the DSC enclosure and the sample calorimeter, respectively. The term T_0 (Tzero) comes from adding the thermocouple that is centrally located in the cell and that controls the furnace temperature. This allows for an absolute temperature measurement at the base of the sensors (Cassel, 2005).

The temperature difference is converted to a heat flow signal through a proportionality factor $E(T)$ that depends on the construction of the differential sensor using this equation:

$$q = E(T)\Delta T \qquad\qquad\qquad\qquad\qquad\qquad\qquad\qquad\text{[A-2]}$$

During the first two steps of the calibration process, with an empty cell and with two sapphire disks with matched masses, the parameters of the four-term heat flow measurement equation are determined as a function of temperature. In Tzero$^{\text{TM}}$ Technology, these first two steps of the calibration are only to calibrate the instrument's thermal analyser and are independent from the type of experimental conditions to be used in the subsequent experiments. The T4 flow rate calibration mode of the instrument only allows the use of a range of heating rates from 10 to 100 °C/min. Also, the instrument gives the options to calibrate in two modes: "Heat Only" and "Heat-Cool". Since this study seeks to investigate the thermal behaviour during cooling, the second mode had always been used for calibration and was thought of as an actual cooling calibration. However, through continued contact with the manufacturer's technicians, we came to know that the machine does not in fact calibrate for cooling but instead uses a no-data acquisition heat-cool cycle as a preparation step before the actual heat calibration. The

notion "Heat-Cool" used by TA instrument could be in this sense misleading and confusing for TA instrument DSC Q series users. Having an instrument with a cleaned cell that has been temperature cycled prior to the Tzero^{TM} calibration provides a signal that is more representative of the instrument response, rather than relying on a single run that is susceptible to "first-run" effect.

TA instruments claims that the DSC with Tzero^{TM} machine performance is independent of the heating rate used in calibration. At the end of each calibration procedure for a given heating rate, different slopes and offset values of ΔT and ΔT_0 are created and used to bring the heat flow values of the reference and sample calorimeters to zero in units of µV. An example of these parameters is shown as following:

	Temperature [°C]	slope	Offset
Tzero Dt	-90.0139	0.0053	-0.621
TzeroDtz	-90.0139	0.0069	0.6307

The first number is the lower temperature limit used for calibration, the second number is the slope applied to ΔT and ΔT_0 in µV/ °C. It is calculated by adding the µV values of the ΔT and ΔT_0 at the lower temperature limit (-90 °C in this example) and at the upper temperature (usually 250 °C) and then dividing that number by the temperature range of the calibration. The third number is the offset number applied to ΔT and ΔT_0 at the lower temperature limit to bring the heat flow signal to zero. It is recommended by the manufacturer to always use a heating rate of 10, 15 or 20 °C/min for calibration to obtain representative values of the calorimeter's parameters, hence the slopes and offsets for ΔT and ΔT_0 created by these heating rates were plotted and compared as shown in Figure 1. These curves were done once and hence it has no effective statistical meaning; however it

could be a very useful investigative tool to test whether using different heating rates could produce variations in the resultant heat flow values. This is very important since the actual strength of this technology revolves around getting smooth and flat baselines with no need of baseline subtractions as is the case for power-compensated DSCs. So having a comprehensive knowledge on what would affect the flatness or smoothness of the baselines, which ultimately affects the measurements, is mandatory.
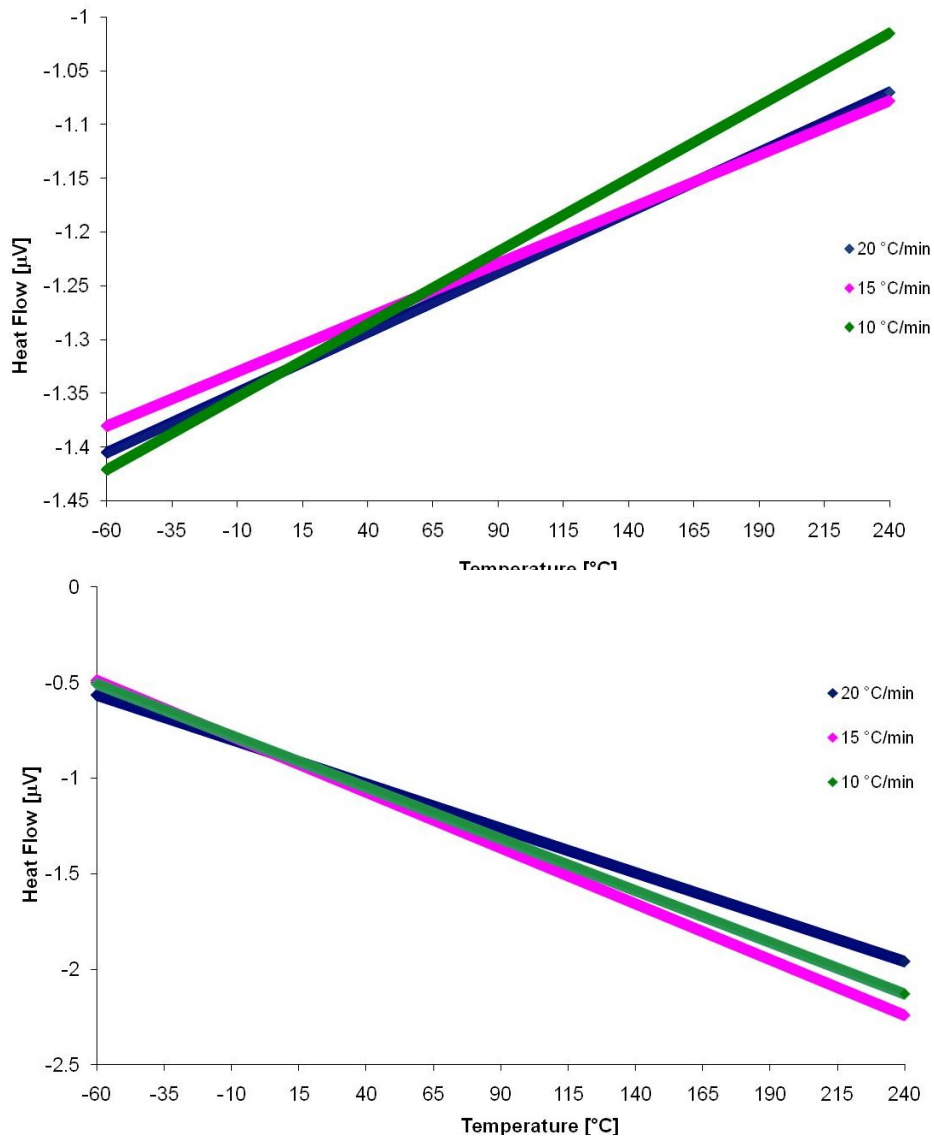
Figure 1: The effect of using different heating ramps on the baseline correction factors obtained during the calibration process over the temperature range from -60 to 240 °C. The top and bottom plots are for the correction factors ΔT and ΔT_0 respectively.

Enthalpy calibration

The determination of enthalpy in the DSC was usually done upon heating, to avoid undercooling effects. However, the phase transitions of TAGs involve polymorphic transformations and they undergo many changes upon melting, rendering the process of thermal analysis and phase identification difficult. The enthalpy calibration corrections (cell constants) are established by the manufacturers for heating, not for cooling, using the enthalpy of melting of Iindium. This was a major concern since heating and cooling are known to produce different readings. This asymmetry appears because the heat transfer is not linearly dependent only on the temperature difference between reference and sample but it is affected by other factors such as the position of the pans; however these differences are typically small and hence symmetry with respect to cooling and heating can sometimes be assumed (Sarge *et al.*, 2000).

With the TzeroTM measuring method the cell thermal resistances that determine the baselines, thermal lags and the calibration constants are relatively invariant with respect to cooling or heating rates, though they depend on temperature.

Another key point is that the DSC calorimeter with the TzeroTM technology is constructed as a vertical cylinder; this creates a symmetric distribution of temperature in the cell. A cross-sectional depiction of the DSC Q series with TzeroTM technology is shown in Figure 2.

Tzero sensor enclosure

Ni cooling rods
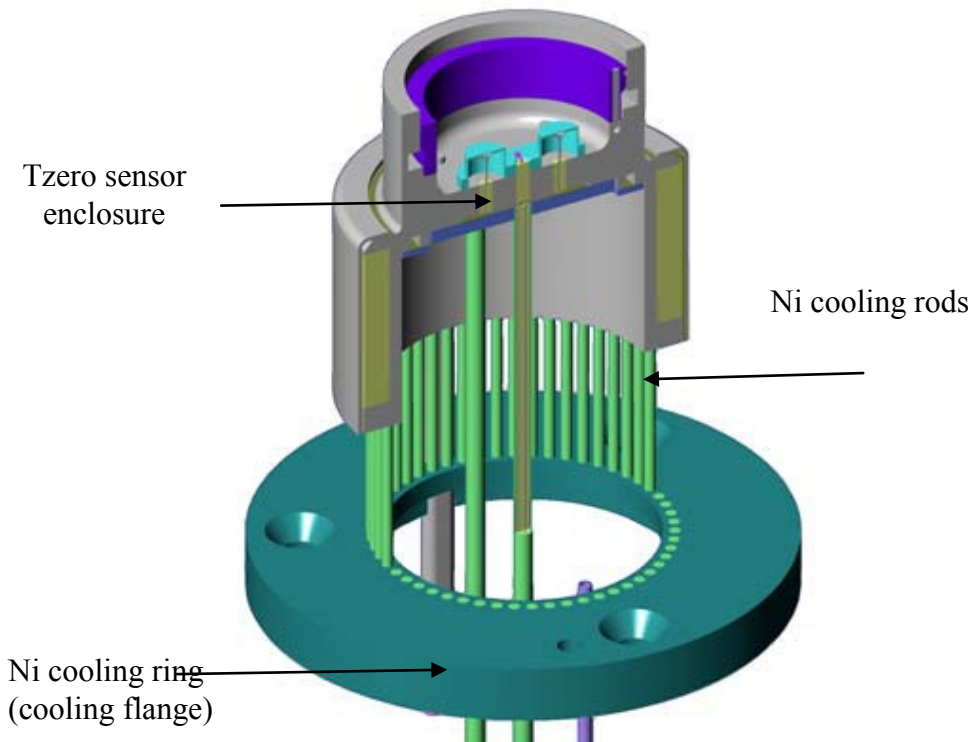
Ni cooling ring (cooling flange)

Figure 2: A cross-sectional depiction of the Q series DSCs cell (Cassel, 2005).

To obtain the most accurate and reliable determination of transition measurements, it is preferable to calibrate using the exact conditions under which the transition of the melt will happen, including the pan type. However, with the use of Tzero technology in Q series DSCs, it is sufficient to use only indium rather than using multiple calibration materials. This was confirmed by an experiment done by Cassel (2005) from TA Instruments by calculating the enthalpy of melting and melting temperatures for four calibration standards; indium, tin, lead and zinc, with melting temperatures of 156.5, 232.03, 327.57 and 417.77 °C, respectively (according to National Institute of Standards and Technology, NIST) using a DSC Q100. The average cell constant for these materials was found to be 1.0034 ±0.006 (Cassel, 2005). This was very convenient because the melting temperature of indium (156.6 °C) is well above the highest melting temperature of the materials under study (β polymorph for pure MMM at, 57

°C). The experiment of Cassel (2005), however, does not indicate how many times each material was performed nor does mention the heating rate used to obtain these results.

The effect of using different heating rates on the cell constant was also studied by a TA Instruments team. An indium sample of 7.54 mg encapsulated in an Al pan was heated through its melting temperature using a range of heating rates between 1 and 40 °C/min. A DSC Q1000 with advanced Tzero[TM] was used; this technology incorporates the pan type resistance contribution to the four-term heat flow measurements (TP4), which produces heat flow signals with higher resolution. It was found that the change in the melting temperature onsets from the theoretical value ranged from -0.03 to 0.02 °C, and from -0.02 to -0.07 J/g in the case of the enthalpy of melting. With Tzero[TM] heat flow measurement, the difference in heating rate through the melting is taken into account in the fourth term of the equation whose contribution is high if the melt is very endothermic or the heating rate is high.

It can be concluded that the enthalpy calibration constant with the use of only indium as a calibration material can be used for the investigation of materials that are not within the same melting and enthalpy of melting of Iindium irrespective of the heating rate used in calibration. If the calibration constants were influenced by the heating rates, then it would be necessary to calibrate for each heating rate and consequently obtain a cell constant for each heating rate used in the sample runs.

In spite of all that has been said, one cannot explicitly use the cell constants generated in the heating mode to correct for the enthalpy of crystallization during cooling. It was reported, however, that with Tzero[TM] technology the same results can be obtained with the cooling mode when the same ramp is used (Kasap & Capper, 2006).

The procedure for the calibration DSCs on cooling has been addressed by several authors (Hohne *et al.*, 2003; Martins & Cruz-Pinto, 1999; Menczel, 1997; Sarge *et al.*, 2000) For

the calibration on cooling, it has been always suggested to use thermally stable liquid crystals that do not exhibit hysteresis on cooling (Martins & Cruz-Pinto, 1999), and the use of the same calibration substances for heating has been also recommended to be used in cooling with the consideration for supercooling (Hohne *et al.*, 2003; Martins & Cruz-Pinto, 1999). This could only be achievable if a material with high thermal diffusivity is used. An experiment was performed by a TA instrument technician with the use of a liquid crystal (CE-3) to examine the effect of different cooling and heating rates with a DSC Q1000 on the resultant thermal lags created by different heat/cooling rates. It was concluded from this study that for all practical purposes the DSC with Tzero[TM] can be calibrated at any reasonable heating rate and the DSC temperature data will be correct within a few tenths of Celsius degrees for data taken at other heating or cooling rates (Cassel, 2002).

Appendix B: The Normalization procedure

The Normalization procedure using the Universal Analysis software (TA Instruments) for the calculation of C_p using the classical three steo method.
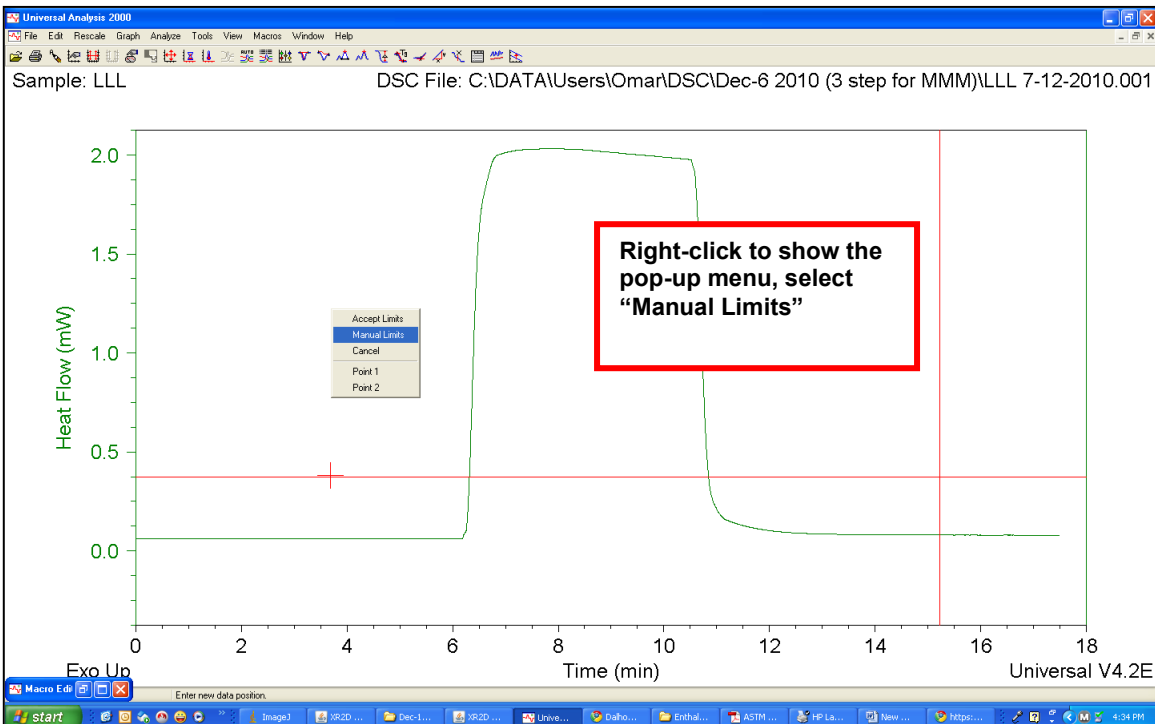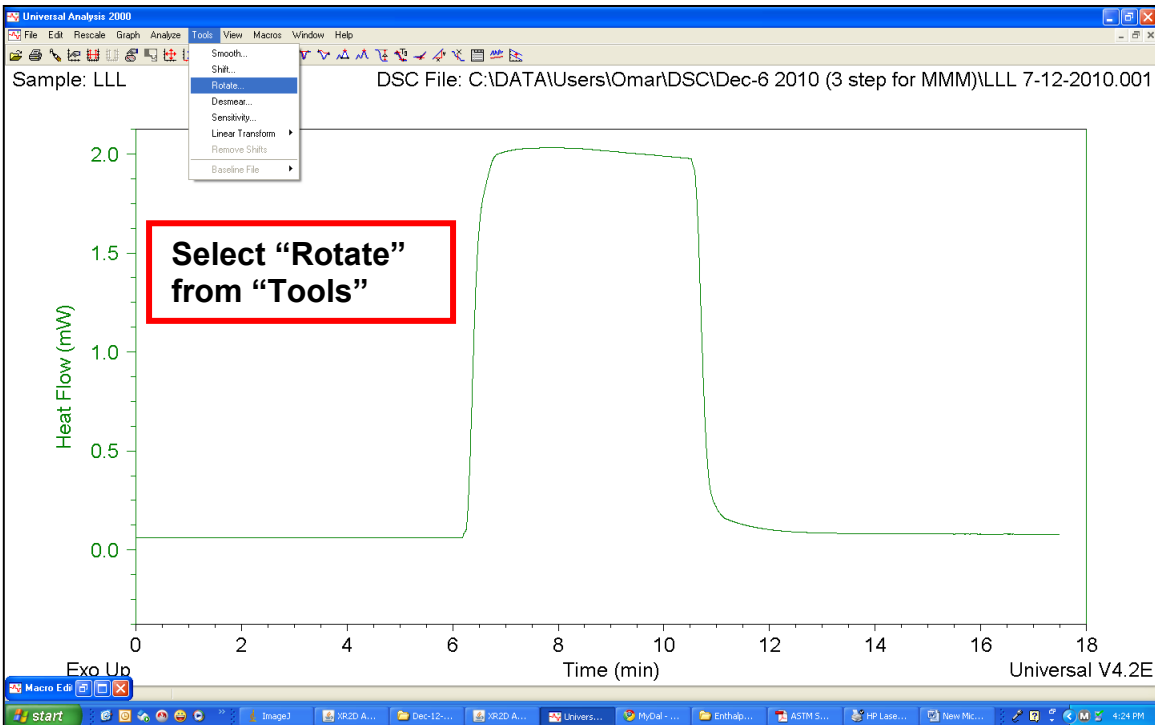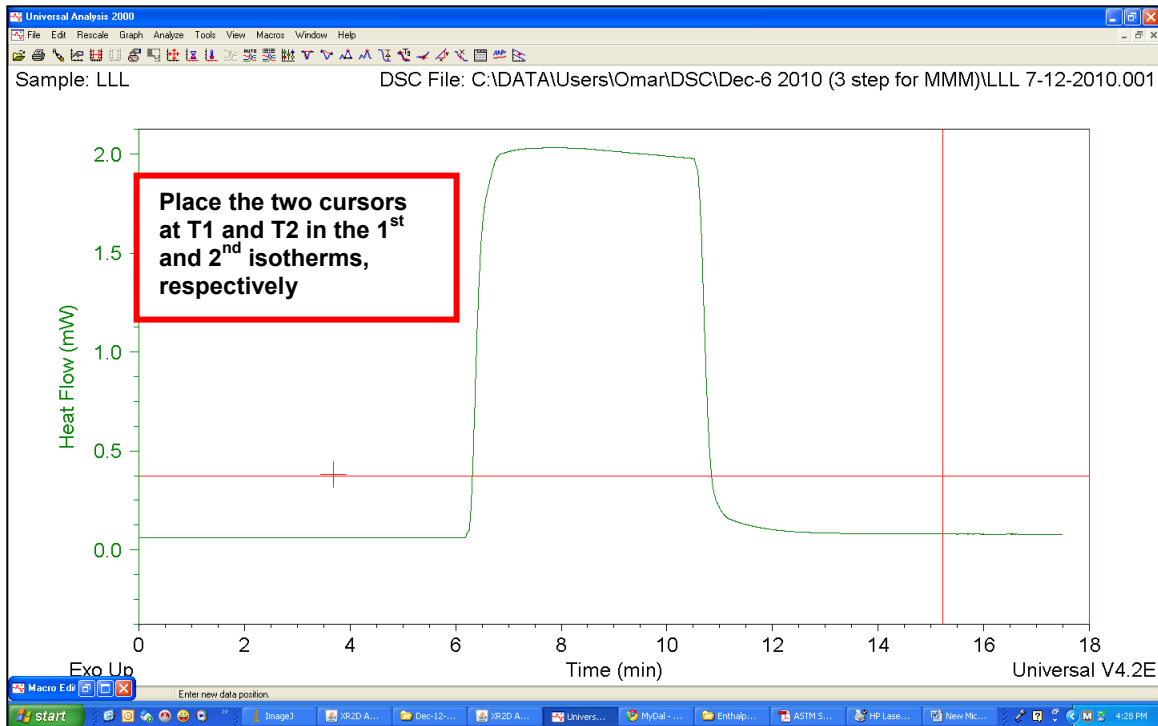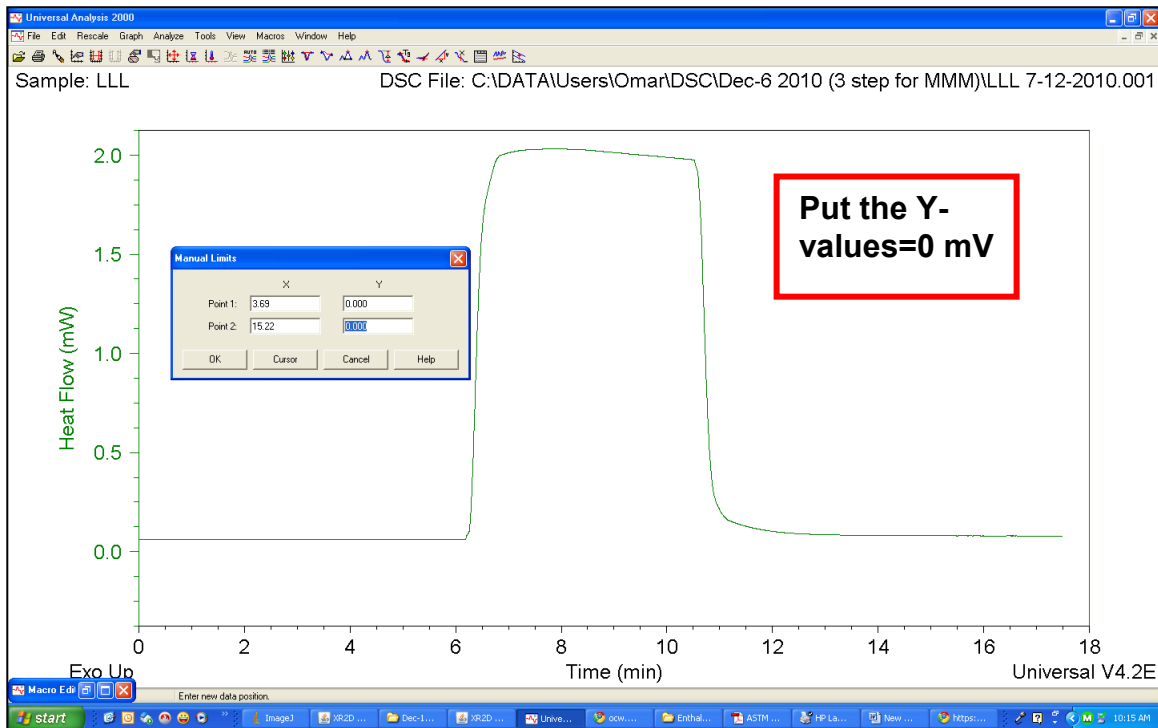
The normalization process was performed using the following equations. The signals should first be plotted as heat flow in mW as a function of time

$$\Delta Y(x) = \frac{Y_2 - Y_1}{X_2 - X_1}(X - X_1)$$

$$Y_0(x) = Y_{Old}(x) + \Delta Y$$

Where $Y_0(x)$ is the normalized heat flow value and Y_{old} is original heat flow before the normalization.

x= t

where t is the time in min

$$\Delta Y(t) = \frac{Y_2 - Y_1}{t_2 - t_1}(t - t_1)$$

The values of Y_2 and Y_1 are replaced with the value if 0 assuming that the heat flow values are zero during the isothermal segments.

Appendix C: A new method of pan crimping

1- In this procedure the AL hermetic lid (TA Instruments 900794.901) serves as the sample container and the non hermetic pan Al pan (TA Instruments 900786.901) serves as the lid. As seen in Figure 1.
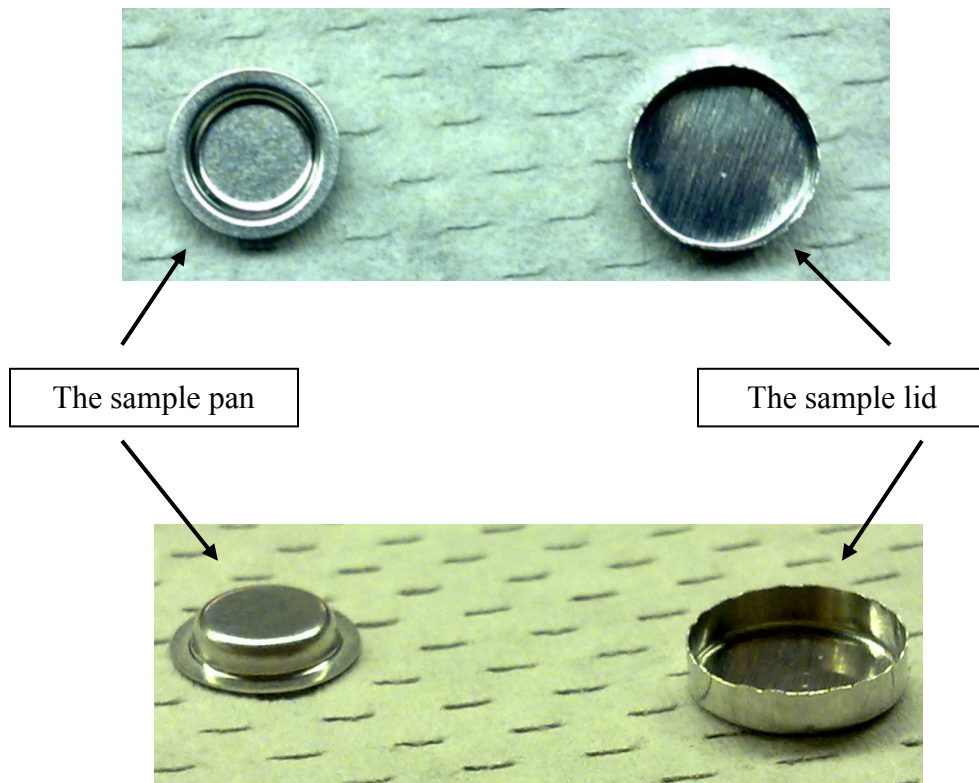

Figure 1: The sample pans and the lid used in this procedure.

2- Place the sample into the sample container while ensuring that the container area is covered with the sample. A sample mass range from 10 to 30 mg is recommended.

3- Before crimping the sample pan, ensure that the sample is solid so it wouldn't spill when the sample container is flipped.

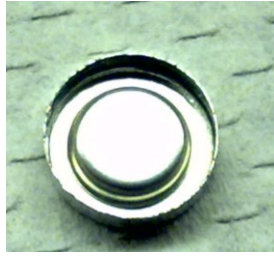4- Flip the sample pan upside down, and place it onto the Al non-hermetic pan as seen in Figure 2.

Figure 2: The sample pan flipped upside down ready to be crimped.

5- The sample pan and the lid are now ready to be crimped, using the TA Instruments blue crimper as shown in Figure 3. The crimping procedure is the same as the one recommended by TA instrument to crimp AL hermetic pans.
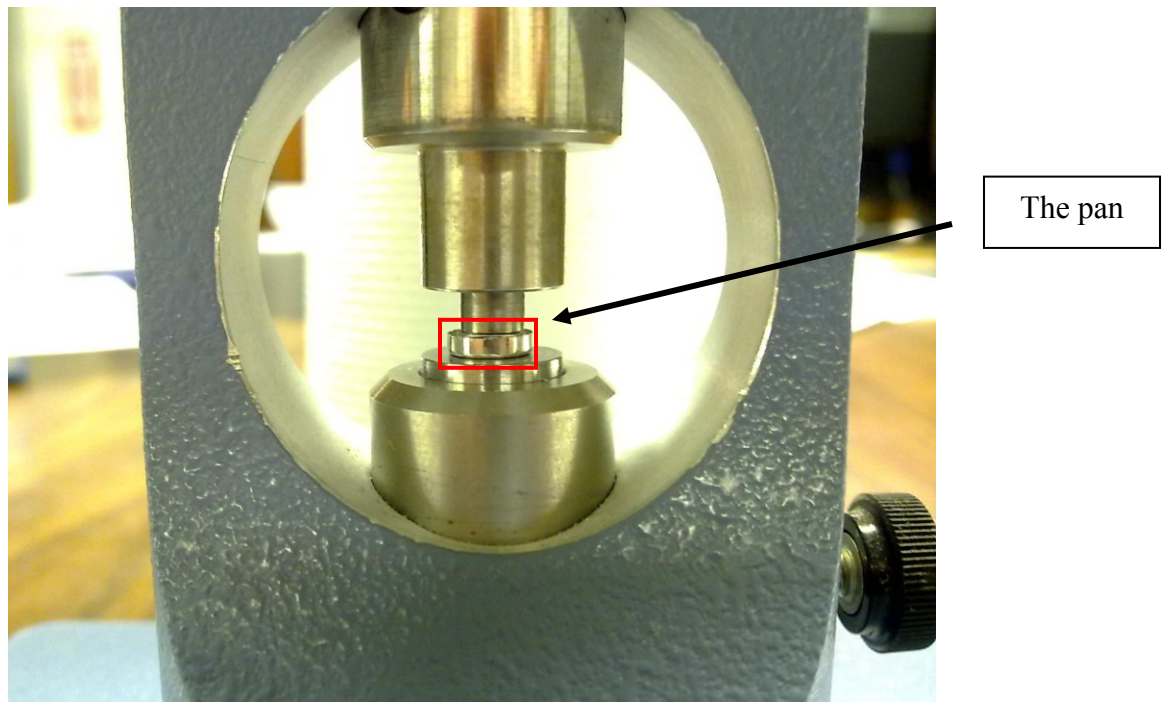

The pan

Figure 3: the crimping process of the pan.

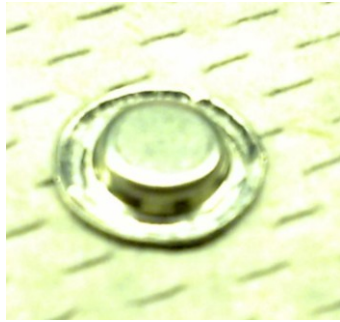6- The sample pan after crimping is shown in Figure 4 and is ready for the experiment.

Figure 4: the sample pan crimped.

7- Another pan should be prepared without a sample to serve as a reference pan, mass matched to within 0.005 mg.

Appendix D: The procedure used to test the effect of "take-out-put-back"

The thermal log used to test the "take-out-put-back" effect on the C_p measurements.

1: Mass flow 50.0 mL/min

2: Sampling interval 0.20 sec/pt

3: Data storage: Off

4: Ramp 20.00 °C/min to 110.00 °C

5: Isothermal for 2.00 min

6: Data storage: On

7: Isothermal for 10.00 min

8: Ramp 15.00 °C/min to -40.00 °C

9: Isothermal for 10.00 min

10: End of method